NEW DERIVATIVES OF TROVACENE (η^7-C_7H_7)V(η^5-C_5H_5): STUDIES OF REDOX SPLITTING, EXCHANGE COUPLING AND HYDROGEN BONDING

INAUGURAL-DISSERTATION

zur

Erlangung des Grades eines Doktors

der Naturwissenschaften

(Dr. rer. nat.)

vorgelegt

dem Fachbereich Chemie

der Philipps-Universität Marburg/Lahn

von

Francesca Paganelli

aus

Rimini

Marburg/Lahn 2003

Dedicated to my father

Danksagung

Herrn Prof. Dr. Ch. Elschenbroich danke ich für die Überlassung des Themas und für seine Unterstützung. Mein ganz besonderer Dank gilt Prof. D. Braga und Prof. F. Grepioni für die Kooperation mit ihrer Arbeitsgruppe.

Herrn Dr. Olaf Burghaus danke ich für die Simulationen der EPR-Spektren und immerwährende Hilfsbereitschaft bei EPR-spektroskopischen Problemen.

Herrn C. Pietzonka danke ich für die Durchführung und Auswertung der magnetischen Messungen, und Herrn Prof. Dr. B. Neumüller für die schnelle Durchführung der Kristallstrukturanalyse.

Bei Herrn Dipl.-Chem. S. Horst und Herrn Dipl.-Chem. B. Schäfer möchte ich mich für die Polymeranalytik bedanken.

Den ehemaligen Mitgliedern des Arbeitskreises danke ich für das hervorragende Arbeitsklima. Mein besonderer Dank gilt Herrn Dr. M. Nowotny für zahlreiche fachliche Diskussionen sowie Frau T. Schmidt für die von ihr durchgeführten Synthesen und die cyclovoltammetrischen Messungen.

Weiterhin danke ich dem Personal der zentralen Serviceeinrichtungen für die erbrachten Leistungen, vor allem den Herren K. Stutz (glastechnische Werkstatt), Prof. Dr. W. Massa (Röntgenstukturanalyse), Dr. K. Steinbach (Massenspektroskopie), Dr. J. Knecht (CHN-Analytik).

Sehr herzlich bedanken möchte ich mich bei meinen Mitbewohnern Roman und Sarah sowie bei meinen AGP-Kollegen Thomas und bei meinen Auslandskorrespondenten Marina, Paolo, Daniele und Domenico für ihre Freundschaft und ihre moralische Unterstützung.

Table of Contents

Numbered Compounds		IV
Abbreviations		VI
1.	Introduction	1
1.1	Crystal Engineering	1
1.2	Research Objectives	3
1.3	Electron Transfer and Exchange Interactions through Hydrogen Bond	4
2.	Metallation of (η^7-Cycloheptatrienyl)(η^5-cyclopentadienyl)vanadium and (η^7-Cycloheptatrienyl)(η^5-pentamethylcyclopentadienyl)vanadium	7
2.1	ENDOR Studies of Trovacene Metallation	13
2.1.1	Fundamentals of ENDOR Spectroscopy	13
2.1.2	Results	15
3.	Determination of the Structure of (η^7-Cycloheptatrienyl)(η^5-cyclopentadienyl)vanadium, **1•,** and (η^7-cycloheptatrienyl)(η^5-pentamethylcyclopentadienyl)vanadium, **2•**	19
3.1	Structure of (η^7-Cycloheptatrienyl)(η^5-cyclopentadienyl)vanadium, **1•**	19
3.2	Structure of (η^7-Cycloheptatrienyl)(η^5-pentamethylcyclopentadienyl) vanadium, **2•**	21
4.	Aldehydes and Carboxylic Acids (η^7-cycloheptatrienyl)(η^5-cyclopentadienyl)vanadium, **1•**, and (η^7-cycloheptatrienyl)(η^5-pentamethylcyclopentadienyl)vanadium, **2•**	25
4.1	Synthesis of (Carboxy-η^7-cycloheptatrienyl)(carboxy-η^5-cyclopentadienyl)vanadium, **13•**, and (Formyl-η^7-cycloheptatrienyl) (formyl-η^5-cyclopentadienyl)vanadium, **14•**	25
4.2	Synthesis of (Carboxy-η^7-cycloheptatrienyl)(η^5-pentamethylcyclopentadienyl)vanadium, **15•**, and (Formyl-η^7-cycloheptatrienyl) (η^5-pentamethylcyclopentadienyl)vanadium, **16•**	26
4.3	Structure of (Carboxy-η^7-cycloheptatrienyl)(carboxy-η^5-cyclopentadienyl)vanadium, **13•**	27
4.4	Structure of (Formyl-η^7-cycloheptatrienyl) (η^5-pentamethylcyclopentadienyl)vanadium,**16•**	30

4.5	Cyclic Voltammetry of **13$^{\bullet}$**, **14$^{\bullet}$**, **15$^{\bullet}$**, **16$^{\bullet}$**	33
4.5.1	Fundamentals of Cyclic Voltammetry	33
4.5.2	Results	34
4.6	Electron Paramagnetic Resonance of **13$^{\bullet}$**, **14$^{\bullet}$**, **15$^{\bullet}$**, **16$^{\bullet}$**	42
4.6.1	Fundamentals of Electron Paramagnetic Resonance	42
4.6.2	Results	44
4.7	ENDOR of **2$^{\bullet}$**, **14$^{\bullet}$**, **16$^{\bullet}$**, **17$^{\bullet}$**	51
5.	A Binuclear Complex of (η^7-Cycloheptatrienyl) (η^5-pentamethylcyclopentadienyl)vanadium	54
5.1	Synthesis of E-1,2-Bis[(η^7-cycloheptatrienyl)(pentamethyl-η^5-cyclopentadienyl)vanadium]ethene, **18$^{\bullet\bullet}$**	55
5.2	Cyclic Voltammetry of **18$^{\bullet\bullet}$**	56
5.2.1	Fundamentals of Cyclic Voltammetry of Binuclear Species	56
5.2.2	Results	57
5.3	Electron Paramagnetic Resonance of **18$^{\bullet\bullet}$**	59
5.3.1	Fundamentals of Electron Paramagnetic Resonance of Biradicals	59
5.3.2	Results	62
5.4	Magnetic Measurement of **18$^{\bullet\bullet}$**	65
5.4.1	Fundamentals of Magnetic Susceptibility	65
5.4.2	Results	67
6.	Sila-trovacenophanes	70
6.1	Synthesis of [1,8-(Diphenylsilanediyl)(η^7-cycloheptatrienyl)(η^5-cyclopentadienyl)vanadium], **24$^{\bullet}$**, and [1,8-(Tetramethyldisilane-1,2-diyl)(η^7-cycloheptatrienyl)(η^5-cyclopentadienyl)vanadium], **25$^{\bullet}$**	71
6.2	Structure of [1,8-(Diphenylsilandiyl)(η^7-cycloheptatrienyl)(η^5-cyclopentadienyl)vanadium] **24$^{\bullet}$**	72
6.3	Structure of [1,8-(Tetramethyldisilan-1,2-diyl)(η^7-cycloheptatrienyl-η^5-cyclopentadienyl)vanadium], **25$^{\bullet}$**	74
6.4	Comparison of the two Structures	77
6.5	Cyclic Voltammetry of **24$^{\bullet}$** and **25$^{\bullet}$**	79
6.6	EPR of **24$^{\bullet}$** and **25$^{\bullet}$**	84
6.7	Poly(trovacenylsilane)	86
6.7.1	Polymerisation Attempts and Analysis of the Products	88

7.	Benzoic Acid and Benzoate π-Complexes of Chromium	92
7.1	Synthesis of 1,1'-Bis(carboxy-η^6-benzene)chromium, **4**	93
7.2	Structure of 1,1'-Bis(carboxy-η^6-benzene)chromium, **4**	94
7.3	Synthesis of [1,1'-Bis(carboxy-η^6-benzene)chromium][hexafluorophosphate], **$[4(H)_2]^+ \bullet [PF_6]^-$**, (α and β forms) and [1,1'-Bis(carboxyl-η^6-benzene)chromium] [ammoniumhexafluorophosphate], **$[4(H)^\bullet] \bullet [NH_4PF_6]$**	96
7.4	Polymorphic Modification of the Salt **$31^{+\bullet}$**	97
7.4.1	Fundamentals of Polymorphism	97
7.4.2	Structures of **$[4(H)_2]^+ \bullet [PF_6]^-$** α and β Form	98
7.5	Structure of the Zwitterion as Co-crystal with $[NH_4][PF_6]$, **$[4(H)^\bullet] \bullet [NH_4PF_6]$**	102
7.6	Hydrogen Bonding Interaction in the three Species	105
8.	Summary	107
9.	Zusammenfassung	111
10.	Experimental Section	115
10.1	Materials	115
10.2	Instrumental Analysis	116
10.3	Preparations	118
11.	Literature	125
Appendix A		132
Appendix B		138
Appendix C		148

Numbered Compounds

1$^{\bullet}$ (η^7-Cycloheptatrienyl)(η^5-cyclopentadienyl)vanadium, [trovacene]

2$^{\bullet}$ (η^7-cycloheptatrienyl)(η^5-pentamethylcyclopentadienyl)vanadium

3 Bis(benzene)chromium

4 1,1'-Bis(carboxyl-η^6-benzene)chromium

[4(H)$_2$]$^+$•[PF$_6$]$^-$ [1,1'-Bis(carboxy-η^6-benzene)chromium][hexafluorophosphate], (α and β forms)

[4(H)$^{\bullet}$]•[NH$_4$PF$_6$] [1,1'-Bis(carboxyl-η^6-benzene)chromium] [ammoniumhexafluorophosphate]

4$^{\bullet-}$ [1,1'-Bis(carboxyl-η^6-benzene)chromium]

5 [1,1'-Bis(carboxyl-η^6-benzene)chromium][squarate]

6$^{\bullet}$ (η^7-Cycloheptatrienyl)(carboxy-η^5-cyclopentadienyl)vanadium

7 Ferrocene

8 (η^7-Cycloheptatrienyl)(η^5-cyclopentadienyl)titanium

9 (η^7-Cycloheptatrienyl)(η^5-cyclopentadienyl)chromium

10 Tetracarbonyl(η^5-cyclopentadienyl)vanadium

11$^{\bullet}$ (Deuterio-η^5-cyclopentadienyl)(η^7-cycloheptatrienyl)vanadium

12$^{\bullet}$ (Deuterio-η^5-cyclopentadienyl)(deuterio-η^7-cycloheptatrienyl)vanadium

13$^{\bullet}$ (Carboxy-η^7-cycloheptatrienyl)(carboxy-η^5-cyclopentadienyl)vanadium

14$^{\bullet}$ (Formyl-η^7-cycloheptatrienyl)(formyl-η^5-cyclopentadienyl)vanadium

15$^{\bullet}$ (Carboxy-η^7-cycloheptatrienyl)(η^5-pentamethylcyclopentadienyl)vanadium

16$^{\bullet}$ (Formyl-η^7-cycloheptatrienyl)(η^5-pentamethylcyclopentadienyl)vanadium

17$^{\bullet}$ (η^7-Cycloheptatrienyl)(formyl-η^5-cyclopentadienyl)vanadium

18$^{\bullet\bullet}$ **E**-1,2-bis[(η^7-cycloheptatrienyl)(η^5-pentamethylcyclopentadienyl)vanadium]ethene

19$^{\bullet\bullet}$ [5-5]-Bitrovacene

20$^{\bullet\bullet}$ [7-7]-Bitrovacene

21$^{\bullet\bullet}$ Bis([5]-trovacenyl)ethene

22$^{\bullet\bullet}$ 1,4-Bis([5]trovacenyl)benzene)

23 1,1'-Ferrocenyldiphenylsilane

24$^{\bullet}$ [1,8-(Diphenylsilanediyl)(η^7-cycloheptatrienyl)(η^5-cyclopentadienyl)vanadium]

25$^{\bullet}$ [1,8-(Tetramethyldisilane-1,2-diyl)(η^7-cycloheptatrienyl)(η^5-cyclopentadienyl)vanadium]

26 μ-(1,1'-Ferrocenyldiphenylsilane)

27 μ-(1,1',6,6'-Tetraphenylsilanechromium)

28 μ-(1,1'-Ferrocenyltetramethyldisilanylene)

29$^{\bullet}$ [5]-Trovacenol

30 1,1-Dimethyl-1-silaferrocenophane

31$^{\bullet}$ [1,8-(Dimethylsilandiyl)(η^7-cycloheptatrienyl)(η^5-cyclopentadienyl)vanadium]

32 1,1'-Ferrocenedicarboxylic acid

33^{+} [1,1'-Cobaltoceniumdicarboxylic acid][hexafluorophosphate]

34$^{\bullet}$ 1,1'-Bis(carboxyl-η^6-benzene)vanadium

Abbreviations

a, A	isotropic, anisotropic hyperfine coupling constant
a, b, c	lattice constants
AO	atomic orbitals
β	Bohr magneton
BBC	bis(benzene)chromium
c	concentration
BuLi	*n*-butyllithium
Cp	cyclopentadienyl
C	Curie constant
D	zero field splitting
DME	1,2-dimethoxyethane
DMF	dimethylformamide
E	energy, zero field splitting
$E_{1/2}$	half wave potential
E_λ	switching potential
E_{pa}, E_{pc}	anodic, cathodic peak potential
EPR	electron paramagnetic resonance
ENDOR	electron-nuclear double-resonance
f	frequency
g	g-value
G	Gauss
h	Planck constant
H_{ab}	electronic matrix element
HOMO	highest occupied molecular orbital
I	nuclear spin, current
I_{pa}, I_{pc}	anodic, cathodic peak current
IR	infra red
J	exchange coupling interaction
K	equilibrium constant
k_B	Boltzmann constant
λ	reorganization term

LUMO	lowest occupied molecular orbital
M	transition metal
μ	magnetic moment
m_I	nuclear spin quantum number
M_s	magnetic electronic quantum number
Me	methyl
MS	mass spectroscopy
MO	molecular orbital
NMR	nuclear magnetic resonance
ν	sweep velocity
PE	petroleum ether
Ph	phenyl
r	distance, radius
ROP	ring opening polymerization
S	electronic spin
SCE	saturated calomel electrode
T	temperature
TBAP	tetrabutylammoniumperchlorate
THF	tetrahydrofurane
TMEDA	N,N,N',N'-tetramethylethylenediamine
Tr	cycloheptatrienyl, tropylium ($C_7H_7^+$)
TVC	trovacene, (η^7-tropilium)vanadium(η^5-cyclopentadienyl)
TVC*	(η^7-cycloheptatrienyl)(η^5-pentamethylcyclopentadienyl)vanadium
Θ	Weiss constant
χ	susceptibility

1. Introduction

The independent discovery of ferrocene[1] in 1951 by Pauson and Miller and the rational synthesis of bis(benzene)chromium[2] by Fischer and Hafner in 1955 heralded a new era in organometallic chemistry, that of "sandwich-complexes".

The introduction of substituents in the ring periphery leads to molecules with new structural, electronic and electrochemical properties. Variation of metal and ligands offers a great number of combinations obtained by different synthetic methods. In this context should be mentioned:

a) the metallation reaction employing *n*-butyllithium,[3] which gives mono- and 1,1'-dimetallated products. Subsequent reactions give a variety of mono- and 1,1'-disubstituted bis(arene)metal derivatives including 1,1'-heteroatom substitution in the ring periphery;

b) the metal-ligand co-condensation, introduced in 1969 by Timms.[4] Thanks to this technique, complexes containing a large variety and number of substituents as well as complexes containing different types of transition- and post-transition metals became accessible.

Sandwich complexes play a central role in many areas:

-ligands in catalysts for stereoselective synthesis (i.e. 1,1'-bis(diphenylphosphino)ferrocene derivatives);[5]

-building blocks of redox active macrocycles in supramolecular chemistry;[6]

-application in medical science (biosensors, anti tumor agens);[7]

-components of molecular magnets;[8]

-utilization in non linear optics.[9]

1.1 Crystal Engineering[10]

Originally, crystal engineering was concerned with the design of more efficient topochemical[11] reactions, but now has greatly increased its scope to the design of molecular crystals for a wide variety of physical and chemical purposes.

Crystal engineering is the planning and the execution of a crystal structure synthesis from the constituent molecules.[12] Molecules and ions, chosen on the basis of their size, shape, and extramolecular bonding capacity, are the ultimate constituents. The assembly of these, i.e., the nucleation and growth of a molecular crystal, is one of the most basic processes in solid-state

chemistry and also one of the most impressive examples of molecular recognition. Crystal Engineering proceeds via the essential steps of analysis, synthesis and application.

Molecular crystal engineering is an area where supramolecular chemistry and material chemistry meet[13]: both disciplines are concerned with the utilization of non-covalent interactions to predetermine chemical and physical properties of supramolecular aggregates. The interest in organometallic crystal engineering stems from the enormous potential arising from the possibility of combining, inter alia, the electronic and magnetic characteristics of metal-bound ligands with those of metal atoms. The properties of solid organometallic materials depend on the electronic nature of the metals as well as on the characteristic of the ligands. These are in general organic molecules as fragments that, in most cases, retain their original extramolecular bonding capacity upon metal coordination because the peripheral atomic groups are not affected.

The crystals are the most accessible systems for a detailed study of geometry and energy of non-covalent interactions. X-ray crystallography has always played an important role in the development of organometallic chemistry. Ferrocene[14] represents the earliest example of an organometallic crystal structure determination. The relevance of X-ray crystallography in this chemistry arose because the complex structural features of organometallic compounds (many of which are air- and moinsture-sensitive) could not be determined by any other known methods.[15] This is particularly true for paramagnetic complexes where high-resolution NMR spectroscopy fails as an analytical tool. Despite this, the almost exclusive interest of organometallic chemists lay in the molecular structure and stereochemistry of organometallic compounds rather than in their crystal structures and packing characteristics.[16] However, crystals of organometallic complexes are molecular in nature, and so they must be held together by interactions that are, at least, similar to the interactions responsible for the assembly of purely organic molecular crystals.[17] The interactions utilized in the construction of the desired superstructure are

a) the coordinative bonds between multidentate ligands and metal centers, in the case of coordinative networks, and

b) van der Waals and hydrogen bonding between building blocks that possess a defined structure in solution, in the case of molecular networks.

The hydrogen bond,[18] that may most generally considered to be a three-center four-electron interaction, is the master-key interaction in crystal engineering because it combines directionality with strength (nevertheless anion-cation[19] and van der Waals[20] interactions take part to the process of molecular recognition and crystal cohesion). Length and directionality

permit the planning of molecular aggregates formed by molecules bearing donor and acceptor groups opportunely chosen.[21] This idea is now largely used to produce new crystalline materials[22] with suitable characteristics to confer useful properties in non linear optics, optoelectronics and photonics, magnetism, conductivity, nanoporosity, as well as applications in catalysis, molecular traps, reservoirs and sieves, solid state reactivity, mechanics *etc*.

1.2 Research Objectives

Organometallic complex offers the possibility to combine the large variety of the organic synthetic methods with the stability of paramagnetic complexes. In particular our research is focused on the paramagnetic complexes [(η^7-C_7H_7)(η^5-C_5H_5)V] (TVC) [trovacene, (η^7-tropilium)vanadium(η^5-cyclopentadienyl)], **1**$^{\bullet}$, and [V(η^7-C_7H_7)(η^5-C_5Me_5)V] (TVC*), **2**$^{\bullet}$, in their neutral form, and the paramagnetic complex [(η^6-C_6H_6)$_2$Cr] (BBC), bis(benzene)chromium, **3**$^{+\bullet}$, in its cationic form.

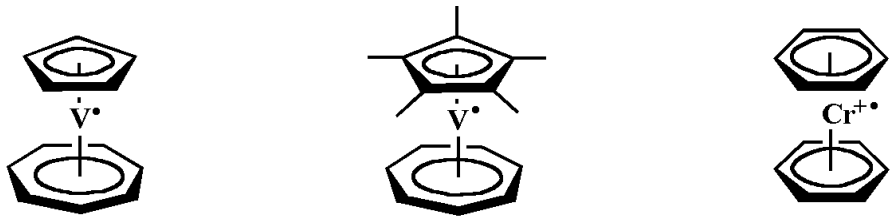

1$^{\bullet}$ **2**$^{\bullet}$ **3**$^{+\bullet}$

The followed line of research is devoted to preparation and characterization of novel building blocks and of their precursors for the construction of crystalline materials via cooperative strong and weak hydrogen bonds.[23] The prerequisites of the chosen candidate building blocks are essentially 3-fold: (a) chemical stability to yield robust materials, (b) specific and predictable capacity for the formation of a large number of extramolecular interactions, in particular O–H---O and C–H---O types[24], and (c) suitable shape for molding intermolecular H-bond networks to achieve highly organized superstructures.

Carboxylic acids and aldehydes of **1**$^{\bullet}$, and **2**$^{\bullet}$ were chosen as buildings blocks, since, due to their paramagnetic properties, they permit an investigation of the electron spin-exchange interactions mediated by O–H---O hydrogen bonds in solution, employing EPR[25] spectroscopy, in addition to that in solid state, employing X-ray diffraction.

When paramagnetic complexes are linked by a bridging ligand to give a binuclear complex, it is possible to observe intermetallic interactions between both spin centers, depending on the nature of the spacers. The study of electron spin exchange coupling aid in understanding which factors control the rate of electron-transfer, as found in oxidation-reduction, and electrochemical processes. The bridged complexes of $\mathbf{1}^{\bullet}$, and $\mathbf{2}^{\bullet}$ provide the opportunity to study intramolecular electron-transfer between electron-donor and electron-acceptor as a function of the relative orientation and separation of donor and acceptor. In this context, is of interest, which factors determine both magnetic exchange and intramolecular electron-transfer.[26]

Moreover, varying the oxidation states of the individual metal centers can be used to control the spin state, hence the magnetic properties of the complex. Magnetic materials, that are based on organometallic open-shell complexes, have been studied extensively. Hence, in organometallic systems the neutral or charged nature of the ligands, combined with the variable oxidation states of metal atoms, allows the study of the same building block in both neutral and ionic environments.[10] Bis(benzoic acid)chromium, $[Cr(\eta^6\text{-}C_6H_5COOH)_2]$, **4**, is a good candidate to prepare magnetic materials due to the possibility of combining in a controlled manner the charge (varied via a redox process) with the hydrogen bonding capacity.

1.3 Electron Transfer and Exchange Interactions mediated through Hydrogen Bonding

Electron transfer reactions are known to be transmitted through non-covalent interactions such as hydrogen bonds, which play an important role in biological electron-transfer systems for example, non-covalent bonded proteins, model complexes for photosynthesis.[27]

Long range donor-acceptor electron transfer, mediated by a molecular bridge, represents one of the fundamental charge transfer processes in chemical and biological systems.

Due to the possible relation between k_{et} and J (exchange interaction coupling), the more facile experimental access to J could deliver valuable information about electron transfer processes through hydrogen bonds in biological molecules.

The hydrogen bond is the principal non-covalent interaction in the formation of molecular crystals, because it combines strength with directionality.[28] Etter's elaboration[29] of Linus Pauling's definition describes "a hydrogen bond as an interaction that directs the association

of a covalently bonded hydrogen atom with one or more others atoms, groups of atoms, or molecules into an aggregate structure that is sufficiently stable to make it convenient for the chemist to consider it as independent chemical species". However, for most purposes, hydrogen bonding is defined as an interaction between a X-H donor and a Y acceptor, X and Y being electronegative atoms or electron-rich groups, in the same or in another molecule (X–H--Y).[30] This interaction is generally stronger (often much stronger) than the strongest intra- and intermolecular van der Waals interactions (X–H--Y). The H-Y and X-Y separations are shorter than van der Waals contact distances, and X-H-Y angles tend to adopt the linearity. Hydrogen bridges can be found in the solid state, in solution, and in the gas-phase.[31] Charge assistance[32] to hydrogen bond is the enhancement of donor and acceptor systems' polarity by utilizing cationic donors and anionic acceptors instead of neutral systems. The favourable location of charges increases proton acidity and acceptor basicity.
Spectroscopic characteristics, and detection methods of hydrogen bond are shown in Table **1**.

Properties	**Detection Methods**
The distance H--Y is shorter than the sum of van der Waals radii	X-ray Diffraction Neutron Diffraction
The distance X–H increases compared to the free molecules	X-ray Diffraction/Neutron Diffraction Red-Shift of X---H Stretching in IR
The electron density at the H atom decreases with the formation of hydrogen bridges	Low Field Shift in NMR

Table **1**: Properties and detection methods of hydrogen bonds.

The classical O-H···O hydrogen bonds formed by COOH and OH groups are among the strongest neutral hydrogen bonds. However, the bond can be strengthened if the polarity of the acceptor is increased via deprotonation. Negatively charged O-H···O^- bonds have been shown to possess dissociation energies in the range 60-120 $kJmol^{-1}$.[33]
The utilization of carboxylic acids permits the simultaneous use of neutral O-H···O and charged O-H···O^- bonding interactions. The latter interactions can be grouped in two distinct categories: the O-H···O^- interactions, in which the donors belongs to a neutral molecule and the acceptor is an anion, and the interaction O-H^-···O^-, where both donor and acceptor groups belong to an anion. In all cases the O···O distances are considerably shorter than the sum of the van der Waals radii and there is a marked preference for linearity. O-H···O^- and O-H^-···O^-

interactions, although possessing the same geometrical properties as neutral O-H···O bonds, are generally associated with O···O distances shorter than in the case of neutral systems (roughly 2.45 against 2.65 Å).[34]

A recent example of engineering of a supramolecular arrangement with target magnetic properties is provided by crystalline [1,1'-bis(carboxyl-η^6-benzene)chromium][squarate], $[(\eta^6\text{-}C_6H_6)_2Cr^I]^+[HC_4O_4]^-$, **5**, obtained by reacting squaric acid (3,4-dihydroxy-3-cyclobutene-1,2-dione) with $[(\eta^6\text{-}C_6H_6)_2Cr^I]^+$, $\mathbf{3}^{+\bullet}$.[35] The anion $[HC_4O_4]^-$ self-assembles into chains linked by $^{(-)}$O-H···O$^{(-)}$ interactions and simultaneously intercalates between the benzene ligands forming π-stacking interactions. The presence of a charge transfer transition was detected by diffuse reflectance UV-spectroscopy.

An EPR study of exchange interactions mediated by O-H---O bonds for hydrogen bonded dimmers of the paramagnetic complex (η^7-cycloheptatrienyl)(carboxy-η^5-cyclopentadienyl)vanadium, $[(\eta^7\text{-}C_7H_7)(\eta^5\text{-}C_5H_4COOH)V^0]$, $\mathbf{6}^{\bullet}$, has been reported previously.[25]

2. Metallation of (η^7-Cycloheptatrienyl)(η^5-cyclopentadienyl)vanadium, 1$^\bullet$ and (η^7-Cycloheptatrienyl)(η^5-pentamethylcyclopentadienyl)vanadium, 2$^\bullet$

The reaction between an organic (organometallic) compound containing a relatively acidic hydrogen atom (R-H) and an organolithium reagent (R'-Li) is of considerably synthetic utility since the resulting new organolithium reagent (R'-Li) can be used in a wide variety of subsequent reactions:[36]

$$\text{R-H} + \text{R'-Li} \rightarrow \text{R-Li} + \text{R'-H}$$

Ring hydrogen atoms of cyclopentadienyl- as well as arene-metal complexes have weakly acidic character. Reactions with alkyllithium reagens result in ligand metallation under formation of highly reactive products, which can be converted into a wide variety of ring-substituted complexes.

The extent of polylithiation, which may occur in the case of the more acidic complexes, can be controlled to some degree by an appropriate choice of the reaction conditions. For example, addition of tertiary amines, such as N,N,N',N'-tetramethylethylendiamine (TMEDA), and 1,4-diazabicyclo[2.2.2]octane (DABCO), accelerates lithiation by coordination to the lithium, which in turn promotes dissociation of aggregated structures.[37] The stable coordination complexes formed are considerably more reactive in the metallation reaction than the organolithium reagents alone.

The enhanced metalating ability of the couple *n*-butyllithium/TMEDA may possibly arise from the interation of the diamine with vacant 2*p* orbitals of the lithium ion. Such a process may polarize the carbon-lithium bond to such an extent that the butyl group becomes a considerably more powerful nucleophile than *n*-butyllithium alone. The presence of the diamine does not affect subsequent reactions of the newly formed organolithium compounds.

The ability of various (η^5-cyclopentadienyl)metal compounds to undergo the hydrogen lithium exchange (metallation) reaction has played an important role in the development of the chemistry of metallocenes. Metallation of ferrocene, **7**, with *n*-butyllithium in ether solution, first reported independently by two research group in 1954,[38] leads to lithio-ferrocene and 1,1'-dilithio-ferrocene, that are very readily converted to numerous derivatives.

Studies of the early transition metals have shown that (η^7-cycloheptatrienyl)(η^5-cyclopentadienyl)titanium, **8**, is readly monometalated by 1 equiv of *n*-butyllithium in ether solution at 0°C, and the metallation take place preferentially at the seven membered ring.[39] Treatment of this mixed sandwich complex with 2.4 equiv of *n*-butyllithium/TMEDA affords

the dimetalated product in high yield.[40] This is in contrast to the behaviour of the corresponding vanadium and chromium compounds which are preferentially metalated at the five-membered ring. The mono-metallation of (η^7-cycloheptatrienyl)(η^5-cyclopentadienyl)vanadium can be achieved by employing 1.5 equiv of *n*-butyllithium in ether solution at room temperature overnight[41], whereas the metallation of (η^7-cycloheptatrienyl)(η^5-cyclopentadienyl)chromium, **9**, is more difficult, but again the products isolated are substituted mainly in the five-membered ring.[42]

These results have been interpreted with the aid of MO calculations and ESCA measurements, which suggest that the more negatively charged ring of these unsymmetrical sandwich complexes is the more reactive towards lithiation. These observations are discussed in terms of qualitative molecular orbital considerations on the charge distribution in the complex.[39]

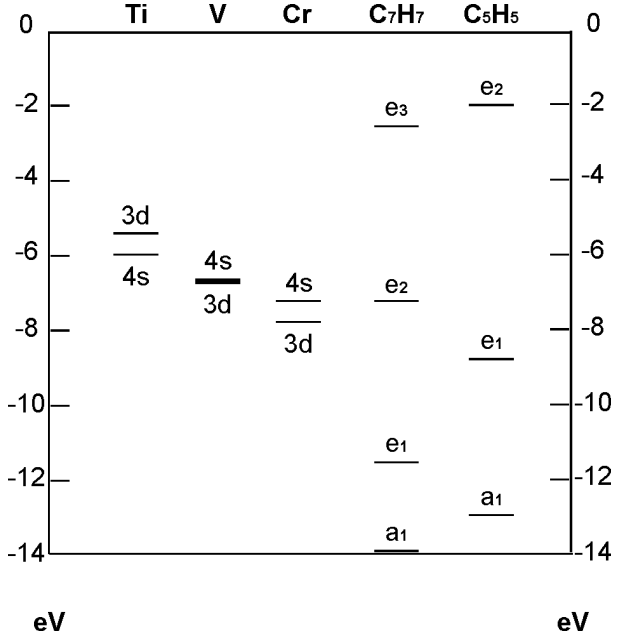

Fig.**1**: Estimated energies of the 3*d* and 4*s* orbitals of Ti, V, Cr, and of the π-orbitals of neutral C_7H_7 and C_5H_5.[39]

The rate of metallation employing *n*-butyllithium at room temperature increases in the sequence M= Cr< V< Ti. This observation indicates that the negative charge on the carbon atoms of the seven-membered ring increases in the same sequence, leading to an enhanced susceptibility for metallation, while the charge on the five-membered ring is much less affected. A qualitative consideration of the molecular orbitals formed from the π-orbitals of the cyclic ligands and the 3*d*-orbitals of the metals is shown in the Fig. **2**.[39]

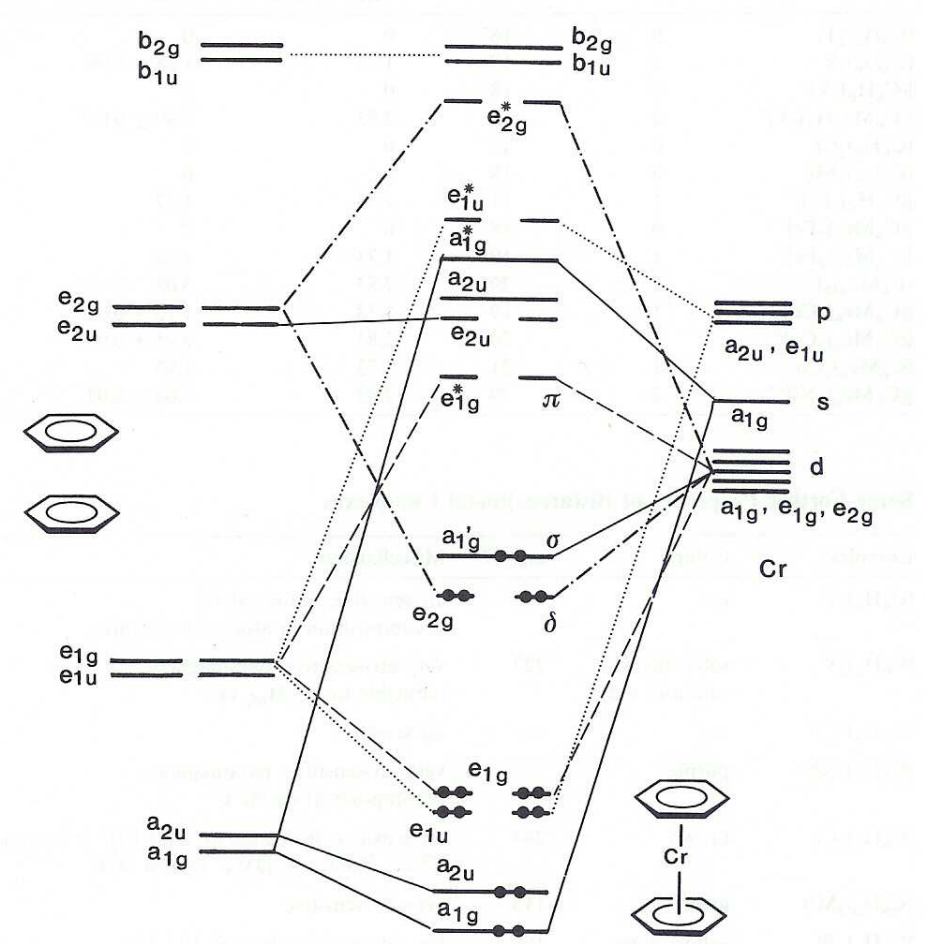

Fig. **2**: MO diagram for bis(benzene)chromium.[36]

Taking the line connecting the metal with the centers of the two rings as the *z*-direction, the $3d_z^2$, the 4s and the $4p_z$ orbitals of the metal, and the a_1 orbitals of the two rings have σ-symmetry. The bonding σ-orbitals, occupied by four electrons, are essentially ligand orbitals; the d_z^2 orbital is almost non bonding (unoccupied in the titanium sandwich, occupied by one electron in the vanadium sandwich, and by two electrons in the chromium sandwich). Eight electrons occupy molecular orbitals of π-symmetry (the e_1 orbitals of the two rings), and the d_{xz}, d_{yz}, $4p_x$, and $4p_y$ orbitals of the metal. It is obvious that the occupied bonding orbitals are essentially ligand orbitals, while the empty anti-bonding orbitals are metal orbitals. The remaining four valence electrons are placed in the bonding molecular orbitals of δ-symmetry (the d_{xy} and $d_{x^2-y^2}$ orbitals of the metal, and the e_2 orbitals of the seven-membered ring); the e_2 orbitals of the cyclopentadienyl (Cp) ligand have too high energy to be considered. The character of the bonding MO's of δ-symmetry is strongly dependent on the nature of the

metal, as the 3*d*-orbitals of the metals (which increase in the sequence Cr< V< Ti)[43], and the e_2 orbitals of the seven-membered ring are close in energy.[44]

It is argued that the ligand character of these occupied orbitals will increase in the sequence Cr< V< Ti. This picture predicts that the bonding MO's of δ-symmetry are mainly metal orbitals in **9**, but mainly C_7H_7 orbitals in **8**. Hence, the Cp ligand is more negative than the cycloheptatrienyl ligand in the chromium compound, and vice versa in the titanium compound, whereas in **1**$^{\bullet}$ the two rings carry about an equal (negative) charge.[45]

In this case the charge of the seven-membered ring resides predominantly on the hydrogen atoms, the carbon atoms being almost neutral, while the charge of the Cp ring is distributed over the carbon and hydrogen atoms. In any case, it is shown that the negative charge on the seven-membered ring of $(C_5H_5)M(C_7H_7)$ increases in the sequence M= Cr< V< Ti. The interatomic distances in **9**[39] [Cr-C(C_5H_5)= 2.18 Å; Cr-C(C_7H_7)= 2.16 Å] and $(C_5H_5)V(C_7H_7)$ [V-C(C_5H_5)= 2.210 Å; V-C(C_7H_7)= 2.208 Å] (see next section for the values) have normal values; while **8**[46] [Ti-C(C_5H_5)= 2.32 Å; Ti-C(C_7H_7)= 2.19 Å] displays abnormally short Ti-C(C_7H_7) distances, as a result of the very short distance (1.49 Å) of the metal to the plane of the seven-membered ring.

This observation demonstrates the importance of δ-bonding in the Ti-(C_7H_7) moiety; a decrease of the distance of the metal from the ring plane greatly increases the overlap of the ligand e_2 orbitals with the $d_{x^2-y^2}$ orbitals of the metal.

Mono-substituted complexes of trovacene are known, carrying the functional groups in the cycloheptatrienyl- or in the Cp-ring. Compounds of the first type, $[V^0(\eta^5\text{-}C_5H_5)(\eta^7\text{-}C_7H_6R)]$, (where R= -$CH_3$, -Ph, -CN, -$OCH_3$…) are obtained by refluxing the appropriate cycloheptatriene derivative with tetracarbonyl(η^5-cyclopentadienyl)vanadium, $[V^0(\eta^5\text{-}C_5H_5)(CO)_4]$, **10**.[47] This method is limited by the accessibility of the cycloheptatrienyl-derivative (for example, it is very difficult to introduce aldehyde and acid groups to the cycloheptatrienyl ring).

Because of the only marginally greater negative charge on the Cp, with respect to that on the cycloheptatrienyl ligand, trovacene reacts slowly with *n*-buthillithium (1 equivalent of trovacene and 1.5 equivalent of *n*-buthillithium) in ether at room temperature (maximum yield: 50%),[39] resulting in metallation of the five-membered ring, as indicated by a colour change of the solution from violet to dark-red. The mono-lithio derivative can be converted to compounds of the type $[V^0(\eta^5\text{-}C_5H_4R)(\eta^7\text{-}C_7H_7)]$, where R= -$CH_3$[48], -CHO[49], -COOH[50], -I[51], -Br[52], -PPh_2[53], -$B(OH)_2$[54]…

The low yield of mono-metallation might be explained by assuming a scrambling reaction, which, in its simples case, would amount to a dismutation of monolithio-trovacene to trovacene and 1,1'-dilithio-trovacene, as it is postulate for the equivalent reaction of ferrocene[55]:

$$2FcLi \rightleftharpoons Fc + FcLi_2$$

This reaction is confirmed by mass-spectroscopy analysis, by quenching the reaction mixture with D_2O. The fragmentations obtained in mass-spectroscopy are displayed in Table **2**.

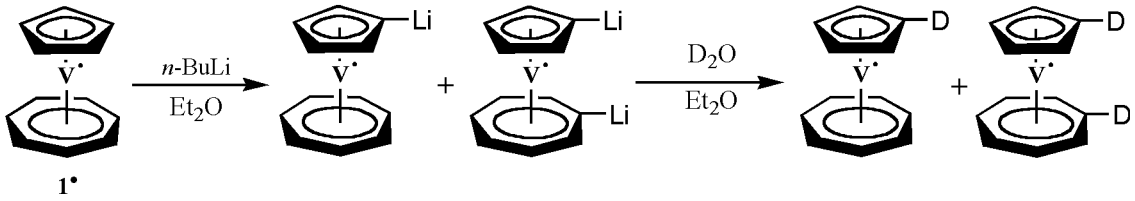

It is known that dimetallation reactions of metallocenes give very good yields: in almost all cases more than 90% of dilithio-metallocene is obtained (the percentage of unreacted metallocene and monolithio-derivative is minimal).[56]

When 1 equivalent of trovacene is treated with a combination of 4 equivalents of TMEDA, and 4 equivalents of *n*-butyllithium in ether at reflux temperature for 4 hours, transmetallation in both rings is effected as indicated by a colour change of the solution from violet to brown, and the formation of a violet precipitate. The extent of the transfer of lithium to trovacene was determined by quenching the reaction mixture with D_2O and examination of its mass spectrum.

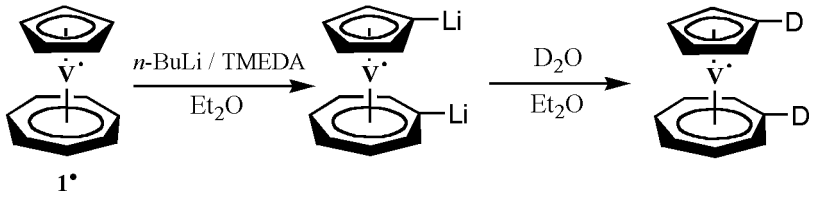

The detected fragmentations in the resulting mass spectrum are displayed in the following table (the spectra reveal a fragmentation pattern involving C_7-ring contraction and C_5-ring expansion, as it has been reported in literature from studies of trovacene).[57]

		TVC-D	TVC-D_2
51	V^+	98%	77%
116	$C_5H_4HV^+$	24%	3%
117	$C_5H_4DV^+$	32%	39%
129	$C_6H_6^+$	14%	5%
130	$C_6H_5D^+$	39%	69%
208	$C_{12}H_{11}D_1V^+$	100%	2%
209	$C_{12}H_{10}D_2V^+$	24%	100%

Table **2**: Fragmentation pattern in the mass spectrum of the reactions of mono- and di-metallation of trovacene quenched with D_2O. The column named TVC-D corresponds to the product isolated from the reaction of mono-lithiation; the column named TVC-D_2, to that isolated from the reaction of di-lithiation. %-values represent relatives intensity.

In addition, a study of the deuterated complexes was performed employing ENDOR spectroscopy in order to avoid the hydrogen/deuterium scrambling reaction, which can occurs in mass spectrometry analysis (see section 2.1.2).

A new strategy to prepare [7]-trovacene derivatives, was developed by employing a trovacene derivative bearing a pentamethylcyclopentadienyl (Cp*) ligand. When 1 equivalent of (η^7-cycloheptatrienyl)(pentamethyl-η^5-cyclopentadienyl)vanadium, **2•** is treated with 2 equivalents of TMEDA, 2 equivalents of potassium-*tert*-butoxide and 2 equivalents of *n*-butyllithium in petroleum ether at low temperature (-20°C), metallation in the seven-membered ring was effected as indicated by a colour change of the solution from clear violet to brown.

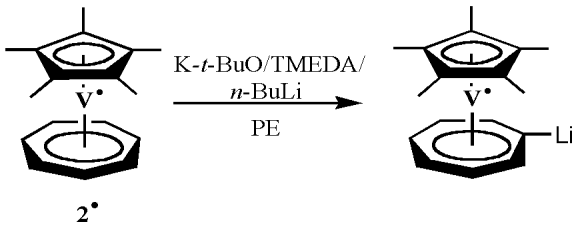

2•

The presence of the Cp* ligand results in favourable properties in terms of increased stability and solubility and lowered oxidation potential, due to its amplified donor capacity. In addition, the 1,8-substitution pattern of trovacene derivatives achieved under analogous

reaction conditions of metallated intermediates with electrophiles, is of course not possible in the case of (η^7-cycloheptatrienyl)(pentamethyl-η^5-cyclopentadienyl)vanadium moiety, which might be of advantage with regard to a selective 1'-monofunctionalization.

2.1 ENDOR Studies of Trovacene Metallation

2.1.1 Fundamentals of ENDOR Spectroscopy[58]

ENDOR (Electron-Nuclear Double-Resonance) spectroscopy is a multiple-resonance technique in which the spin system is simultaneously irradiated by a microwave and a radio frequency field. This technique was introduced in 1956[59] to resolve hyperfine and nuclear quadrupole interactions which were not accessible in the EPR spectra.

One disadvantage of EPR spectroscopy in rigid media is that the EPR lines are additionally broadened by the g anisotropy and the hyperfine anisotropy of the interacting nuclei. As a consequence, ligand hyperfine couplings are often not resolved in the EPR display.

In an ordinary EPR experiment the magnetic field is swept through the region of resonance $H= \hbar\omega_e/g\beta$ (where H= magnetic field strength, $\hbar = h/2\pi$, ω_e = microwave frequency, g= spectroscopic splitting factor, β= Bohr magneton). An ENDOR experiment uses two frequencies: a microwave frequency to partially saturate electronic Zeeman transitions and monitor the intensity of the EPR signal, and a strong radio frequency, which is varied in order to excite nuclear (NMR) Zeeman transition. The induced NMR transitions alter the spin polarization or the spin alignment, leading to a change of the EPR signal intensity. By plotting these EPR intensity changes versus the radio frequency, the ENDOR spectrum is obtained.

In Fig. **3** the hyperfine coupling of one unpaired electron with four equivalent nuclei (I= ½) in a high field is show.

The four nuclear spins can be combined and classified according to their total spins values I= 2, 1, 0 with degeneracies D(I=2) = 1, D(I=1) = 4, D(I=0) = 6. Owing to the transition frequency degeneracies, five EPR transitions are obtained with binomial intensity distribution (1:4:6:4:1). The ENDOR spectrum, on the other hand, exhibits only two signals, since all NMR transitions in the same M_s state are degenerate. To generalize, each group of equivalent nuclei contributes only two ENDOR lines to the spectrum. Addition of non-equivalent nuclei to the system causes a multiplicative increases of the number of signals in the EPR spectrum,

but only an additive increase in the ENDOR spectrum. The number of lines in an ENDOR spectrum is considerably less, so the effective resolution is much greater.

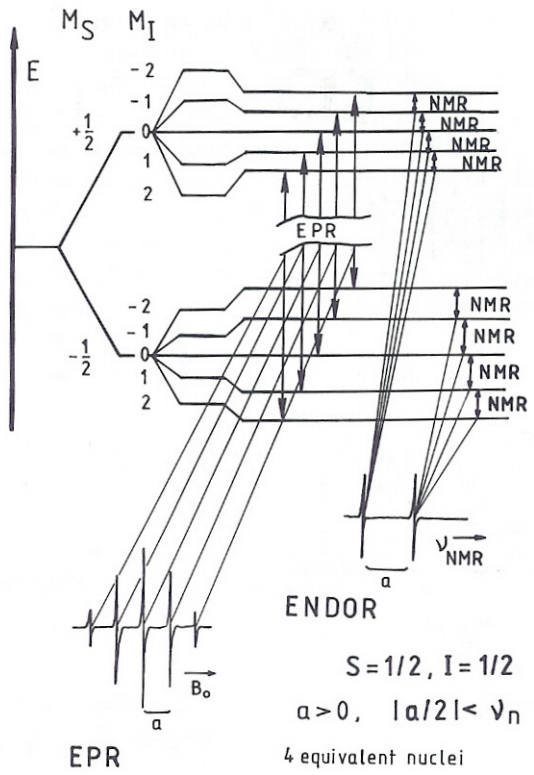

Fig. **3**: Energy-level diagram of a hyperfine-coupled spin system in a high magnetic field, consisting of one unpaired electron (S= ½) and four equivalent nuclei (I= ½).[58]

The narrow signal usually achieved in fluid solutions or in single crystals are no longer obtained in ENDOR experiments of disordered solid, i.e., glasses or powders. Due to absorption from a range of orientations of the radicals with respect to the direction of the magnetic field, the ENDOR lines broaden and may become very weak. In this situation the ENDOR absorptions are spread out over a range of anisotropic hyperfine coupling values with some buildup of intensity at three values corresponding to those radicals that have their principal axes along the magnetic field (see Fig. **4**). Fairly narrow lines are observed only if the hyperfine anisotropy pertaining to the nucleus is small.

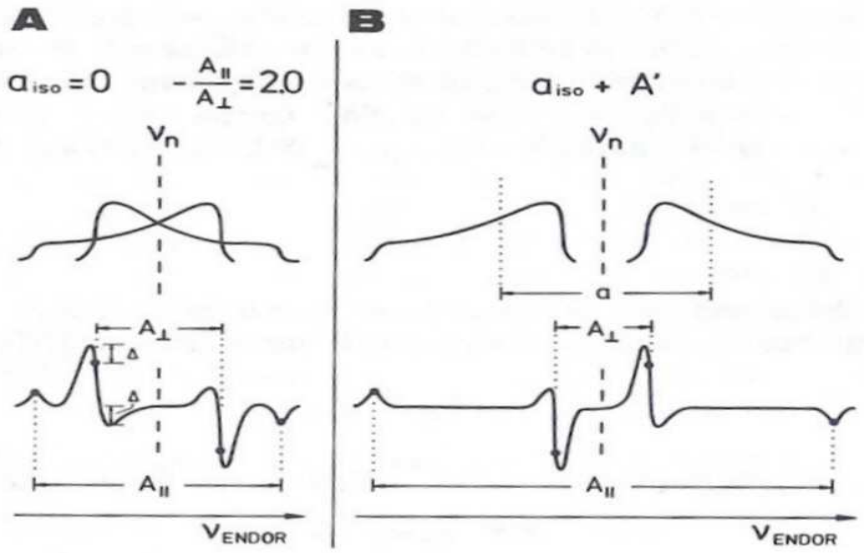

Fig. **4**: ENDOR lines shapes (absorption: top, first derivate: bottom) resulting from axially symmetric hyperfine tensor.[58]

2.1.2 Results

^{1}H ENDOR experiments of trovacene and the deuterated derivatives obtained by metallation reactions were performed in frozen toluene solution, in order to check the presence of the deuterium atom in the five and in the seven-membered ring in both mono- and di-metallation reaction.

The ^{1}H ENDOR lines appeared symmetrically around the free nuclear (hydrogen) frequency (around 14.2 MHz). In the case of compound **1**$^{\bullet}$, the isotropic hyperfine coupling constants are 5.0 and 12.1 MHz for the five- and seven-membered ring, respectively. These values are supported by NMR studies: $a(^1H_{cp})$= 1.8 G (corresponding to 5.04 MHz), and $a(^1H_{tr})$= 4.3 G (corresponding to 12.05 MHz).[60] Resonance in sandwich complexes in liquid solution can not be EPR saturated, which is a prerequisite for ENDOR. Therefore, in this work, the ENDOR spectra of **1**$^{\bullet}$, of mono-, **11**$^{\bullet}$, and di-deuterated trovacene, **12**$^{\bullet}$ have been recorded in frozen toluene solution. The deuterated compounds have been prepared and isolated as described above. The experimental spectra are displayed in Figs. **5**-**6**.

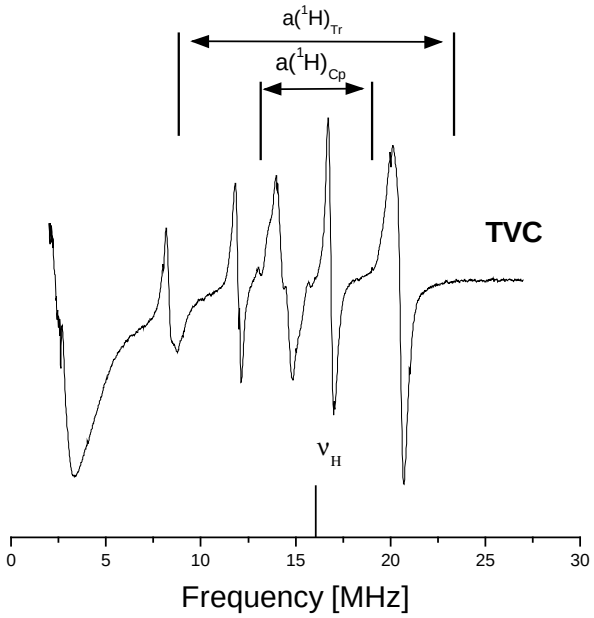

Fig. **5**: ^{1}H ENDOR spectra in toluene of **1**$^{\bullet}$ at 130 K, frequency 9.5494 GHz, microwave power 7 dB (42 mW), radio frequency power 3 dB (500 W), static field 3371 G. The vertical line indicates the free proton frequency (15.30 MHz).

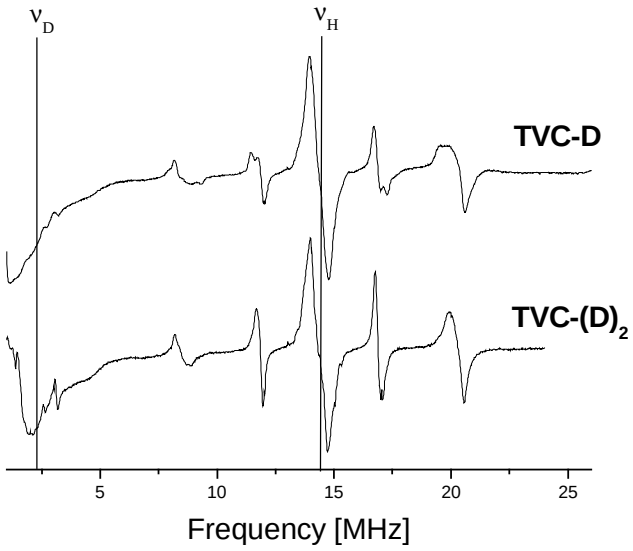

Fig. **6**: ^{1}H ENDOR spectra in toluene of **11**$^{\bullet}$ (top) at 130 K, frequency 9.4889 GHz, microwave power 7 dB (42 mW), radio frequency power 3 dB (500 W), static field 3365 G, and **12**$^{\bullet}$ (bottom) at 129 K, frequency 9.4901 GHz, microwave power 6 dB (53 mW), radio

frequency power 3 dB (500 W), static field 3360 G. The vertical lines indicate: the free deuterium frequency (2.4 MHz) and the free proton frequency (14.33 MHz).

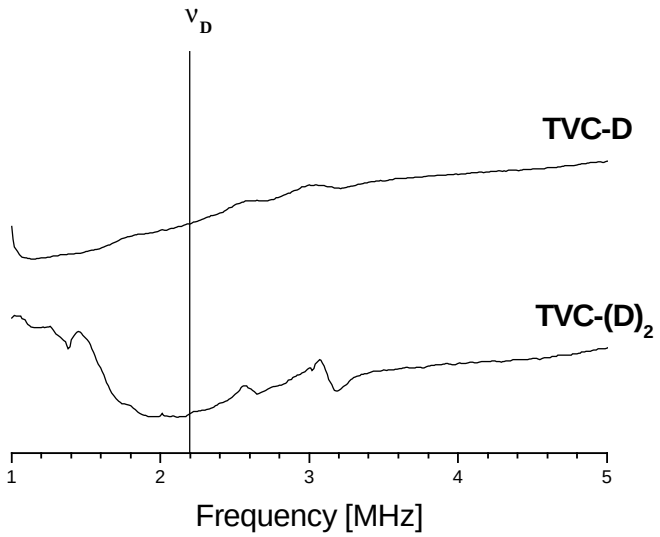

Fig. **7**: Enlargement of the deuterium frequency range of the ENDOR spectra of **11**$^{\bullet}$ (top) and **12**$^{\bullet}$ (bottom). The vertical line indicates the free deuterium frequency (2.2 MHz).

In the spectra, the line at 14.40 MHz (for **1**$^{\bullet}$), 14.37 MHz (for **11**$^{\bullet}$) and 14.34 MHz (for **12**$^{\bullet}$) corresponds to the matrix signal (unresolved hyperfine interactions with the solvent), while the other lines arise from the hyperfine interaction of the cycloheptatrienyl and cyclopentadienyl protons: the signals spread out between 11.9 and 16.8 MHz, for **1**$^{\bullet}$, between 11.6 and 17.2 MHz for **11**$^{\bullet}$and **12**$^{\bullet}$, (assigned to hyperfine interactions of the cyclopentadienyl ring protons); between 8.3 and 20.5 MHz, for **1**$^{\bullet}$, between 1.9 and 20.5 MHz for **11**$^{\bullet}$and **12**$^{\bullet}$, (assigned to hyperfine interactions of the cycloheptatrienyl ring protons). Differences noted between the spectra may be attributed mainly to variations in the experimental conditions (e.g., experimental parameters, freezing of the solution). In the spectrum of **12**$^{\bullet}$, the frequency range below 1.5 MHz shows a structure that is an instrumental disturbance.

Applying the ENDOR selection rules $\Delta M_I = \pm 1$, $\Delta M_S = 0$, two ENDOR transitions at the frequencies $\nu_{ENDOR} = |\nu_D \pm a/2|$ are obtained.[58] Taking into account the ratio (6.51) of the gyromagnetic moment from hydrogen (267.51 MHz/T)) and deuterium (41.06 MHz/T), one can easily calculate the deuterium ENDOR transitions for the deuterium substituents in the five and the seven-membered ring. Quadrupole couplings are not resolved. Calculated values for the five-membered ring: 1.75 MHz, 2.65 MHz; measured values: 1.8 MHz, 2.65 MHz.

Calculated values for the seven-membered ring: 1.3 MHz, 3.1 MHz; measured values: 3.15 MHz, the value in the range of 1 MHz could not be obtained because of the lower limit of the spectrometer.

Both, **11**$^{\bullet}$ and **12**$^{\bullet}$, show two deuterium signals, thereby confirming the scrambling reaction postulated above, which would lead to a dismutation of mono-lithiotrovacene to trovacene and 1,1'-di-lithiotrovacene. Hence, the ENDOR results confirm also the results obtained from mass spectroscopy (see Table **2** in Section 2). Moreover, during the long accumulation time (1 h) no decrease of the deuterium signal was observed, confirming that no H/D exchange occurs.

3. Determination of the Structure of (η^7-Cycloheptatrienyl)(η^5-cyclopentadienyl)-vanadium, $1^\bullet$ and (η^7-Cycloheptatrienyl)(η^5-pentamethylcyclopentadienyl)-vanadium, $2^\bullet$

3.1 Structure of (η^7-Cycloheptatrienyl)(η^5-cyclopentadienyl)vanadium, $1^\bullet$

The first low precision determination of the structure of trovacene, **$1^\bullet$** (present discrepancy factor, R= 9.6%) was published in 1963.[61] In the present work, a redetermination of the unsymmetric sandwich complex was undertaken in order to improve the low accuracy of the original determination, which did not allow for a precise discussion of structural parameters.
Crystals suitable an X-ray crystallographic determination were grown by sublimation as violet hexagonal plates.
Crystals are orthorhombic with space group Pnma; lattice constants *a*= 10.8759(8) Å; *b*= 10.6309(11) Å; *c*= 7.8759(6) Å. In the adopted centrosymmetric space group Pnma, having a eightfold general position, the molecule must occupy a special position in the unit cell, as Z=4.

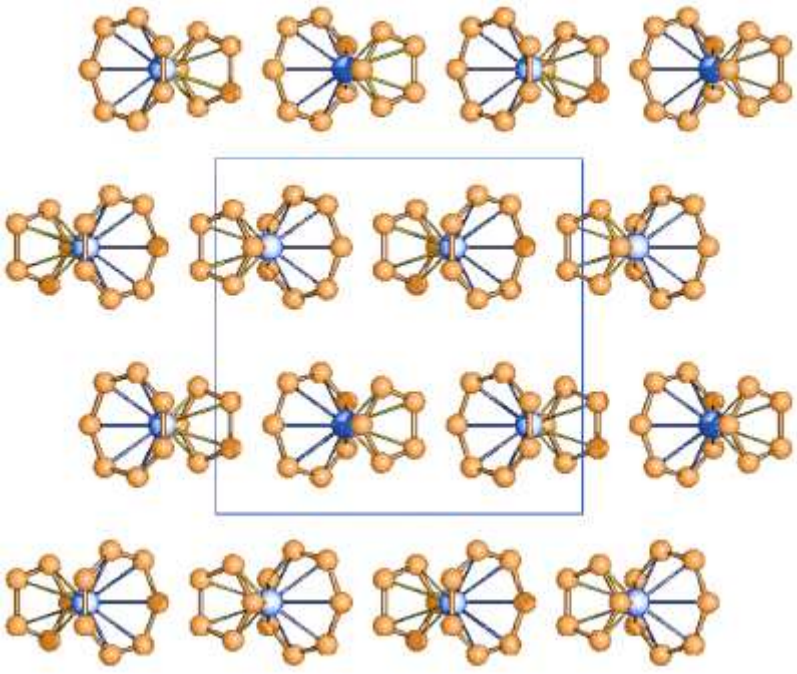

Fig.**8**: **$1^\bullet$** view down the c-axis.

The rings are bisected by a mirror plane, which passes through one apex carbon atom of each ring. The carbon atoms bisected by the mirror plane are syn-periplanar.

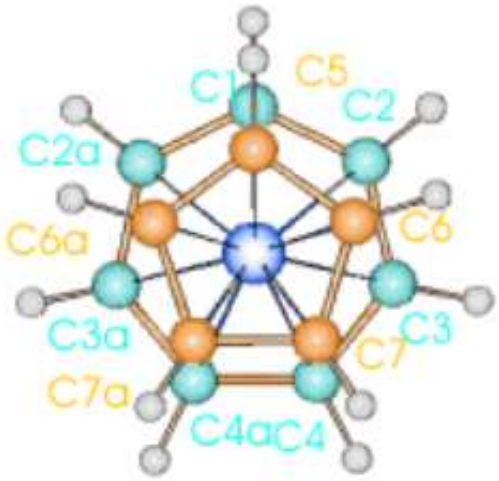

Fig.**9**: Projection of **1**• perpendicular to the molecular axes.

V(1)–C(1)	2.1789(17)	V(1)–C(2)	2.1898(12)
V(1)–C(3)	2.1936(11)	V(1)–C(4)	2.1924(11)
V(1)–C(5)	2.2508(15)	V(1)–C(6)	2.2612(11)
V(1)–C(7)	2.2680(12)	V(1)–C(2a)	2.1899(12)
V(1)–C(3a)	2.1937(11)	V(1)–C(4a)	2.1925(11)
V(1)–C(6a)	2.2612(11)	V(1)–C(7a)	2.2680(12)
C(1)–C(2)	1.4157(15)	C(1)–C(2a)	1.4157(15)
C(2)–C(3)	1.4154(18)	C(2a)–C(3a)	1.4154(18)
C(3)–C(4)	1.4127(17)	C(3a)–C(4a)	1.4127(17)
C(4)–C(4a)	1.420(2)	C(5)–C(6)	1.4143(16)
C(6)–C(7)	1.4128(18)	C(7)–C(7a)	1.416(3)
C(5a)–C(6a)	1.4143(16)	C(6a)–C(7a)	1.4128(18)

Table **3:** Selected bond lengths (Å) for **1**•.

C(3)–C(2)–C(1)	128.51(11)	C(4)–C(3)–C(2)	128.68(11)
C(5)–C(6)–C(7)	107.95(11)		

Table **4:** Selected bond angles (deg) for **1**•.

The average V-C distances for the five-membered and in the seven-membered ring amount to 2.211(3) and 2.190(5) Å, respectively. Accordingly, the distance from the metal to the ring centers differ in that larger rings are approached more closely by the metal. This situation

leads to the relatively poor metal-ligand orbital overlap, so that centrosymmetric bonding of a first row transition metal to a large ring is less favourable than to a smaller ring. No significant differences have been observed between the mean C-C bond lengths of both rings (1.414(2) and 1.415(2) Å for the five-membered and the seven-membered ring, respectively). The hydrogen atoms of the cycloheptatrienyl ring are bent towards the central metal, as it can be also observed in metal arenes such as bis(benzene)chromium.[62]

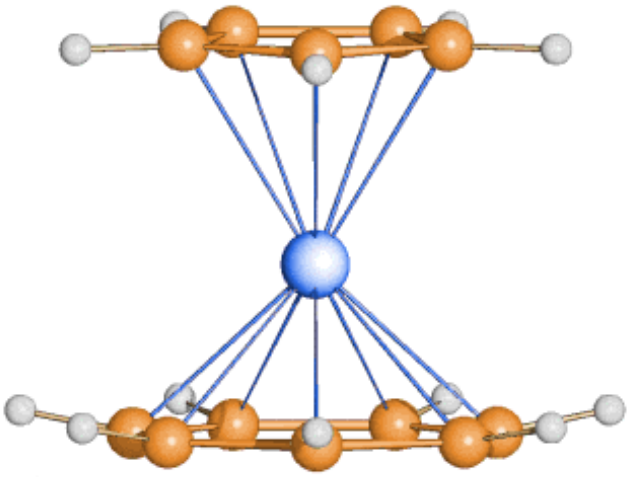

Fig.**10**: Bending of the hydrogen substituents of the seven-membered ring toward the vanadium central metal.

3.2 Structure of (η^7-Cycloheptatrienyl)(η^5-pentamethylcyclopentadienyl)vanadium, 2•

(η^7-Cycloheptatrienyl)(pentamethyl-η^5-cyclopentadienyl)vanadium, **2•** crystallizes from a petroleum ether solution at –20°C in form of violet needles.

Crystals are orthorhombic with space group Pnma; lattice constants *a*= 1021.1(1) pm; *b*= 1261.5(1) pm; *c*= 1103.1(1) pm; with four molecules per unit cell. The vanadium atom is located on a crystallographic mirror plane, which bisects the two aromatic rings. However, the carbon atom of the five-membered ring, C(5), and of the seven-membered ring, C(1), which are bisected by the mirror plane, are trans to one another. This situation is opposite to the conformation found for trovacene, in which the carbon atoms on the mirror plane are syn-periplanar. Hence, the increased steric demand of the methyl substituents in **2•** results in an anti-periplanar conformations.

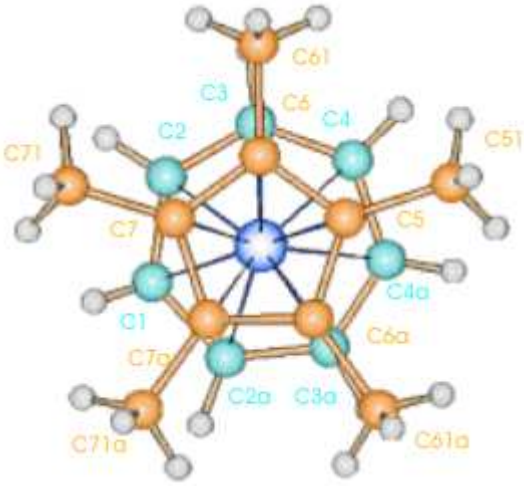

Fig.**11**: Projection of **2**• perpendicular to the molecular axes.

V(1)–C(1)	2.179(3)	V(1)–C(2)	2.181(2)
V(1)–C(3)	2.183(2)	V(1)–C(4)	2.195(2)
V(1)–C(5)	2.247(2)	V(1)–C(6)	2.251(2)
V(1)–C(7)	2.261(2)	C(1)–C(2)	1.420(3)
C(2)–C(3)	1.404(4)	C(3)–C(4)	1.393(4)
C(5)–C(6)	1.420(2)	C(6)–C(7)	1.423(2)
C(5)–C(51)	1.507(3)	C(6)–C(61)	1.501(2)
C(7)–C(71)	1.495(2)	C(7)–C(7a)	1.427(3)
C(1)–H(1)	0.86(5)	C(2)–H(2)	0.97(3)
C(3)–H(3)	1.01(3)	C(4)–H(4)	0.94(3)
C(51)–H(511)	0.95(4)	C(51)–H(512)	0.98(3)
C(61)–H(611)	0.98	C(61)–H(612)	0.98
C(61)–H(613)	0.98	C(71)–H(711)	0.98
C(71)–H(712)	0.98	C(71)–H(713)	0.98

Table **5:** Selected bond lengths (Å) for **2**•.

C(1)–C(2)–C(3)	127.9(2)	C(3)–C(4)–C(4a)	128.4(2)
C(5)–C(6)–C(7)	107.9(1)	C(6)–C(5)–C(51)	125.8(1)
C(7)–C(6)–C(61)	125.6(2)	C(6)–C(7)–C(71)	126.6(2)

Table **6:** Selected bond angles (deg) for **2**•.

As expected, the two ligand planes are essentially parallel (angle of Tr plane to Cp^* plane is 3°). The average distances of the vanadium atom to the carbon atoms of the cycloheptatrienyl- and Cp*-ring are 2.185(7) and 2.254(6) Å, respectively. The virtual identity of the average carbon-vanadium bond distances for the Cp ligand in **1**• and **2**• despite the higher steric

demand of the Cp* ligand may be attributed to a very small structural trans effect, indicating the tighter bonding of the more electron-rich Cp* ligand. The static structural differences in M-Cp and M-Cp* bonding should reflect related electronic differences in M-Cp and M-Cp* interactions. By a comparison of the free ligands Cp^- and Cp^{*-}, the consequences of the pentamethyl substitution upon the relevant π-MOs of Cp^- is shown in Schema **1**.[63]

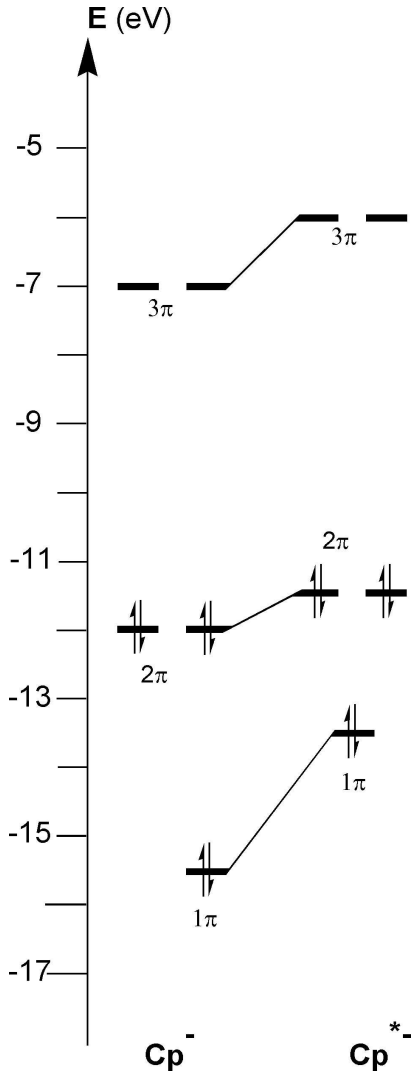

Schema **1**: π-MOs of the free ligands Cp^- and Cp^{*-}.[63]

All π-levels are destabilized significantly for Cp^{*-}, and this must lead to non equivalent metal-ring interactions for V-Cp* vs V-Cp. The π-orbitals of Cp^{*-} to a certain extent are delocalized over the five methyl groups. As the main bonding interaction between the metal and the ring comes from the interaction of d_{xz} and d_{yz} with the 2π set of the cyclic ligands, the higher lying and thus much better π-donor levels 2π of Cp^{*-} causes a stronger bonding from the metal to

the carbon atoms of the pentamethyl substituted ring and, the weaker donating Cp^- ligand keeps more of its electron density in its 2π-level set.

In conclusion, the new electronic and steric environment created by the Cp* moiety does not greatly effect the overall structure.

4. Aldehydes and Carboxylic Acids of (η^7-Cycloheptatrienyl)(η^5-cyclopentadienyl)vanadium, **1$^\bullet$** and (η^7-Cycloheptatrienyl)(η^5-pentamethylcyclopentadienyl)vanadium, **2$^\bullet$**

Whereas the study of intramolecular electron transfer requires highly sophisticated techniques of time resolved spectroscopy, intramolecular communication, namely spin exchange interaction in biradicals, can be explored by measuring the exchange coupling constant J via EPR.[64]

A structural unit that plays an important role in electron transfer pathway in non-covalently linked proteins and in photosynthetic models is the hydrogen bond. Organometallic molecules bonded by hydrogen bonds have been widely studied in recent years.[65]

The synthesis of paramagnetic organometallic aldehydes and carboxylic acids permits to combine the two seemingly unrelated fields, in order to study electron-electron spin-spin exchange in the dimers formed by hydrogen bridge interactions.

For this purpose, as a supplement to the previously prepared mono-aldehyde[49] and mono-carboxylic acid[50] of **1$^\bullet$**, in which the functional groups had been introduced into the Cp ligand, in the present work the dicarboxylic acid, **13$^\bullet$**, and the bis-aldehyde of **1$^\bullet$**, **14$^\bullet$**, have been prepared. Furthermore, the mono-carboxylic acid, **15$^\bullet$**, and the mono-aldehyde, **16$^\bullet$,** derivatives of **2$^\bullet$**, bearing the respective functional group in the seven-membered ring have been synthesized. All new compounds have been studied by EPR spectroscopy and cyclic voltammetry, and **13$^\bullet$** and **16$^\bullet$** have been further characterized by X-ray diffraction.

4.1 Synthesis of (Carboxy-η^7-cycloheptatrienyl)(carboxy-η^5-cyclopentadienyl)vanadium, [(η^7-C_7H_6COOH)(η^5-C_5H_4COOH)V^0], 13$^\bullet$, and (Formyl-η^7-cycloheptatrienyl)(formyl-η^5-cyclopentadienyl)vanadium, [(η^7-C_7H_6CHO)(η^5-C_5H_4CHO)V^0], 14$^\bullet$

(Carboxy-η^7-cycloheptatrienyl)(carboxy-η^5-cyclopentadienyl)vanadium, **13$^\bullet$**, was synthesized by dilithiation of **1$^\bullet$** in ether solution with *n*-BuLi and TMEDA.

CO_2 was bubbled through the solution containing the 1,1'-dilithiated product. Finally, the free dicarboxylic acid was obtained by hydrolysis with dilute aqueous HCl. **13$^\bullet$** is obtained as clear-green powder, low soluble in almost organic solvents.

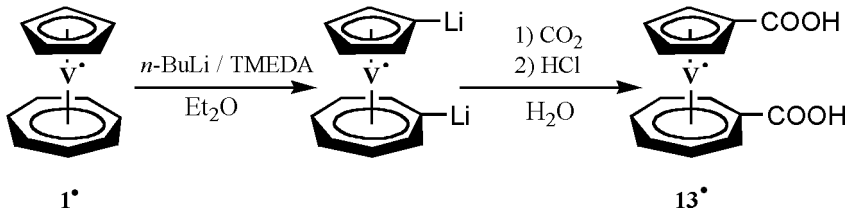

1• **13**•

(Formyl-η^7-cycloheptatrienyl)(formyl-η^5-cyclopentadienyl)vanadium, **14**•, was synthesized by dilithiation of **1**• in ether solution with *n*-BuLi and TMEDA followed by addition of dimethylformamide, and hydrolysis with dilute aqueous HCl. **14**• is obtained as a dark-green solid, very good soluble in organic solvents.

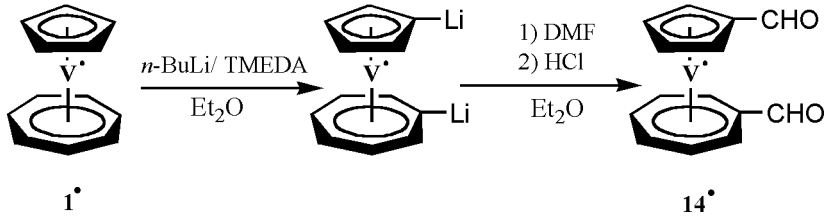

1• **14**•

4.2 Synthesis of (Carboxy-η^7-cycloheptatrienyl)(η^5-pentamethylcyclopentadienyl)-vanadium, [(η^7-C_7H_6COOH)(η^5-C_5Me_5)V^0], 15•, and (Formyl-η^7-cycloheptatrienyl)(η^5-pentamethylcyclopentadienyl)vanadium, [(η^7-C_7H_6CHO)(η^5-C_5Me_5)V^0], 16•

The metallation of **2**• proved to be quite difficult: no reaction is observed with the common deprotonanting agent *n*-butyllithium in diethyl ether or in petroleum ether as solvent, neither in presence nor in absence of TMEDA as metal chelating co-solvent. In contrast to **1**•, where these metalating agents are sufficiently basic to effect mono- or di-metallation, in this case stronger bases are necessary, due to the donor effect of the five methyl groups. Deprotonation of **2**• was finally achieved under employment of a mixture of *n*-butyllithium and potassium-*t*-butoxide as superbase.[66]

15•, was synthesized by regioselective lithiation in the seven-membered ring of **2**• by use of a mixture of TMEDA, K-*t*-butoxide and *n*-BuLi in petroleum ether solution. CO_2 was subsequently bubbled through the solution containing the mono-lithiated product. Finally, the

free mono-carboxylic acid was obtained by hydrolysis with dilute aqueous HCl. **15•** is obtained as clear-green powder, low soluble in almost organic solvents.

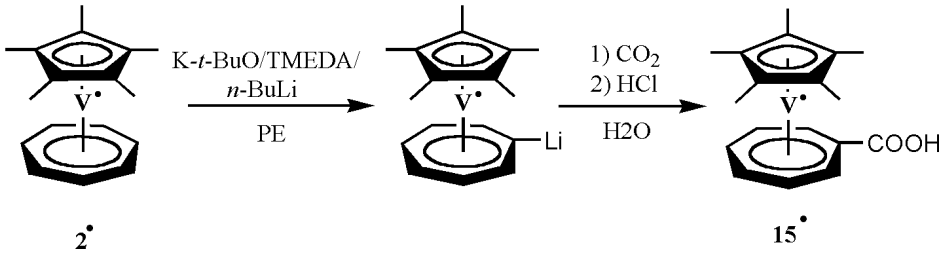

2• **15•**

16•, was synthesized analogously by selective mono-lithiation of **2•**, followed by addition of dimethylformamide, and hydrolysis with dilute aqueous HCl. **16•** is obtained as a dark-green solid, very good soluble in organic solvents.

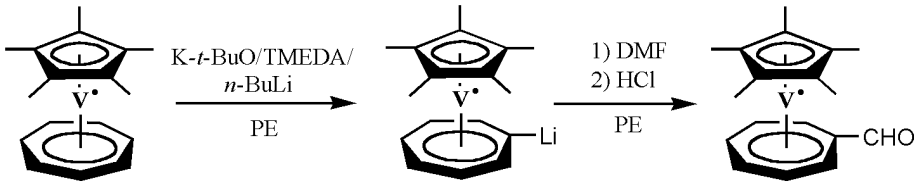

2• **16•**

The pentamethylation of Cp ring is a chemical modification of the complex that perturbs the electronic structure, and thereby provides much information on the orbital character and sensitivity. The pentamethyl derivatives of trovacene exhibit altered crystallization characteristics and increased solubility.

4.3 Structure of (Carboxy-η^7-cycloheptatrienyl)(carboxy-η^5-cyclopentadienyl)vanadium, 13•

Crystals were obtained by suspension of the crude product in water, followed by addition of dilute aqueous NaOH. The solution was then layered with ether containing HBF_4.

Crystals are monoclinic with space group $P2_1/c$; lattice constants *a*= 6.9723(14) Å; *b*= 7.8419(16) Å; *c*= 21.642(4) Å; with four molecules per unit cell. The molecular structure of one of the dimers in the unit cell is presented in Fig. **12**, while the packing of the molecules inside the unit cell is displayed in Fig. **13**.

The hydrogen bonds of the two carboxylic groups give rise to strong intermolecular forces and are limiting the thermal motion of the molecule. Two molecules related by a center of symmetry form a hydrogen bonding dimer. The formation of these dimers appears to influence strongly many features of the molecular geometry and crystal packing. The unit cell contains two crystallographically independent dimers, which for their part are each linked by hydrogen bonds between the carboxylic groups.

Both, the oxygen of the C=O and that of the H-O group can serve as acceptor, with hydrogen bond distance values of: O(1)---O(4) 2.618(14) Å, and O(2)---O(3) 2.573 Å. The carbon oxygen distances within the carboxylate substituents are almost equal, indicating a virtually completely delocalised system.

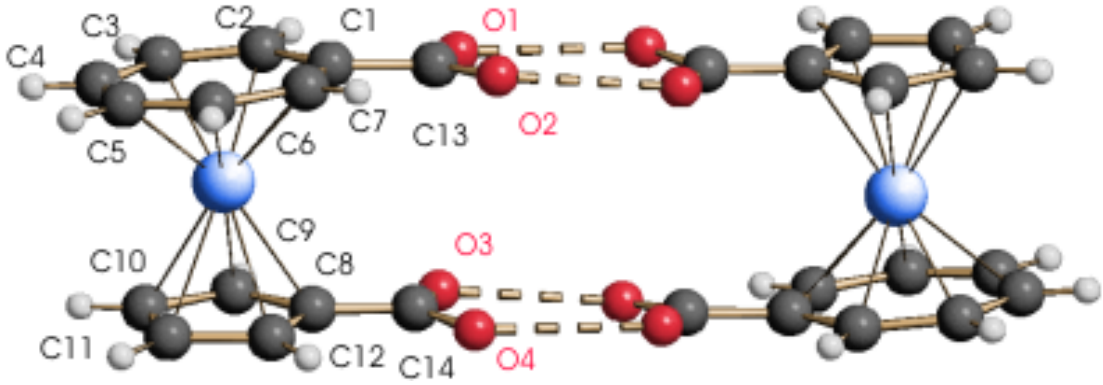

Fig.**12**: Representation of the dimer formed by molecules of **13**$^{\bullet}$ in the solid state. The dimer contains a center of inversion.

Both trovacene units of the hydrogen bonded dimer adopt an almost perfectly eclipsed configuration with both planar and parallel rings. The two carboxylic groups and the attached ring carbon atoms are planar but are twisted slightly with respect to the corresponding ring. The angle between the plane of C(13)-O(1)-O(2) and the ring to which it is connected 122.4(12)°, while the corresponding angle for C(14)-O(3)-O(4) is 123.9°. The large twist for the C(14) carboxylic group appears to be related to crystal packing forces. Both carboxylic groups are bent slightly out of the plane of the rings towards each other.

The vanadium atom is centered between the arene rings. The average V-C distance is 2.254(9) Å to the five-membered ring, and 2.177(13) Å to the seven-membered ring. Hence, there is virtually no difference in comparison to the respective average distances in **1•**. Apparently, the electronic modification due to the introduction of the carboxylate substituents remains without influence on the strengths of the arene-metal bonds.

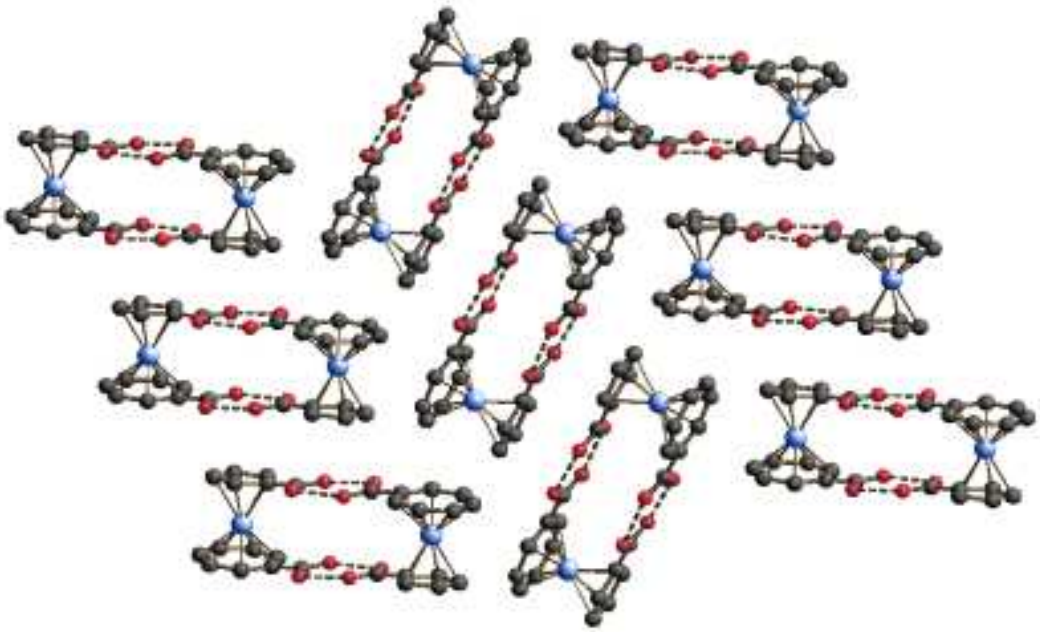

Fig.**13**: **13•** view down the c-axis.

V(1)–C(1)	2.167(11)	V(1)–C(2)	2.198(12)
V(1)–C(3)	2.178(12)	V(1)–C(4)	2.184(13)
V(1)–C(5)	2.169(13)	V(1)–C(6)	2.168(14)
V(1)–C(7)	2.174(14)	V(1)–C(8)	2.244(8)
V(1)–C(9)	2.274(9)	V(1)–C(10)	2.277(9)
V(1)–C(11)	2.248(9)	V(1)–C(12)	2.227(9)
C(1)–C(2)	1.433(16)	C(1)–C(7)	1.464(17)
C(1)–C(13)	1.492(17)	C(2)–C(3)	1.399(17)
C(3)–C(4)	1.351(19)	C(4)–C(5)	1.382(18)
C(5)–C(6)	1.392(17)	C(6)–C(7)	1.40(2)
C(8)–C(9)	1.4200	C(8)–C(12)	1.4200
C(8)–C(14)	1.442(14)	C(9)–C(10)	1.4200
C(10)–C(11)	1.4200	C(11)–C(12)	1.4200
C(13)–O(1)	1.282(14)	C(13)–O(2)	1.251(15)
C(14)–O(3)	1.275(15)	C(14)–O(4)	1.263(15)

Table **7:** Selected bond lengths (Å) for **13•**.

C(2)–C(1)–C(7)	126.7(12)	C(3)–C(2)–C(1)	126.9(13)
C(4)–C(3)–C(2)	131.6(14)	C(3)–C(4)–C(5)	128.8(13)
C(4)–C(5)–C(6)	129.2(14)	C(5)–C(6)–C(7)	129.0(14)
C(6)–C(7)–C(1)	127.7(13)	C(9)–C(8)–C(12)	108.0
C(10)–C(9)–C(8)	108.0	C(10)–C(11)–C(12)	108.0
C(11)–C(10)–C(9)	108.0	C(11)–C(12)–C(8)	108.0
C(2)–C(1)–C(13)	117.3(12)	C(7)–C(1)–C(13)	115.7(12)
C(9)–C(8)–C(14)	125.9(8)	C(12)–C(8)–C(14)	125.8(8)
O(2)–C(13)–O(1)	122.4(12)	O(2)–C(13)–C(1)	118.7(12)
O(1)–C(13)–C(1)	118.9(13)	O(4)–C(14)–O(3)	123.9(12)
O(4)–C(14)–C(8)	118.1(11)	O(3)–C(14)–C(8)	117.9(12)

Table **8:** Selected bond angles (deg) for **13**•.

4.4 Structure of (Formyl-η^7-cycloheptatrienyl)(η^5-pentamethylcyclopentadienyl)-vanadium, 16•

(Formyl-η^7-cycloheptatrienyl)(pentamethyl-η^5-cyclopentadienyl)vanadium, **16**•, crystallizes from a petroleum ether/diethyl ether solution at –20°C in form of green-brown needles.

Crystals are orthorhombic with space group Pnma; lattice constants *a*= 1061.7(1) pm; *b*= 1248.5(1) pm; *c*= 1115.5(1) pm; with four molecules per unit cell. As for the structure of the parent molecule **2**•, in **16**• no equivalent vanadium-ligand distances are observed, (average value for V-C(Cp*): 2.251(2) Å; average value for V-C(Tr): 2.190(3) Å). Again, these average vanadium-carbon distances are identical within the margins of error to those observed in the structure of **2**•, and **15**•, indicating the inertness of the trovacene framework from electronic effect of substituents. The structure is isotypical to that of **2**•, bearing one formyl function.

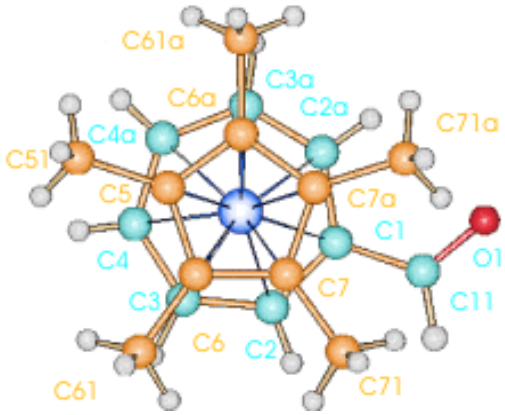

Fig.**14**: Projection of **16**• perpendicular to the molecular axis.

The complex resides on a crystallographic mirror plane containing the vanadium atom and bisecting both aromatic rings. For this reason the C(O)H-function is disordered equally over two positions (thermal ellipsoid 20%).

V(1)–C(1)	2.186(3)	V(1)–C(2)	2.179(2)
V(1)–C(3)	2.204(3)	V(1)–C(4)	2.192(3)
V(1)–C(5)	2.249(3)	V(1)–C(6)	2.250(2)
V(1)–C(7)	2.254(2)	O(1)–C(11)	1.252(8)
C(1)–C(2)	1.428(3)	C(1)–C(11)	1.452(6)
C(2)–C(3)	1.397(4)	C(3)–C(4)	1.408(4)
C(4)–C(4a)	1.406(6)	C(5)–C(6)	1.426(3)
C(6)–C(7)	1.424(3)	C(7)–C(7a)	1.429(5)
C(6)–C(61)	1.499(3)	C(7)–C(71)	1.499(3)
C(2)–H(2)	0.92(3)	C(3)–H(3)	1.02(4)
C(4)–H(4)	0.91(3)	C(11)–H(11)	0.96(8)
C(51)–H(151)	0.92(5)	C(51)–H(152)	0.92(3)
C(61)–H(161)	0.98	C(61)–H(162)	0.98
C(61)–H(163)	0.98	C(71)–H(171)	0.98
C(71)–H(172)	0.98	C(71)–H(173)	0.98

Table **9:** Selected bond lengths (Å) for **16•**.

C(2)–C(1)–C(2a)	126.3(3)	C(2)–C(1)–C(11)	116.4(2)
C(1)–C(2)–C(3)	129.6(2)	C(3)–C(4)–C(4a)	129.0(3)
C(2)–C(3)–C(4)	128.1(3)	C(5)–C(6)–C(7)	108.1(2)
C(6)–C(5)–C(51)	126.0(1)	C(6)–C(5)–C(6a)	107.9(2)
C(51)–C(5)–C(6a)	126.0(1)	C(5)–C(6)–C(61)	125.8(2)
C(7)–C(6)–C(61)	126.1(2)	C(6)–C(7)–C(71)	126.6(2)
C(6)–C(7)–C(7a)	107.9(2)	C(71)–C(7)–C(7a)	125.4(2)
O(1)–C(11)–C(1)	122.8(4)	O(1)–C(11)–H(11)	120.(6)
O(1)–C(11)–H(11a)	10.(6)	O(1a)–C(11)–H(11a)	120.(6)

Table **10:** Selected bond angles (deg) for **16•**.

Similar to the analoguous molecule (η^7-cycloheptatrienyl)(formyl-η^5-cyclopentadienyl)-vanadium, [(η^7-C_7H_7)(η^5-C_5H_4CHO)V^0], **17•**,[49] no hydrogen bonding exist between the formyl groups of adjacent molecules. However, intermolecular hydrogen contact interactions were found between the formyl oxygen atoms and methyl protons of neighboring molecules, indicated by an underrun of the sum of van der Waals radii: C(71)-H(173)---O(1) 2.39 Å (C-H not normalized).

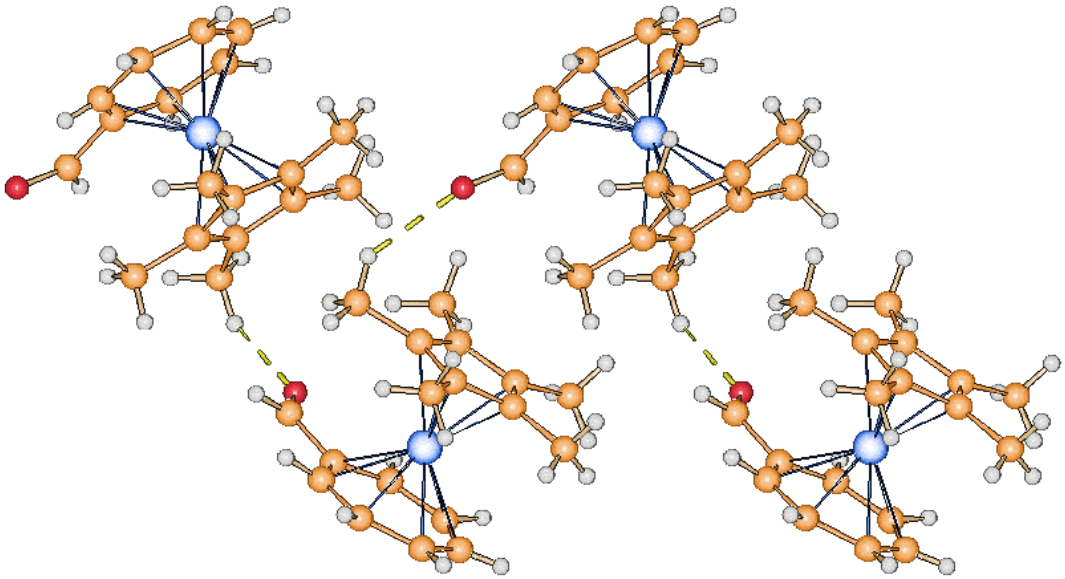

Fig.**15**: Intermolecular hydrogen bonding in **16**$^{\bullet}$ (only one of the two disorder images is shown).

As expected, the two ligand planes are essentially parallel (angle of cycloheptatrienyl plane to Cp* plane is 2°). The angle of Cp plane to C(O)H plane amounts to 14°.

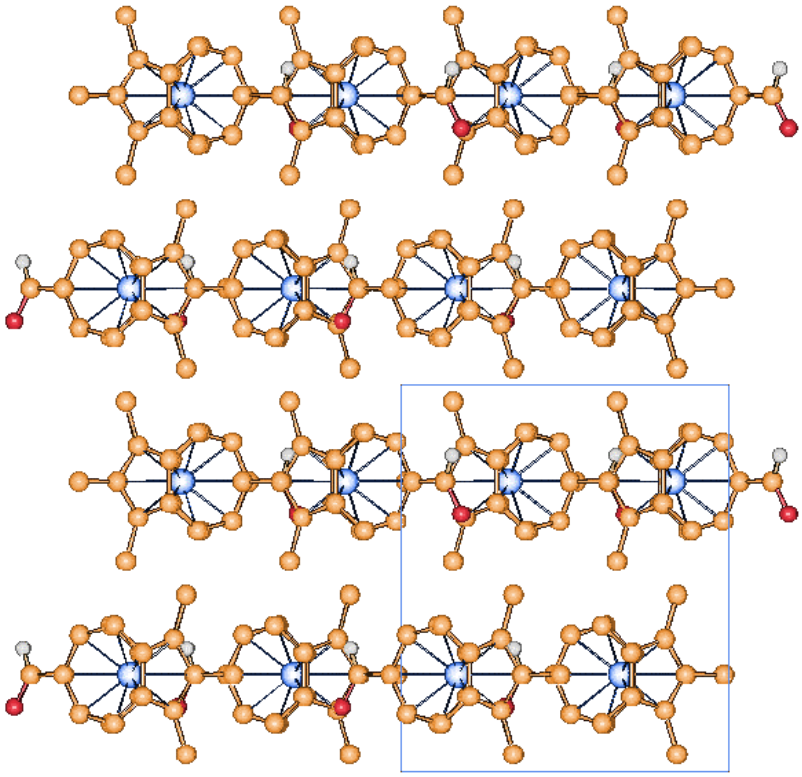

Fig.**16**: **16**$^{\bullet}$ view down the c-axis (only one of the two disorder images is shown).

4.5 Cyclic Voltammetry of $13^{\bullet}$, $14^{\bullet}$, $15^{\bullet}$, $16^{\bullet}$

4.5.1 Fundamentals of Cyclic Voltammetry[67]

Cyclic Voltammetry is used to characterize the redox properties of compounds and to study their redox reactions. In cyclic voltammetry the potential of a small, stationary working electrode, which is immersed in an unstirred solution, is changed linearly with time starting from a potential where no electrode reaction occurs and moving to potential where reduction or oxidation of a solute (the material being studied) sets in. A supporting electrolyte is present to repress migration of charged reactants and products (in this case tetrabutylammonium salt was used). The voltage applied to the working electrode is scanned linearly from an initial value, E_i, to a predetermined limit (known as the switching potential, E_λ) where the direction of the scan is reversed. The potential of this working electrode is controlled versus a reference electrode such as a saturated calomel electrode (SCE) or a silver/silver chloride electrode (Ag/AgCl). A cyclic voltammogram is obtained by measuring the current at the working electrode during the potential scan. The voltammogram is a display of current (vertical axis) versus potential (horizontal axis).

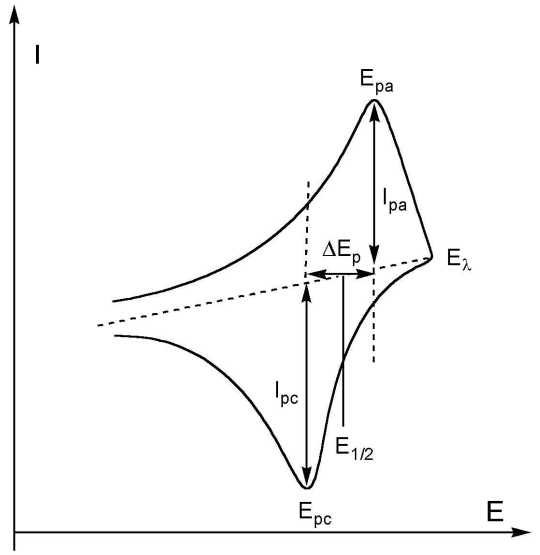

Definition of the parameters:

E_{pa}, E_{pc}= anodic and cathodic peak potentials

$E_{1/2}$= half-wave potential

I_{pa}, I_{pc}= anodic and cathodic peak currents

ΔE_p= peak separation

E_λ= switching potential

Fig.**17**: Schematic representation of a cyclic voltammogram, and definition of the parameters.

By examination of these parameters, the electron transfer process can be assigned to one of the three categories: reversible, quasi-reversible, irreversible reactions. Decisive for the

electrochemical reversibility is the rate of heterogeneous electron transfer at the electrode surface given by k_s (standard heterogeneous electron transfer rate constant).

a) Reversible process

$k_s > 2 \cdot 10^{-2}$ cm/s: the electron transfer process is faster than the diffusion.

The reaction is diffusion-controlled (no other processes limit the current). The criteria for diffusion control is that I_{pc} increases with $v^{1/2}$ (v is the sweep rate, dE/dt) and is directly proportional to the concentration. The electron transfer reaction at the electrode surface is so rapid that equilibrium conditions are maintained even with a substantial net current and a rapidly changing potential. The criteria of reversibility are $\Delta E_p = E_{pa} - E_{pc} = 57/n$ mV at 298 K, where n is number of electrons transferred per ion (equivalent/mol), values which must be independent of scan rate and concentration. The $E_{1/2}$ value is situated exactly (within 2/n mV) midway between E_{pa} and E_{pc}. The values of I_{pa} and I_{pc} should be identical for a simple reversible (fast) couple, that is $I_{pa}/I_{pc} = 1$.

b) Quasi-reversible process

$2 \cdot 10^{-2}$ cm/s $> k_s > 5 \cdot 10^{-5}$ cm/s: the rate of the electron transfer process is equal to that of the diffusion.

The rate of electron transfer and diffusion are comparable. The peak separation ΔE_p of a quasi-reversible process increases with $v^{1/2}$. The values of I_{pa} and I_{pc} should be identical, that is $I_{pa}/I_{pc} = 1$. I_{pa} and I_{pc} are not proportional to $v^{1/2}$.

c) Irreversible process

$k_s > 5 \cdot 10^{-5}$ cm/s: the electron transfer process is slower than the diffusion.

Electrochemical irreversibility is caused by slow electron exchange of the redox species with the working electrode. Irreversibility manifest itself through $\Delta E_p > 57/n$ mV at 298 K, ΔE_p increasing with increasing v, and it is characterized by a separation of peak potentials greater than indicated by the expression $\Delta E_p = E_{pa} - E_{pc} \cong 0{,}059/n$.

4.5.2 Results

The 17-VE-complex trovacene, **1**$^{\bullet}$, exhibits in its crystalline phase air stability of a few minutes.[68] This property is confirmed by the cyclovoltammetry experiment, indicated by a redox potential $E_{1/2}^{(+/0)}$ of 0.26 V, [vs. 0.54 V of ferrocene, **7**, a sandwich complex stable to

air] (these values have been measured in DME/0.1 M TBAP; T=–40 °C; ν= 100 mV/s; glassy carbon electrode vs. SCE). Neutral trovacene possesses the ground state configuration $[(e_2)^4(a_1)^1(e_1)^0]$, while the cationic form has the low spin configuration $[(e_2)^4(a_1)^0(e_1)^0]$. The e_2-orbitals are so low in energy, that the configuration $[(e_2)^4]$ is more favorable also in the ionized state. The introduction of electron-withdrawing substituents on the rings of trovacene causes a reduction of the electron density at the central metal. In consequence, the effective positive charge at the vanadium atom increases, resulting in a contraction of the essentially non-bonding a_1 (V-3d_z^2) redox orbital and in a stronger binding of the occupying electron. Therefore, the oxidation becomes more difficult and an anodic shift of the redox potential is observed. Similar to the parent molecule trovacene, the derivatives (carboxy-η^7-cycloheptatrienyl)(carboxy-η^5-cyclopentadienyl)vanadium, **13**$^\bullet$, and (formyl-η^7-cycloheptatrienyl)(formyl-η^5-cyclopentadienyl)vanadium, **14**$^\bullet$ show a second oxidation wave (2+/+), that is irreversible for all complexes (the species formed has not been identified so far). Trovacene is reversibly reduced to the mono-anion at –2.55 V: the transferred electron will occupy the metal dominated a_{1g}-orbital. The derivatives **13**$^\bullet$ and **14**$^\bullet$ are reduced also, but more readily. This effect is explained by the increase of stability of the a_{1g}-orbital, due to the presence of the electron-withdrawing substituents. It has to be noted, that the anodic shifts of the oxidation steps to the monocations are smaller than the shifts of the corresponding reduction steps to the monoanions. Hence, a transfer of an electron into a ligand-centered LUMO would also be conceivable, resulting in the formation of a paramagnetic biradical species. This explanation may be adopted also for the second reduction of the formyl complexes. The π-bonded arene ring bearing a carbonyl substituent has the ability to stabilize an electron transferred into a ligand-centered LUMO by delocalization. Due to the low energy and the corresponding higher electron affinity of this ligand-centered LUMO, a further reduction of the previously formed monoanion would be facilitated.

Cyclovoltammetric data for (carboxy-η^5-cyclopentadienyl)(η^7-cycloheptatrienyl)vanadium,[25] **6**$^\bullet$, (carboxy-η^7-cycloheptatrienyl)(carboxy-η^5-cyclopentadienyl)vanadium, **13**$^\bullet$, (formyl-η^5-cyclopentadienyl)(η^7-cycloheptatrienyl)vanadium,[49] **17**$^\bullet$, (formyl-η^7-cycloheptatrienyl)-(formyl-η^5-cyclopentadienyl)vanadium, **14**$^\bullet$, and for the parent molecule trovacene, **1**$^\bullet$, are shown in Table **11.** Typical cyclovoltammetric traces for **13**$^\bullet$ and **14**$^\bullet$ are depicted in Figs. **18-19**.

	1•	**6•**	**13•**	**17•**	**14•**
$E_{1/2}^{(+/0)}$ [V]	0.260	0.480	0.615 [c]	0.496	0.688
ΔE_p [mV] [a]	64	74	74	90	60
r= i_{pa}/i_{pc}	0.93	0.94	0.52	1	0.34
E_{pa} [V]	1.03	1.043 [b]	1.034	1.100	1.102
$E_{1/2}^{(0/-)}$ [V]	-2.55	-2.687	-2.554 [c]	-2.088	-1.843 [c]
ΔE_p [mV] [a]	66		88	96	66
r= i_{pa}/i_p	1		0.56	0.41	0.96
$E_{1/2}^{(-/2-)}$ [V] [c]				-2.499	-2.070
ΔE_p [mV] [a]				136	152
r= i_{pa}/i_p				0.30	0.86

[a] $\Delta E_p = (E_{pa} - E_{pc})$ [b] irreversible [c] the r values do not strictly confirm reversibility

Table **11**: Cyclovoltammetric data for **1•**, **6•**, **13•**, **17•**, **14•** measured in DME/0.1 M TBAP, vs. SCE, ν= 0.1 V/s, T=-40°C.

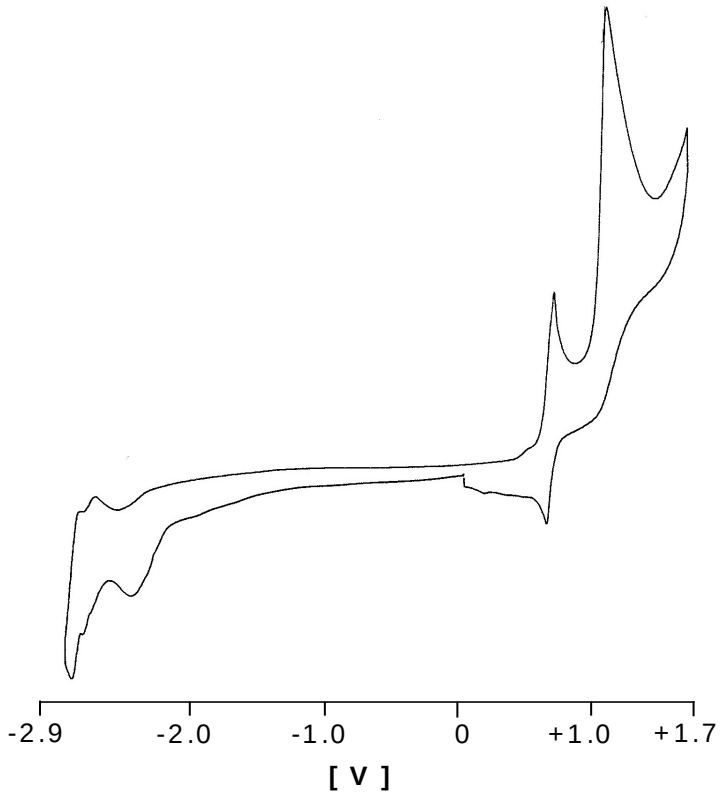

Fig.**18**: Cyclovoltammetric trace for **13•**.

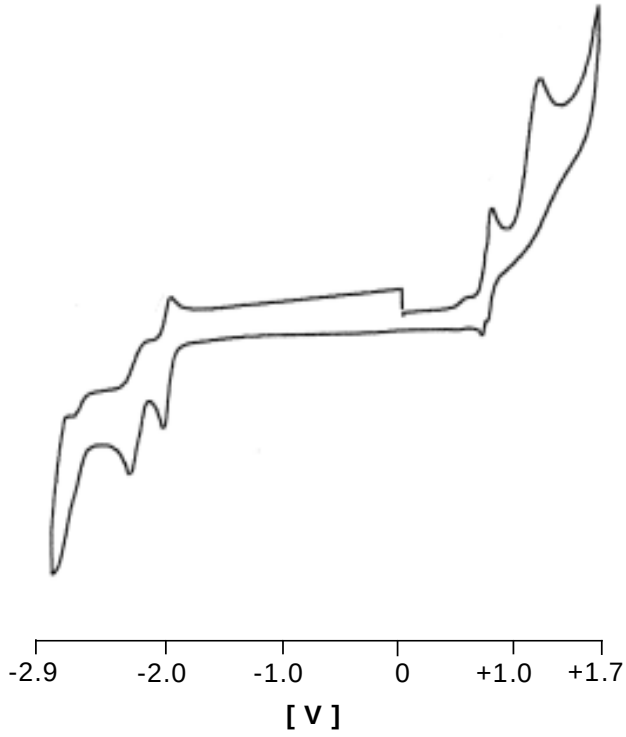

Fig.**19**: Cyclovoltammetric trace for **14**$^{\bullet}$.

The introduction of a second electron-acceptor group on the Tr ring of trovacene in **13**$^{\bullet}$ leads to more positive oxidation potential, higher also than that of ferrocene, **7**, amounting to 0.54 V. This observation explains why the new derivatives are stable to air. Tests to confirm this property were performed in solid state and in solution, by repeated X-ray diffraction of the crystals (in the case of the acid) stored without inert atmosphere over a period of two days, and by measuring the EPR spectrum of a solution of the complex which had been exposed to air.

By a comparison of the oxidation potentials of the mono- and di-substituted derivatives of **1**$^{\bullet}$ a trend in the anodic shift, which could provide the additive value per carboxy or formyl group introduced in the trovacene moiety was not recognized. However, it was noted that the anodic shift of the oxidation potential is more pronounced in the cases of formyl derivatives. In addition, it is evident that the introduction of the first acceptor group causes the major shift of the oxidation potential.

Comparing the function of cyclopentadienyl and cycloheptatrienyl as ligands, it is noted that in the free ligand the *e* levels are progressively stabilized with increasing ring size.[69] This has important consequences on their ability to bind to metals. It can be deduced, on grounds of the

energy separation, that the interaction of the e_1 orbitals with a metal is likely to decrease with increasing ring size, while that of the e_2 orbitals is likely to increase. Because of energy of the metal valence orbitals concerned is approximately intermediate between the e_1 and e_2 orbitals for the early transition metals, both the e_1 and e_2 molecular orbitals, will increase in ligand character with increasing ring size. When π-Cp is a ligand, interaction of the e_1 orbitals is the most important source of bonding, and as these orbitals are not fully occupied in the free ligand (the Cp radical), this interaction is able to remove charge from the metal. When π-cycloheptatrienyl is a ligand, its e_1 interaction with the metal is likely to be very small and chief source of bonding is the e_2 interaction. This theoretical consideration is supported by a systematic analysis of the species [M(η^m-C_mH_m) (η^n-C_nH_m)] (M= Ti, Cr, V; m, n= 5, 6, 7, 8) by photoelectronic-spectroscopy, which confirmed that the contribution of the ring to the e_2-MO's of sandwich complex increases with increasing ring size, while it decreases with increasing atomic number of the transition metal.[70]

The substitution of Cp for Cp* is one of the best known methods for increasing steric congestion at a metal center. This modification results also in increasing stability of reactive metal complexes and altering of their catalytic properties. The favorable properties of the Cp* ligand, such as increased electron donation, steric bulk, and enhanced solubility in comparison to the ubiquitous Cp ligand, are finding increasing use in organometallic chemistry.[71]

The ligand-field strength of the Cp ring is significantly enhanced by the complete replacement of the hydrogens with electron-donating methyl groups. The increased electron density, and donor strength of the permethylated ring reflects itself, for instance, in low oxidation potential.[72]

The influence of the introduction of Cp* into the trovacene framework has been studied by cyclic voltammetry measurements, demonstrating a cathodic shift of the redox potential relative to parent **1**$^{\bullet}$.

Cyclovoltammetric data for **15**$^{\bullet}$, **16**$^{\bullet}$, and for (η^7-cycloheptatrienyl)(pentamethyl-η^5-cyclopentadienyl)vanadium, **2**$^{\bullet}$ are shown in Table **12**. Typical cyclovoltammetric traces for the three compounds are depicted in Figs. **20**-**22**.

	2•	**15•**	**16•**
$E_{1/2}^{(+/0)}$ [V]	0.080	0.304	0.314
ΔE_p [mV] [a]	98	72	48
r= i_{pa}/i_{pc}	1	1	1
E_{pa} [V] [b]	1.232	1.294	1.430
$E_{1/2}^{(0/-)}$ [V]	-2.592	-1.723	-2.090
ΔE_p [mV] [a]	36	58	60
r= i_{pa}/i_p	0.96	0.45	1
$E_{1/2}^{(-/2-)}$ [V]		-2.504	-2.617
ΔE_p [mV] [a]			50
r= i_{pa}/i_p			1

[a] $\Delta Ep = (E_{pa} - E_{pc})$ [b] irreversible

Table **12**: Cyclovoltammetric data for **2•**, **15•**, **16•** measured in DME/0.1 M TBAP, vs. SCE, ν= 0.1 V/s, T=-40°C.

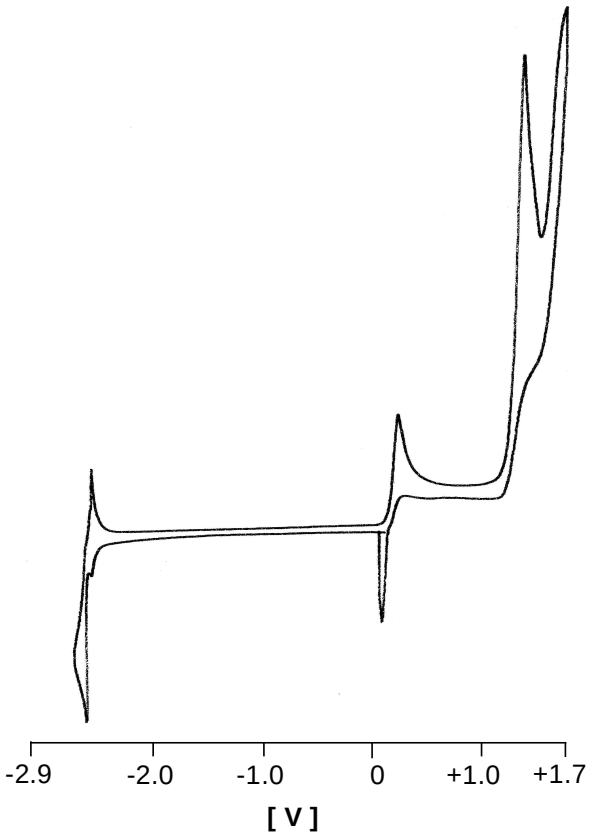

Fig.**20**: Cyclovoltammetric trace for **2•**.

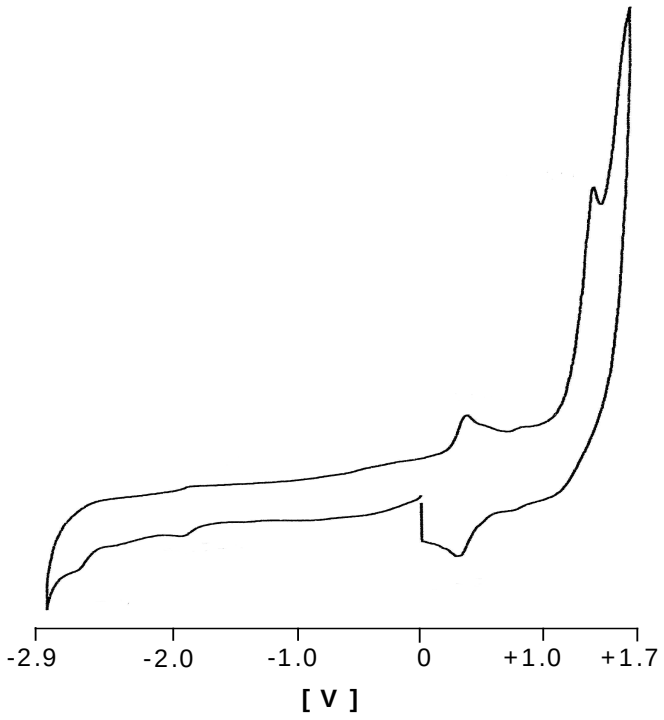

Fig.**21**: Cyclovoltammetric trace for **15**$^{\bullet}$.

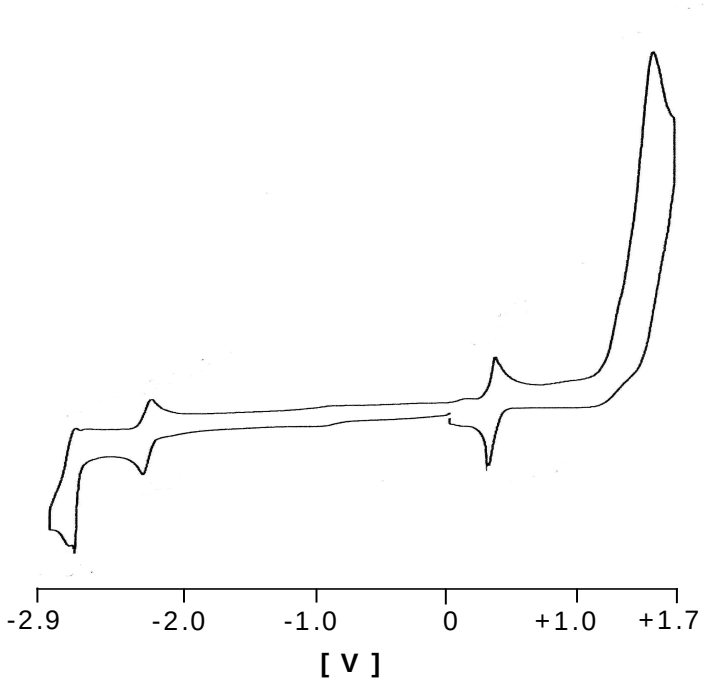

Fig.**22**: Cyclovoltammetric trace for **16**$^{\bullet}$

All complexes show a fully reversible oxidation step, and the carboxylic acid and formyl derivatives show an anodic shift due to the electron withdrawing character of the subtituent groups, as expected. For **16•**, as for all formyl derivatives, a further reduction of the formed anion is possible due to the increased electron affinity.

The effect of the transition from Cp to Cp* on the redox potential of the Fe(0)/Fe(+1) couple has been studied on a series of substituted ferrocenes.[73] In this study, a shift of the redox potential by –0.203 V due to the replacement of Cp by Cp* was determined. Moreover, it was revealed that the contributions of various substituents to the overall potential shift were additive.

Table **13** shows the increase of the redox potentials with increasing acceptor strength of the functional group attached to the (η^7-cycloheptatrienyl)(pentamethyl-η^5-cyclopenta-dienyl)vanadium moiety.

Substituent	$\mathbf{E_{1/2}^{(+/0)}}$ **of TVC-R**	$\mathbf{E_{1/2}^{(+/0)}}$ **of TVC*-R**	$\mathbf{\Delta E_{1/2}}$
H	0.260	0.080	0.180
CHO	0.496	0.314	0.182
COOH	0.480	0.304	0.176

Table **13**: Electrochemical data of TVC and TVC* derivatives.

A comparison between the oxidation potential of trovacene and its pentamethylated analogue **2•** shows that the electronic contribution due to the five methyl groups amounts to a cathodic shift of 0.180 V, with an average contribution of 0.36 V per methyl group. A comparison, as was undertaken in the case of ferrocene, can not be carried out due to the impossibility to synthesize the couple of complexes TVC*-R, and TVC-R, which bear the same functional group R in the seven-membered ring. However, the shift of 0.180 V obtained from the difference of the oxidation potentials of TVC and TVC* can be used to predict the oxidation potential of the hypothetical compound TVC-[7]R. Unexpected, the addition of the cathodic shift due to five methyl substituents to the potential values of the trovacene derivatives **6•** and **17•**, bearing one carbonyl substituent in the five-membered ring affords exactly the potential values of the respective pentamethylated derivatives **15•** and **16•**, which bear the same carbonyl substituent in the seven-membered ring (see Table **15**). Hence, it may be deduced that the shift of redox potential caused by the introduction of a carbonyl substituent into the trovacene framework is independent from its ring location.

4.6 Electron Paramagnetic Resonance of $13^{\bullet}$, $14^{\bullet}$, $15^{\bullet}$, $16^{\bullet}$

4.6.1 Fundamentals of Electron Paramagnetic Resonance[74]

Electron paramagnetic resonance is a technique applicable to systems with net electron spin angular momentum. Free radicals in solid, liquid or gaseous states are systems that fulfil this condition. The unpaired electron with spin S= 1/2 has two possible values of the quantum numbers M_S, +1/2 and –1/2. A strong and homogeneous magnetic field is employed along the *z* direction of laboratory coordinates, to separate the formerly degenerate spin states (Zeeman effect). The magnetic moments of the electron spin μ_Z are oriented along the direction of the applied magnetic field H:

$$\mu_Z = -M_S\, g\, \beta_e = \pm 1/2\, g\, \beta_e$$

where, g= electronic gyromagnetic ratio (g= 2.0023 for a free electron), β_e= Bohr magneton (= $e\hbar/2m$= $9.2740 \cdot 10^{-24}$ JT^{-1}).

The quantization of spin angular momentum in a specified direction leads to the quantization of energy levels of a system of magnetic dipoles in a magnetic field. Application of the expression $E = -\mu_Z H_o$ (E= energy of a magnetic dipole of moment μ_Z in a field H_o) and substitution of $-M_S\, g\, \beta_e$ for μ_Z, gives a set of energies:

$$E_{1,2} = \pm 1/2\, g\, \beta_e H_o$$

The application of the field H_o splits E into two levels E_1 and E_2.

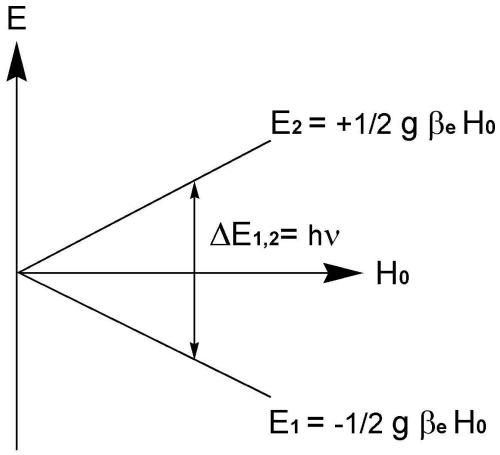

Fig. **23**: Zeeman-Effect.

The separation, that can also be written $\Delta E_{1,2} = g\, \beta_e H_o$, between the Zeeman levels increases linearly with the magnetic field. Transition between the two Zeeman levels can be induced by an electromagnetic field (hν) of appropriate frequency ν and polarization. If the photon

energy hν of the electromagnetic field the matches energy level separation $\Delta E_{1,2}$, than the resonance condition is fullfilled: $\Delta E_{1,2} = h\nu = g\,\beta_e\,H_o$

where, h= Planck constant= $6.624 \cdot 10^{-34}$ Js, ν is expressed in hertz (Hz), H_o= magnetic field at which the resonance condition is met.

A radical in an external magnetic field (when it is not subjected to an electromagnetic radiation), shows a Boltzmann's distribution of spins in the levels E_1 and E_2 :

$$\frac{N_2}{N_1} = e^{-(\Delta E_{1/2} / k_B T)}$$

where, N_1= population in level E_1, N_2= population in level E_2, k_B= Bolzmann's constant (= $1.3805 \cdot 10^{-23}$ JK^{-1}), T= absolute temperature.

The population difference increases with decreasing temperature and increasing $\Delta E_{1,2}$, i.e., with increasing outer magnetic field H. The higher the population difference the higher is the net absorption of the spin system, when irradiated with electromagnetic waves of proper frequency (resonance condition) and polarization (the magnetic field of vectors of ν and H_0 have to be perpendicular for maximum signal intensity). The excited spin relax to the ground state via several relaxation pathways (lattice, solvent, etc.), so that a continuous EPR signal (net absorption) can be maintained for low power irradiation. The spin system dependent relaxation time determines the width of the EPR lines (Bloch equations) and sets limits for the experimental conditions.

Besides the g-factor, which determines the center of gravity for each EPR species, the hyperfine interactions is of most interest to chemists. It arises from interactions of unpaired electron with spin bearing nuclei (for instance, ^1H, ^2H, ^{13}C, ^{51}V…). The hyperfine interaction causes splitting of the EPR lines. The hyperfine interaction can be either anisotropic (orientation dependent) or isotropic (independent of the orientation of H with respect to a molecular axis). The first arises from dipole-dipole interaction between magnetic moments of nucleus and electron. In solution the anisotropic part of hyperfine interaction is usually averaged out, because of the fast rotation of paramagnetic molecules. The isotropic part, also called Fermi's contact interaction, arises from the finite (non zero) spin density at the nucleus. This kind of hyperfine interaction is usually observed for radicals in solution.

For n equivalent nuclei with spin I_i the sum of hyperfine splitting constants (absolute values) for all nuclei must equal the separation in gauss between the outermost lines. This sum is $\Sigma i 2|a_i|NiIi$. The total number of energy levels in the system for one value of M_s is given by Π_i $(2\,I_i + 1)^{n_i}$. The maximum possible number of lines (when second-order splittings are not resolved) is given by $\Pi_i\,(2\,n_i\,I_i + 1)$.

4.6.2 Results

The frontier orbitals configuration of trovacene [$(e_2)^4(a_1)^1(e_2)^0$, corresponding to $^2A_1$ state] gives rise to an EPR spectrum of axial symmetry.[75] The metal a_{1g} orbital is non-bonding, the doubly degenerate e_{2g} level has a high metal character (90%), and the anti-bonding doubly degenerate e^*_{1g} level is covalent (40-60%).[75]

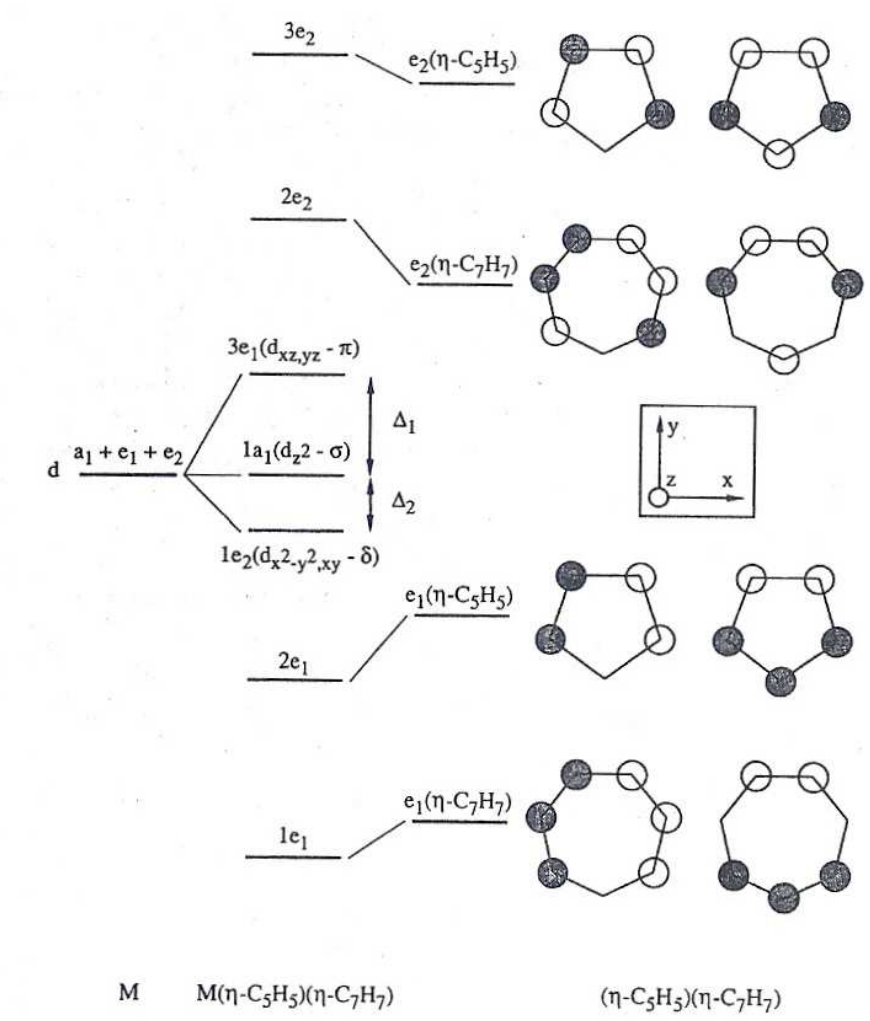

Schema **2**: Qualitative molecular orbital diagram for trovacene.[63]

The metal *d* orbitals split into three sets;[76] d_{z^2} $(1a_1)$, d_{xz}, $d_{yz}(3e_1)$, and $d_{x^2-y^2}$, d_{xy} $(1e_2)$, which are of σ, π, and δ symmetry with respect to the metal-ring centroide axis. The $1a_1$ orbital is the HOMO and is occupied by one electron. The relative energies of these ligand *e* orbitals and the metal *d* orbitals are such that the main contribution to metal-ligand bonding for Cp rings comes from the π MOs (e_1). However, for the bonding of the Tr ring, the δ MOs (e_2) are more

important. The $1a_1$ orbital is essentially non-bonding (as the nodal cone of the d_z^2 orbital intersects the metal-directed lobes of the p_z orbitals of the rings close to their region of maximum electron density). The $3e_1$ orbitals are strongly antibonding and the $1e_2$ orbitals metal→carbon back bonding in nature. The a_1-e_1 (Δ_1) separation is greater than that of a_1-e_2 (Δ_2). On energy grounds we expect the (η-C_7H_7) e_1 orbitals to be the principal contributors to the e_1 complex MOs, and the (η-C_5H_5) e_1 levels to be the main contributors to the $2e_1$.

The isotropic EPR spectrum of trovacene consists of an octet of lines caused by hyperfine structure coupling to the nucleus ^{51}V I=7/2. The coupling constant a(^{51}V)= -6.98 mT bears a negative sign because the hyperfine interaction is thought to be caused by spin polarization of filled inner s shells by the unpaired electron in the vanadium $3d_z^2$.[70] The super hyperfine interaction of the electron with the protons of the rings is not resolved, due to overlapping, and can only be observed with special methods like ENDOR. The isotropic g-value, g_{iso}, is 1.987. The EPR spectrum of trovacene in fluid solution shows a m_I dependence of the line width. This is due to the slow movement of the molecule, which leads to an incomplete averaging of the g- and A- tensors.[77] The anisotropic spectrum in rigid solution yields a value of $g_{\parallel}$= 2.003 (in the range of value of free-spin g_e), and $g_{\perp}$= 1.9784, through spin-orbit-coupling with unoccupied e_{1g}-level,[78] according to the equation: $g_{\perp}=g_e-\frac{6\lambda}{\Delta E}$

with λ= spin-orbit-coupling constant and $\Delta E= [E(e_{1g}) - E(a_{1g})]$.

The value of $g_{\perp}$ is comparable to the free spin value, g_e, diminished by contribution due to spin-orbit-coupling with the unoccupied e_1-level.

The isotropic EPR spectra of the compounds **13**$^{\bullet}$and **14**$^{\bullet}$ in fluid (295 K) and rigid (100 K) solution are shown in Fig. **24**. Important parameters, along with data for **1**$^{\bullet}$, **6**$^{\bullet}$, and **17**$^{\bullet}$, are collected in Table **14**.

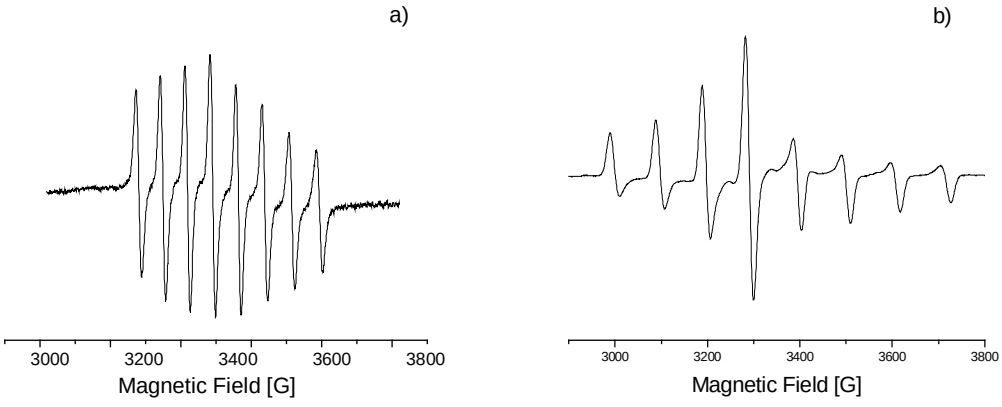

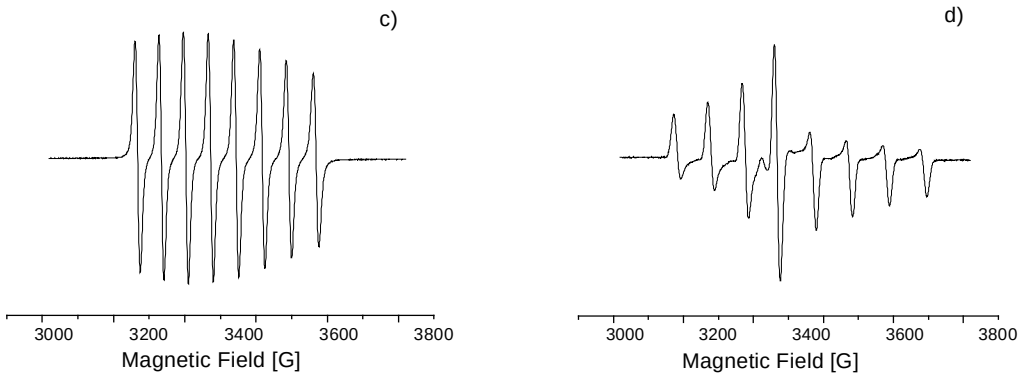

Fig. **24**: EPR spectra of **13•** a) in THF at 295 K and b) 100 K; frequency 9.2175 GHz; and of **14•** c) in toluene at 295 K and d) 100 K, frequency 9.2156 GHz.

	1•	**6•**	**13•**	**17•**	**14•**
<g>	1.9876	1.9809	1.9823	1.9817	1.9823
a(^{51}V) [a]	-6.98	-7.34	-7.31	-7.29	-7.16
$g_\perp$	1.978		1.9745	1.9723	1.9745
$g_\parallel$	2.005		1.9970	2.0005	1.9974
$A_\perp$ [a]	-9.61		-10.38	-10.37	-10.18
$A_\parallel$ [a]	-1.39		-1.18	-1.28	-1.10

[a] coupling constants in mT

Table **14**: EPR parameter for **1•** ,**6•**, **13•**, **17•**, and **14•**, verified by simulation.

13• and **14•**, as in the case of **1•**, show spectra with axial symmetry with $g_\perp < g_\parallel \cong g_e$.

A comparison of the EPR parameters of **1•**, and its mono-derivatives demonstrates that the hyperfine coupling constants a(^{51}V) increases in the sequence **1•**< **17•**< **6•**. This observation reveals an increase of the *s* orbital spin density on the vanadium atom along the series. This effect may be explained by a slight contraction of the non-bonding SOMO a_1, due to the electron-acceptor character of the substituents in the rings. The substituents remove electronic density from e_2-molecular orbital (metal dominated), but not from the metal-dominated a_{1g}-orbital. Hence, the effective positive nuclear charge on vanadium increases and leads to the contraction of a_1-orbital. The effect of the diminution of the spatial extension is an increase of the spin-density on a_{1g}-orbital. Hence, the spin polarization of the inner *s*-orbitals by $V(3d_z)^1$ increases and a(^{51}V) rises.[75]

For the disubstitued compounds lower values of a(^{51}V) with respect to the corresponding monosubstituted complexes are found. This observation requires others argumentations than in the previous case. The two acceptor groups do not exercise an additive effect, but rather a contrary effect. In comparison to **1•** the cyclopentadienyl ligand bearing an acceptor group can transfer less electronic density to vanadium, as in the case of **6•** and **17•**. On the other side, the Tr ring is becoming a better acceptor, due to the presence of acceptor substituent, and can withdraw more electron density than in the others compounds. Hence, in this case the vanadium atom possesses higher electron density in comparison to **1•**, but lower in comparison to **6•** and **17•**.

In accordance with the previous work on **6•**,[25] the possible formation of dimers in solution caused by hydrogen bonding in the species **13•** and **14•** was studied by recording EPR spectra in extra-dry toluene. In the case of **13•**, the very low solubility of the complex in toluene did not permit the recording of a spectrum (this could be obtained only in THF solution). However, in the case of **14•**, an eight-line spectrum was obtained. This observations in accordance with the results from the studies of **17•** and **16•** in the solid state, in which no formation of hydrogen bridges between two formyl groups could be detected in the highly disordered structure. In general, formyl groups form weak hydrogen bonding, weaker than those between carboxylic groups.

The EPR spectra of the compounds **2•**, and **16•** in fluid and rigid toluene solution are shown in Fig. **25**. Important parameters for **2•**, **15•**, and **16•** in are collected in Table **15**.

The measurement of the EPR spectra of **2•**, **15•**, and **16•** at 120 K reveals both the isotropic vanadium hyperfine and the proton superhyperfine components. This is attributed to the slowing down of the reorientation frequency of the rings with respect to the magnetic field.

As it is shown in Table **16**, a comparison of the a(^{51}V) values of **2•** and its derivatives leads to a result contrary t the case of **1•** and the correspondent derivatives. In the later case, an increase of a(^{51}V) from **1•**to **6•** and **17•** is observed, explained by the effect of electron withdrawing substituents located in the Cp ring. In fact, the electron density transferred to vanadium from the Cp ring is less than in the case of **1•**, because of the electron acceptor effect of the carboxylic and formyl groups. In addition, the electron density primarily transferred to the central metal is then passed on the Tr ring, leaving on the vanadium a lower electron density and hence higher spin density than in unsubstituted **1•**. In the case of **2•**, a lower value of a(^{51}V) is found (in respect to the value of **1•**), that must be due to the presence of the Cp* ligand, a superior electron donator. Hence, Cp* can transfer more electron density

to the vanadium than Cp. This characteristic of Cp* is evident in presence of electron acceptor groups, as in the cases of compounds **15**$^{\bullet}$ and **16**$^{\bullet}$. Unexpectedly, the values of a(^{51}V) decrease from the parent molecule **2**$^{\bullet}$ to **15**$^{\bullet}$ and **16**$^{\bullet}$. It may be argued that in these cases the Cp* transfers much more electron density into the system, due to the combined electron withdrawing action of the Tr ligand and its acceptor substituent. Apparently, a fraction of the overall electron density transferred to the Tr ring remains on the central metal atom, thereby increasing the electron density and in turn decreasing the spin density on the vanadium atom. MO calculations could be helpful for an accurate description of the situation.

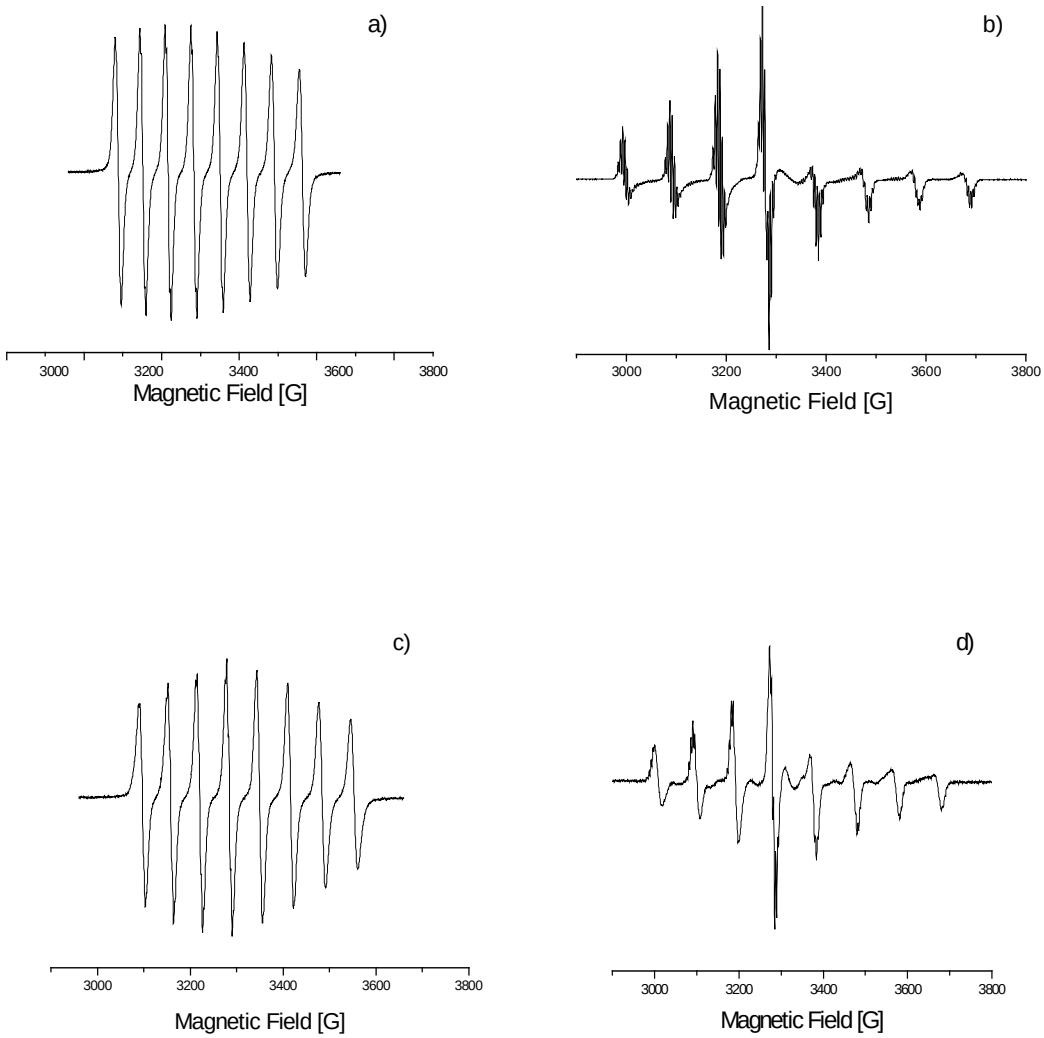

Fig. **25**: EPR spectra of **2**$^{\bullet}$ a) in toluene at 310 K and b) 128 K; frequency 9.2326 GHz, and of **16**$^{\bullet}$ in toluene c) at 300 K and d) 128 K; frequency 9.2335 GHz.

	$2^{\bullet}$	$1^{\bullet}$	$6^{\bullet}$	$15^{\bullet}$	$17^{\bullet}$	$16^{\bullet}$
<g>	1.9852	1.9876	1.9809	1.9861	1.9817	1.9849
a(^{51}V)	-6.78	-6.98	-7.34	-6.54	-7.34	-6.51
$\mathbf{g}_{\perp}$	1.9767	1.978			1.9723	1.9772
$\mathbf{g}_{\parallel}$	1.9968	2.0005			2.0005	1.9953
$\mathbf{A}_{\perp}$ [a]	-9.86	-9.61			-10.37	-9.56
$\mathbf{A}_{\parallel}$ [a]	-0.74	-1.39			-1.28	-0.64

[a] coupling constants in mT

Table **15**: EPR parameter for $\mathbf{2}^{\bullet}$,$\mathbf{1}^{\bullet}$, $\mathbf{6}^{\bullet}$, $\mathbf{15}^{\bullet}$, $\mathbf{17}^{\bullet}$, and $\mathbf{16}^{\bullet}$, obtained by simulation.

To improve the resolution of the EPR experiment of $\mathbf{2}^{\bullet}$ and $\mathbf{16}^{\bullet}$ a second derivate spectrum, shown in Fig. **26,** was calculated.

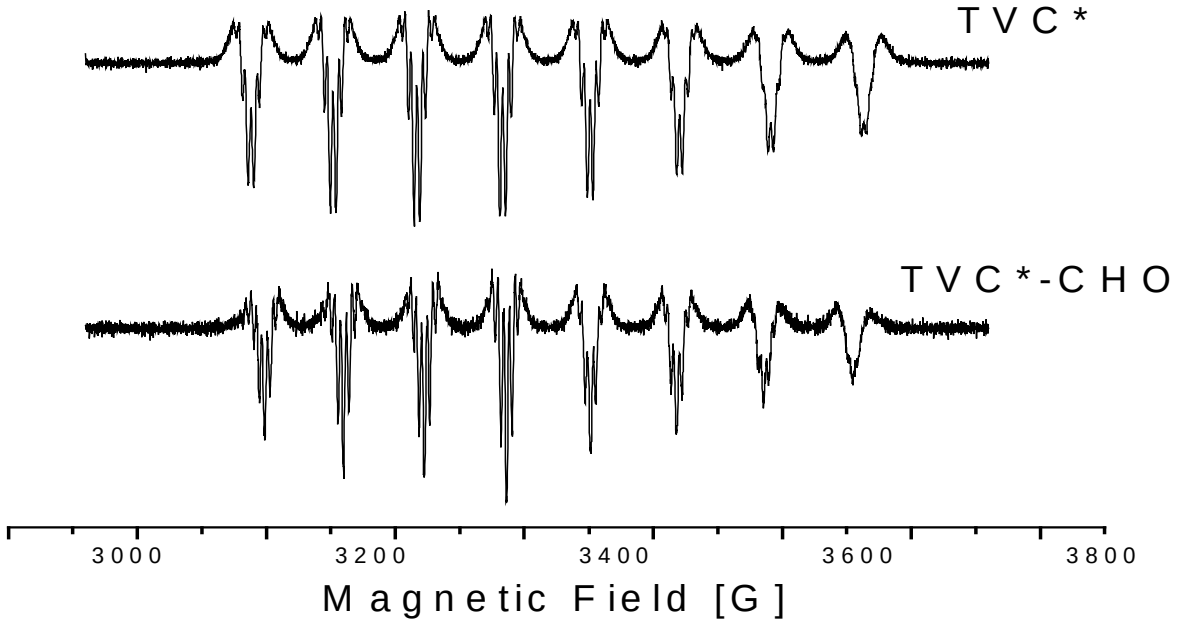

Fig. **26**: Second derivate EPR spectra of $\mathbf{2}^{\bullet}$ and $\mathbf{16}^{\bullet}$ in toluene at 320 K; frequency 9.2468 GHz.

In the spectrum of $\mathbf{2}^{\bullet}$ eight superhyperfine lines are obtained, corresponding to the seven equivalent protons of the Tr ring, while in the spectrum of $\mathbf{16}^{\bullet}$, seven hyperfine lines are

obtained indicanting that in this case only six protons remain almost equivalent. The low intensity lines are not visible because of the poor signal-noise ratio, but simulations undoubtedly show the expected binominal distributions. Computer fits indicate that all ring protons have equal isotropic hyperfine constants within the range of 10-20%.
It is noted that $a(^1H_{Tr})$ are unaffected by substitution as inferred from excellent resolution of ^1H hyperfine splitting. Obviously, π-conjugation of C(O)H group with the Tr-σ-system must be very small, probably due to a twisted position of the formyl group.

The EPR spectrum of **15•** was measured in extra dry toluene (see experimental section) to study the possible formation of hydrogen bridges in solution, as in the case of complex **6•**.[25] The spectrum was recorded at 300 K from a ca. $3 \cdot 10^{-3}$ molar solution. As in the case of **6•**, the spectrum shows the overlapping spectra of monomer and dimer species present in solution.

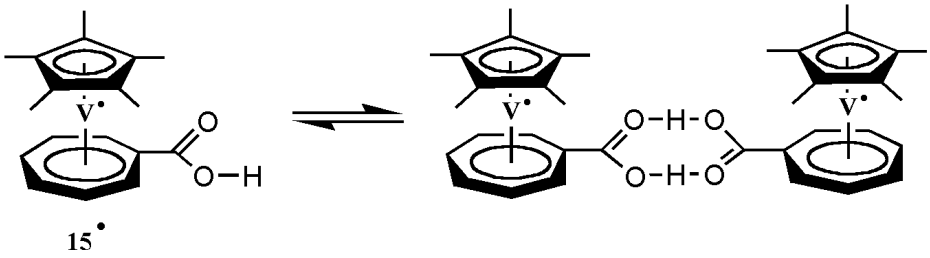

The EPR spectra of the **15•** in fluid extra-dry toluene solution, as well as with addition of methanol are shown in Fig. **27**. EPR parameter obtained by simulation are shown in Table **17**.

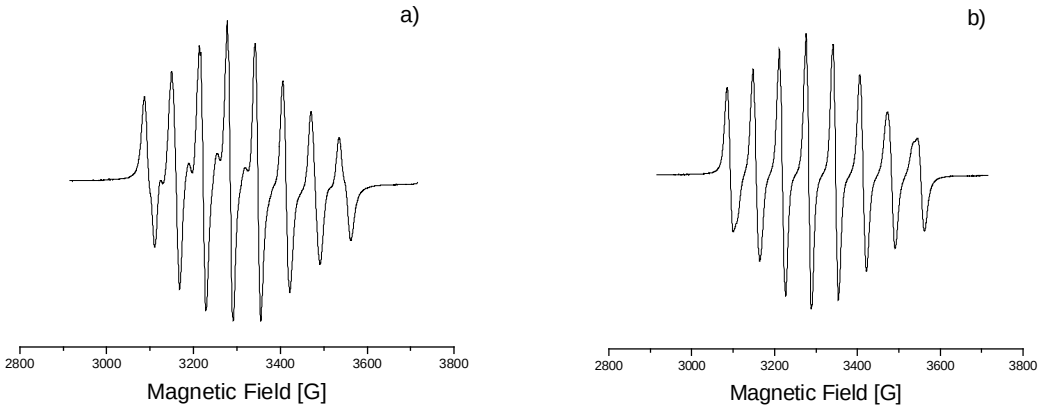

Fig. **27**: EPR spectra of the **15•** at 300 K a) in fluid extra-dry toluene solution, 9.2432 GHz, and b) with addition of methanol, frequency 9.2415 GHz.

The equilibrium is influenced by the variation of concentration, temperature and solvent polarity. In these experiments, it was not possible to obtain a pure dimer spectrum. Subtraction of the monomer spectrum yields a residual dimer spectrum, but the ratio dimer/monomer is too low to permit a simulation. Tests to confirm the presence of the dimeric form in solution were performed by dropwise addition of methanol. The dimer signal disappeared after addition of only one drop, leaving a spectrum for the pure monomer. The ratio dimer/monomer is lower in the case of **15**$^{\bullet}$ than in that of **6**$^{\bullet}$. A possible reason may lie in the steric effect exercised by the Cp* in comparison to Cp. However, the main reason must be ascribed to the inductive effect of the five methyl groups of Cp*, which will reduce the acidic strength in **15**$^{\bullet}$, and likewise the corresponding strength of the hydrogen bridges. In addition, in contrast to the case of **6**$^{\bullet}$, no temperature dependence was observed in the EPR spectra of **15**$^{\bullet}$. This fact must be discuss in term of the too low ratio dimer/monomer observed in solution of complex **15**$^{\bullet}$.

4.7 ^{1}H ENDOR of 2$^{\bullet}$, 14$^{\bullet}$, 16$^{\bullet}$, 17$^{\bullet}$

Electron-Nuclear Double-resonance (ENDOR) experiments of some new trovacene derivatives were undertaken to investigate and confirm their substitution pattern. The assignment of the isotropic hyperfine coupling constants for the five- and seven-membered rings are given in Section 2.1 ($a(^{1}H_{cp})$= 5.04 MHz, and $a(^{1}H_{tr})$= 12.05 MHz).

The ^{1}H ENDOR spectra of compounds **14**$^{\bullet}$, **16**$^{\bullet}$, **17**$^{\bullet}$, are shown in Fig. **28**.

The shift of the spectrum of **14**$^{\bullet}$ with respect to the others is due to the higher magnetic field used in the measurement, which results in a higher ENDOR frequency (nuclear Zeeman term: $\nu_n = g_n\beta_n B_0/h$).

When a substituent is introduced in the seven-membered ring the signal of the protons of the Tr (about 20 MHz) disappears because the protons are no more equivalent. This result is in contrast to that obtained analysing the second derivative spectrum (see Section 4.6.2).

Indeed, the signal of the protons of the Tr-ring remains unvaried (case of **16**$^{\bullet}$). The situation is inverted when there is a selective substitution in the five-membered ring (case of **17**$^{\bullet}$): in this case the Cp-protons are no more equivalent (about 17 MHz). To confirm the effect of the different substitutions, the spectrum of **14**$^{\bullet}$, in which both rings bear a substituent, was

recorded. As expected, both signals, that derived from the protons of the Cp, and that from the protons of the Tr, disappear. (For the parameters assignment see Section 2.1.2).

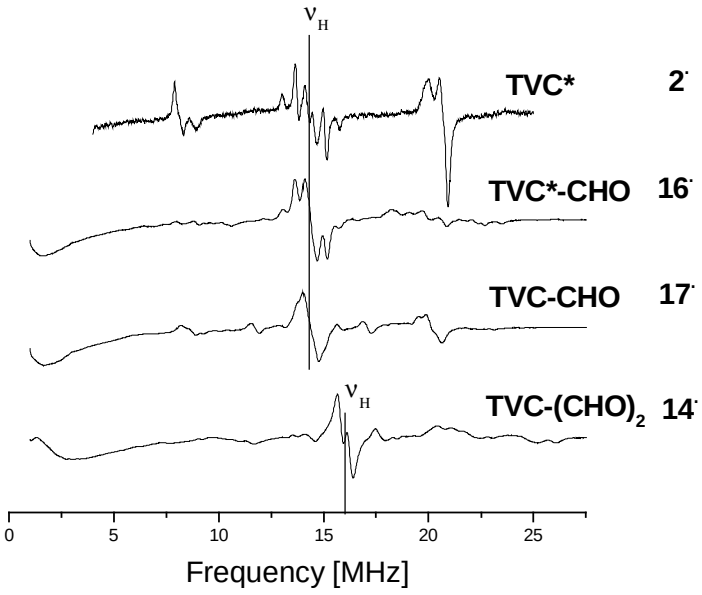

Fig. **28**: ^{1}H ENDOR spectra in toluene of **2**$^\bullet$ at 121 K, frequency 9.5178 GHz, microwave power 13 dB (10 mW), radio frequency power 10 dB (125 W), static field 3373 G; **15**$^\bullet$ at 121 K, frequency 9.5021 GHz, microwave power 7 dB (42 mW), radio frequency power 3 dB (500 W), static field 3373 G; **17**$^\bullet$ at 121 K, frequency 9.5067 GHz, microwave power 7 dB (42 mW), radio frequency power 3 dB (500 W), static field 3372 G; **14**$^\bullet$ at 122 K, frequency, 9.4882 GHz, microwave power 3 dB (100 mW), radio frequency power 3 dB (500 W), static field 3760 G; free proton frequency= 14.38 MHz (spectra of **2**$^\bullet$, **15**$^\bullet$ and **17**$^\bullet$); free proton frequency= 16.03 MHz (spectra of **14**$^\bullet$).

The ENDOR spectrum of **2**$^\bullet$ (shown in Fig. **28**) was also recorded to obtain the values of the proton hyperfine coupling of the methyl groups in the five-membered ring, which are unaccessible by EPR. The following values of a_H(Tr) are obtained: $^1A_1$= 4.7, $^1A_2$= 4.4, $^1A_3$= 3.8 MHz (derived via simulation). From ENDOR the values of a_H(Cp) are obtained: $^1A_1$= 2.7 MHz, $^1A_2$= 1.32 MHz, $^1A_3$= 0.12 MHz (directly measured on spectrometer) reflecting an orthorhombic symmetry. The spectrum shows three lines in the center, one for each methyl proton. All methyl protons are equivalent, because of their free, fast rotation. Moreover, the ENDOR spectrum affords the values of $A_\perp$= 12.79 MHz and $A_{||}$= 11.05 MHz, indicative of

axial symmetry. It is important to taking account that the isotropic hyperfine constants in liquid solution is the time average of all equally possible orientations of the hyperfine tensor with respect to the quantization axis given by the outer magnetic field (see EPR spectrum shown in Fig. **26**). In frozen solutions, in powder (see ENDOR spectrum shown in Fig. **28**), the complete hyperfine tensor has to be taken. The isotropic part, or better the 1/3 trace of this tensor is invariant against transformation of coordinates and is comparable with the isotropic hyperfine constant obtained in liquid solution. Hence, no matter which direction a hyperfine tensor points to, the isotropic part remains constant. The tensor components of the seven-membered ring protons in (η^7-cycloheptatrienyl)(η^5-pentamethylcyclopentadienyl)vanadium, **2**$^{\bullet}$, have equal 1/3 trace <A> value, but different anisotropic parts because of their individual orientations with respect to the seven-membered ring plane. At 130 K (temperature used in the measurement) the seven-membered ring is still rotating faster than the interaction time at the ENDOR experiment. Therefore, time average of all the individual hyperfine tensors are obtained in the ENDOR experiment. The ENDOR seven-membered ring lines of (η^7-cycloheptatrienyl)(η^5-pentamethylcyclopentadienyl)vanadium, **2**$^{\bullet}$, (see also ENDOR of trovacene, **2**$^{\bullet}$) are axial symmetric and relative sharp. At lower temperatures the lines will be broaded and finally all anisotropic hyperfine couplings for each proton in the ring will become visible (T< 4K).[79] Substitution of the Cp or Tr ring slows down the ring rotation and enhances the differences of the anisotropic part as well as the isotropic part of the individual proton hyperfine constants.

5. A Binuclear Complex of (η^7-cycloheptatrienyl)(η^5-pentamethylcyclopentadienyl)vanadium

Since the original studies of mixed-valence ferrocene complexes,[80] metal-metal interactions in linked metallocenes have assumed great attention.

Redox active binuclear organometallic complexes with a conjugated hydrocarbon bridging ligand, correspond to organometallic versions of the multistage redox systems first described by Deutchert and Hüning.[81]

The field has expanded in numerous directions including variation of the central metal atom, and modification of the spacers between the metallocene units. The different nature of the spacer allows to study the mechanism of interaction, that can be through-space or through-bond. The electron-electron spin-spin interaction, J, can be determined by various methods. In this work, the temperature dependent measurement of the magnetic susceptibility was employed in the solid state, and EPR spectroscopy for studies in solution. To complete the study of the exchange interaction, the redox behaviour of the linked trovacenyl-units was examined by cyclic voltammetry.

A great number of dimeric and oligomeric complexes of trovacene, with different bridging ligands, were synthesized and analysed in our group during the last years (some examples are given in Fig. **29**):

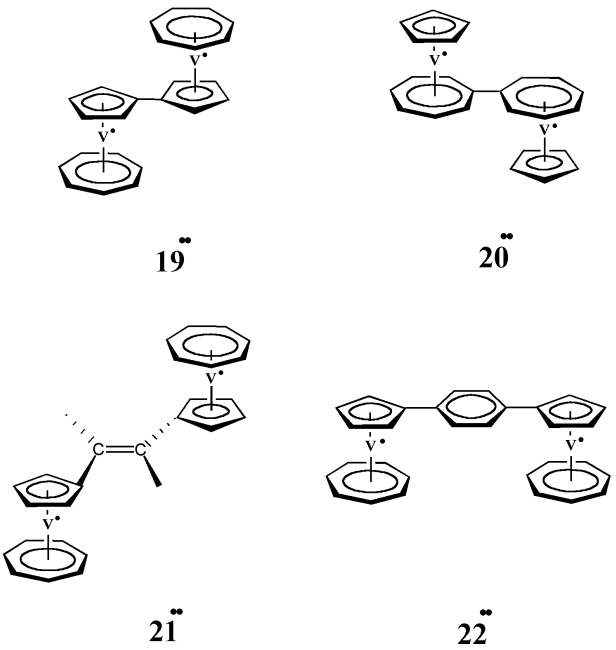

19$^{\bullet\bullet}$ **20**$^{\bullet\bullet}$

21$^{\bullet\bullet}$ **22**$^{\bullet\bullet}$

Fig. **29**: Binuclear complexes of trovacene: [5-5]-bitrovacene,[82] **19**$^{\bullet\bullet}$, [7-7]-bitrovacene,[51] **20**$^{\bullet\bullet}$, Bis([5]-trovacenyl)ethene,[51] **21**$^{\bullet\bullet}$, 1,4-Bis([5]trovacenyl)benzene),[82] **21**$^{\bullet\bullet}$.

These molecules show different intermetallic exchange interactions depending on the spacers. In all cases the exchange interactions are antiferromagnetic.

5.1 Synthesis of E-1,2-bis[(η^7-cycloheptatrienyl)(η^5-pentamethylcyclopentadienyl)-vanadium]ethene, $18^{\bullet\bullet}$

After the well know chemistry of the [5-5]-binuclear trovacenyl derivatives, and the first [7-7]-bitrovacene, the synthesis of first [7-7]-bitrovacenyl compound linked by a spacer was performed in order to compare its electrochemical and electronic properties with those of the [5-5] isomers. The binuclear complex $\mathbf{18^{\bullet\bullet}}$ was synthesized by a modified procedure of the McMurry reaction,[83] a reductive coupling of carbonyl-compounds to olefins by low-valence titanium reagents, that had been optimised for trovacene. Reductive coupling of aldehydes and ketones by titanium(II) salts prepared in situ was described in 1973 independently by two groups[84] and has been further developed by the work of McMurry.[85] While ketones yield both **E**- and **Z**- isomers, the **E**- olefins are formed exclusively from aldehydes.[86] The stereoselectivity of the olefin formation can be accounted for by the calculated energy difference for the **E**- and **Z**- isomers, which will be reflected in the diol deoxygenation, the product determining transition state. When this difference exceeds 4-5 kJmol^{-1}, only the more stable **E**- isomer is isolated.

(Formyl-η^7-cycloheptatrienyl)(η^5-pentamethylcyclopentadienyl)vanadium, $\mathbf{16^{\bullet}}$ was refluxed for 20 hours in a DME solution containing the titanium(II)-reagent ($TiCl_3(DME)_{1,5}$ + Zn/Cu). The product (**E** isomer) was precipitated by petroleum ether as dark-green powder. In contrast to the [5-5] isomers, $\mathbf{18^{\bullet\bullet}}$ is very good soluble in toluene, due to the presence of the Cp* ligand.

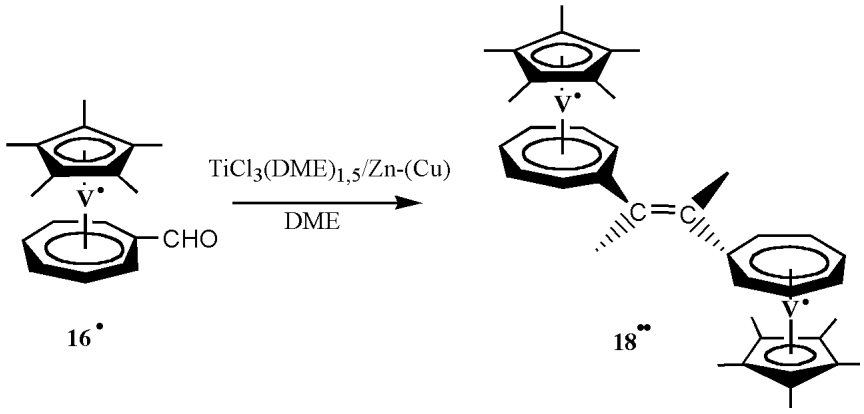

$\mathbf{16^{\bullet}}$ $\mathbf{18^{\bullet\bullet}}$

5.2 Cyclic Voltammetry of $18^{\bullet\bullet}$

5.2.1 Fundamentals of Cyclic Voltammetry of Binuclear Species

In bridged compounds two types of interaction between the two moieties are possible: interaction propagated through the bond (arising from an electronic system delocalised over a diamagnetic spacer or by the mechanism of spin-polarization of the electrons in the double occupied bridging ligand orbitals by the unpaired electrons) and through space (electric field effect, that describes the direct overlapping of both singuly occupied atomic orbitals). Generally, a decreasing interaction with increasing metal-metal distance is observed. The redox properties of dinuclear complexes of transition metal ions depend on the metal, the chemical nature of the bridging ligands, and the geometry of the bridge.

Cyclic voltammetry is a method to study the metal-metal interactions via the parameter of the redox splitting $\delta E_{1/2}$ (potential difference of two subsequent redox steps), complementary to the determination of the exchange interaction, J, between the electronic spins of the metal centers. The redox splitting results from the repulsion between equal charges. In a complex in which the two metal centers are separated from each other two cases are possible:

a) when an electron is transferred from one metal center, the second electron is transferred to the other metal center at the same potential ($\delta E_{1/2} < 70$ mV);

b) when the distance between the two metal centers is small, there is electrostatic repulsion between the first negative charge and the second added negative charge, hence, a shift to cathodic potential is observed in the second electron transfer.

The difference of potential between both electron transfers is the redox splitting $\delta E_{1/2}$. $\delta E_{1/2}$ is a measure of the extent of the interaction between both metal centers. Presupposition for a determination of $\delta E_{1/2}$ from the cyclic voltammogram is the reversibility of the electron transfer.

In an electrochemical experiment,[87] a separation, ΔE, of $(RT/F)\ln 2^n$ is observed between the first and last redox events.[88]

For a molecule with two redox centers, a separation of approximately 36 mV should be expected at 20 °C (rather smaller separation than that typically resolvable in routine electrochemical experiments). Larger, measurable separations are indicative of an interaction between the two sites.

An intramolecular electron transfer can occur between two metal centers of different oxidation states. It can be distinguished between two types of compounds:

a) mixed-valence (electron transfer is slow, the unpaired electron is localised on one metal center),

b) intermediate valence (electron transfer is fast, the unpaired electron is delocalised between the two metal centers).

A comproportionation constant, K_c, gives a measure of the redox splitting:

$$M\text{-}X\text{-}M + [M\text{-}X\text{-}M]^{2-} \rightleftharpoons 2\,[M\text{-}X\text{-}M]^{-}$$

X= spacer; $\delta E_{1/2} = (RT/F)\ln K_c$

Increased separation reflects an increased conproportionation constant, i.e., an increased stabilization of the mixed-valence species. Both electrostatic and electronic effects contribute to this stabilization. In metallocene systems it has been found that ΔE depends on the separation between the metal centers and the degree of conjugation in the bridge linking the two metallocenes.[89]

5.2.2 Results

Cyclic voltammetry data for **18$^{\bullet\bullet}$**, and the [7-7]-bitrovacene[51] **20$^{\bullet\bullet}$** are shown in Table **16**. Typical cyclic voltammetry trace for **18$^{\bullet\bullet}$** is depicted in Fig. **30**.

	18$^{\bullet\bullet}$	**20$^{\bullet\bullet}$**
$E_{1/2}^{(0/+1)}$ [V]	0.158	0.290
ΔEp [mV] [a]	64	80
r= i_{pa}/i_{pc}	0.46	1
$E_{1/2}^{(+2/+1)}$ [V]		0.445
ΔEp [mV] [a]		107
r= i_{pa}/i_{pc}		1
$\delta E_{1/2}$ [mV] [c]		155
E_{pa} [V] [b]	1.228	1.096
$E_{1/2}^{(0/-1)}$ [V]	-2.490	-2.414
ΔEp [mV] [a]	86	80
r= i_{pa}/i_p	1	1
$E_{1/2}^{(-1/-2)}$ [V]		2.739
ΔEp [mV] [a]		63
r= i_{pa}/i_p		1
$\delta E_{1/2}$ [mV] [c]		325

[a] $\Delta Ep = (E_{pa} - E_{pc})$ [b] irreversibile [c] $\delta E_{1/2} = (E_{1/2}^{(n\pm1/n\pm2)} - E_{1/2}^{(n/n\pm1)})$

Table **16**: Cyclic voltammetry data for **18$^{\bullet\bullet}$**, **20$^{\bullet\bullet}$** measured in DME/0.1 M TBAP, vs. SCE, ν= 0.1 V/s, T=-40°C.

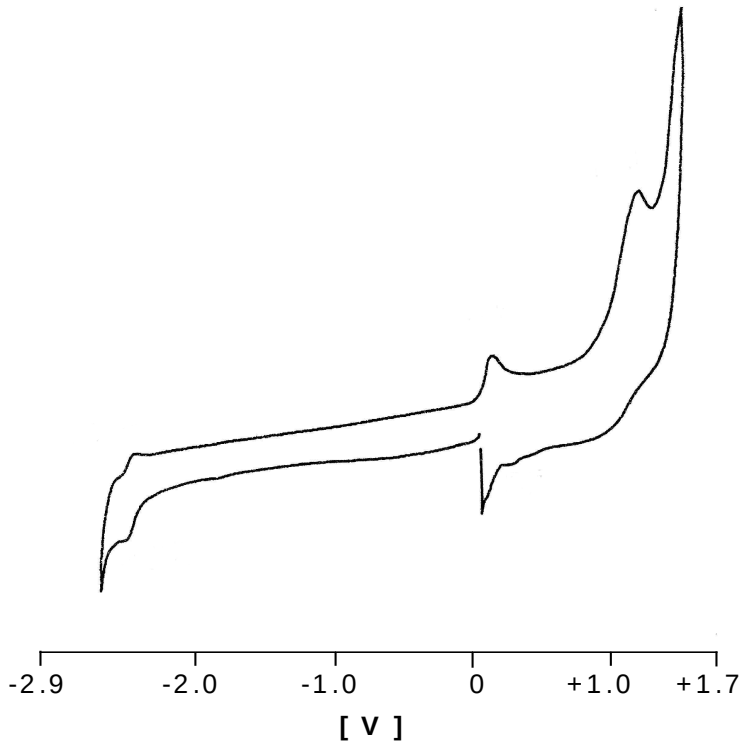

Fig. **30**: Cyclic voltammetry trace for **18$^{\bullet\bullet}$** (mA/V, red→ox).

Surprisingly, the cyclic voltammogram of **18$^{\bullet\bullet}$** shows only one oxidation peak, while in all dimeric analogues a redox splitting is observed. (The disadvantageous start potential of 0 V may be obstacle the observation of a splitting in the region around 0 V).

The redox behaviour of **18$^{\bullet\bullet}$** differs from the others also in the cathodic region: also in this case only one reversible peak is found. A comparison of the peak currents of the reduction and oxidation steps reveals much higher currents in case of the latter process. This might be indicative for a two electron process in the oxidation step and a one electron process in case of the reduction. Hence, a redox splitting of the reduction wave has to be considered. It may be possible that the second peak lies at more negative potentials (< 2.8 V) than the range chosen in the experiment (limited by the redox properties of the solvent).

5.3 Electron Paramagnetic Resonance of $18^{\bullet\bullet}$

5.3.1 Fundamentals of Electron Paramagnetic Resonance of Biradicals[90]

When in a molecule two monomeric units with no interaction between both electrons are present, the molecule acts as double radical. Its EPR spectrum differs to that of a monoradical by the double intensity of the signal (both having the same concentration).
However, when an exchange interaction J between radical centers is present, the isotropic EPR spectrum is governed not only by Zeeman-Effect and the hyperfine coupling, but also by the ratio of the amount of J and the hyperfine coupling constant. In fluid solutions, anisotropic interactions as the dipole-dipole coupling are averaged out, so that for the description of such a system the isotropic Hamilton operator, H_{iso}, results:[90]

$$H_{iso} = g\mu_e B[S(1) + S(2)] + a[I(1)S(1) + I(2)S(2)] + [JS(1)S(2)]$$

Zeeman-effect hyperfine interaction exchange interaction

where, B= magnetic field, I= nuclear spin operator, S= electrons spin operator, A= hyperfine coupling spin constant, J= scalar quantity for the exchange interaction.
This Hamilton operator was used also for the EPR-spectra simulation in this work.
The simulation of the complete spin function with all electrons and nuclear spin quantum numbers leads to the diagonalization of a 256x256 matrix for two vanadium centers with I= 7/2 each. A 4x4 matrix for each permitted combination of $m_I(1)$ and $m_I(2)$ can be obtained by approximation.[91]
For each 4x4 matrix four resonance magnetic fields are obtained, B_x:

$B_1 = nB_0 + [J+R-a(m_I(1)+m_I(2))]/2\ g\beta_e$ S
$B_2 = nB_0 + [J+R-a(m_I(1)+m_I(2))]/2\ g\beta_e$ T
$B_3 = nB_0 + [J+R-a(m_I(1)+m_I(2))]/2\ g\beta_e$ S
$B_4 = nB_0 + [J+R-a(m_I(1)+m_I(2))]/2\ g\beta_e$ T

where, $R = [J^2 - a^2\{m_I(1)-m_I(2)\}]^{1/2}$

S and T determine if the leading contribution to the spin functions is given from singlet or triplet term.
The equation for the relative intensities of the resonance fields are:

$B_1 = B_3 = (R-J)/4R$

$B_2 = B_4 = (R+J)/4R$

When J=0 is inserted in the equation, from all 4x4 matrices only eight different resonance magnetic fields are obtained (spectrum 1 in Fig. **34**). When J and a(^{51}V) are equal the spectra become complex. In this case the singlet and triplet functions are mixed and in addition to the $T_{\pm} \leftrightarrow T_0$ transitions in the S= 1 triplet level spin prohibited transitions between S_0 and $T_{\pm}$ are also observed (Fig. **31**).

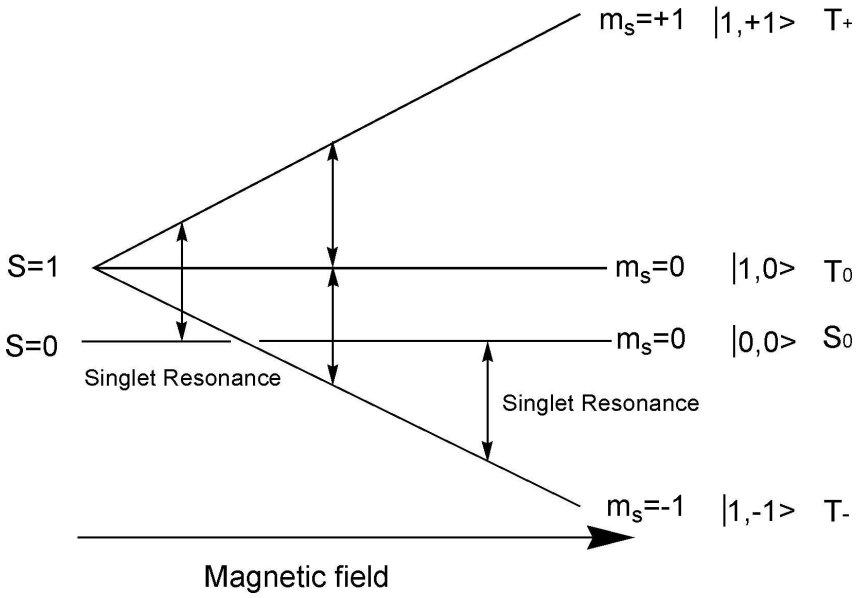

Fig. **31**: Representation of resonances for $|J| \cong |a|$

The observation of the singlet resonance at high- and low-field side of the spectrum (spectra 3 and 4 in Fig. **32**) allows to determine J accurately (see equation given above).[92]

When J increases, these lines are moving further apart and the intensity decreases strongly. When J is essentially grater than a(^{51}V), 2*2I+1 resonance magnetic fields are obtained. In the case of two equivalent vanadium nuclei 15 absorption signals with intensity ratio 1:2:…:2I + 1):…:2:1 occur. The distance between the lines amounts to the half of the hyperfine coupling constant of the individual units.

In Fig. **32** is shown a series of simulated EPR spectra for different J/a ratios.

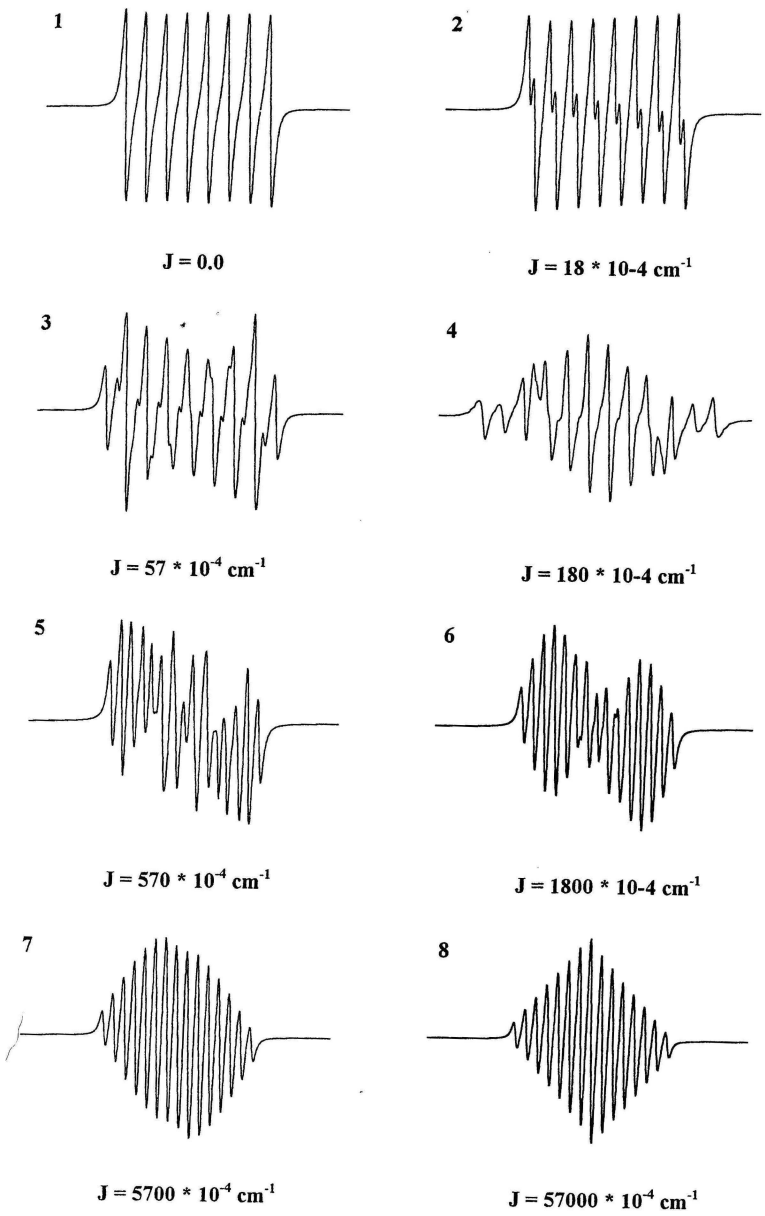

Fig. **32**: Simulated EPR-spectra for binuclear vanadium(0) depending of the ratio J/a, with a= $57*10^{-4}cm^{-1}$, width of lines ΔB= 30 G, without m_I-dependence from ΔB.

The simulation of experimental spectra is obtained by a simplex fit-routine, in which the parameters a, g, and J are varied.[93]

In frozen solution (rigid matrix) anisotropic parameters become accessible, too, because the dipole-dipole exchange interaction between the magnetic moments of both unpaired electrons and both nuclear spins (I= 7/2 each) are not averaged out anymore by the molecular movement. This results in an additional magnetic interaction, called zero-field splitting. For the axial zero-field splitting parameter D the following expression is used:

$$D_z = -\frac{3\cos^2\vartheta - 1}{r^3}\mu_e^z \mu_e^z$$

where, μ_e^z= magnetic moment in in *z*-direction, θ= angle between the distance vector coupling electrons and the z direction, r= distance between both electrons. Therefore, measurements of D_z permits an estimation of the average outer spin distance.

5.3.2 Results

The EPR spectra of the compound **18$^{\bullet\bullet}$** in fluid and rigid toluene solution are shown in Figs. **33-34**. Important parameters for **18$^{\bullet\bullet}$**, and the directly linked dimer **20$^{\bullet\bullet}$** are collected in Table **17**.

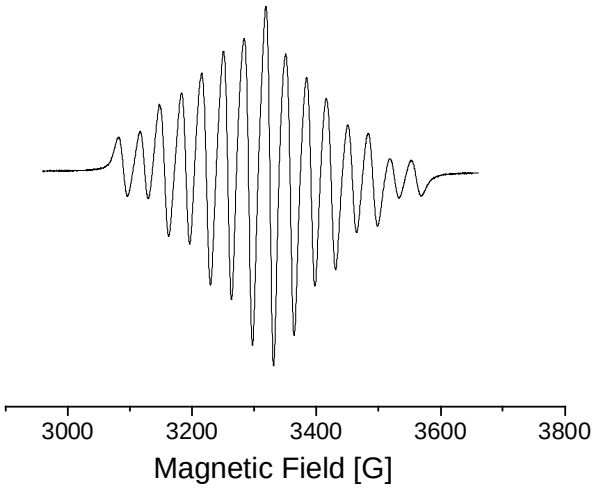

Fig. **33**: EPR spectrum of **18$^{\bullet\bullet}$** in toluene solution at 295 K; frequency 9.2431 GHz.

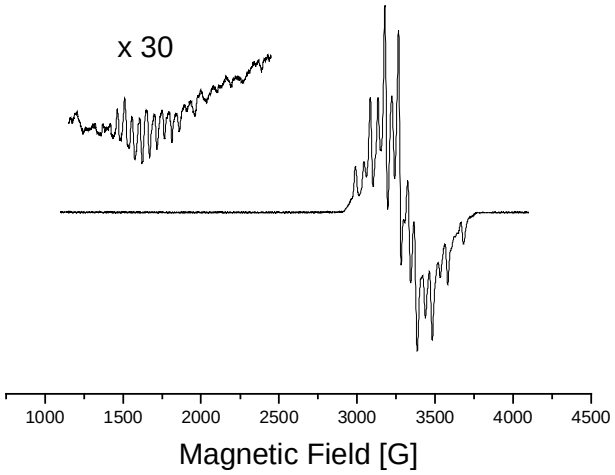

Fig. **34**: EPR spectrum of **18$^{\bullet\bullet}$** in toluene solution at 120 K; frequency 9.2332 GHz.

	18$^{\bullet\bullet}$	**20$^{\bullet\bullet}$**
g_{iso}	1.9860	1.9832
a(^{51}V)	-6.7 mT	-7.19 mT
J	-2.4 cm^{-1}	-2.59 cm^{-1}

Table **17**: EPR parameters for **18$^{\bullet\bullet}$** and **20$^{\bullet\bullet}$** obtained by simulation.

The EPR spectrum in fluid solution (295 K) consists of 15 lines, in the correct binomial intensity distribution of two magnetic equivalent vanadium centers (2∗^{51}V, I=7/2). Therefore, the spectrum points to an exchange coupling constant J, which largely exceeds the hyperfine coupling constant a(^{51}V). The lines distance amounts to 33.5 G. The parameters of the spectrum recorded at 295 K were obtained by simulation, hence the precision for J is not very high, because of the great ratio J/a= 388. Simulations in this J range are not sensitive on changes of J. A lower limit only can be given for the magnitude of exchange interaction. The best fit gives a value of $|J| = 2.4$ cm^{-1}. Considering the results of magnetic susceptometry, a negative sign can be attributed to J, corresponding to an antiferromagnetic interaction. In rigid solution (120 K) a half-field signal is obtained, proving the biradical character. The half-field signal arises from the spin-forbidden $\Delta M_s=2$ transition. The splitting in the $\Delta M_s=2$ multiplet amounts to 47 G, which corresponds to half the value of the hyperfine coupling constant $A_\perp$(^{51}V), amounting to 94 G. This signal for weakly interaction V(d^5) is often not observed

because of the low intensity of the spin-forbidden $\Delta M_s=2$ transitions. According to $3<a>= 2 A_{\perp} + A_{||}$, a value of 13 G is obtained for $A_{||}(^{51}V)$. A value for the zero-field splitting parameter D can be extracted from the rigid solution spectrum, assuming that the distance between the outermost lines (low field, high field, respectively) is equal to $2D + 7 A_{\perp}(^{51}V)$. The value of D= 17 G could be extracted and is used in the relation $D= 0.65 g_{||}^2/ r^3$(based on the point-dipole approximation)[94] for calculating a value for r of r= 5.3 Å, corresponding to the interspin distance in the dimer **18**$^{\bullet\bullet}$. This value is too small compared with those obtained employing molecular models: 7.69 Å for the anti conformation and 7.04 Å for the syn conformation (these value are in accord with those found for **E** and **Z** [5-5]-isomers)[51]. It must be noted that in the formula is not taken account of the changes of $g_{||}$.

In the relation an approximation was used by replacing the value of $g_{||}$ with that of g_{iso}. This is permitted by the consideration that the values of $g_{||}$ found in all trovacene dimers lie in the range of those of monotrovacene derivates. The rotation of the two trovacene units in the dimeric structure does not permit a collinear alignment of the molecule so that the value of $g_{||}$ can be averaged.

A comparison will be carried out with [7-7]-bitrovacene, **20**$^{\bullet\bullet}$, the other known dimer linking the trovacene units through the seven membered rings (see value shown in Table **17**).

As expected, the J values found for the dimer linked by an ethene bridge are lower than those found in the directy linked **20**$^{\bullet\bullet}$. The observation of the half-field signal indicates a strong exchange interaction between the two vanadium centers. The half field signal could not be detected in all the other bridged trovacenes, linked through the five-membered ring except for the directly bridged **19**$^{\bullet\bullet}$, where this signal is considerably weaker and only detectable by spectral accumulation. This observation indicates that electron spin dipolar coupling in [7-7] linked dimers markedly exceeds that exhibited by its [5-5] isomers, and the fact that the deviation from the true value is small compared to the other experimental errors.

Moreover, the decrease of $a(^{51}V)$ in **18**$^{\bullet\bullet}$ confirms a diminution in the exchange interactions due to the presence of the 1,2-ethenediyl bridge, as it was already observed in the series of [5-5] directly and through a bridge linked trovacenes (see **19**$^{\bullet\bullet}$, **21**$^{\bullet\bullet}$ and **22**$^{\bullet\bullet}$).[82,51]

5.4 Magnetic Measurement of $18^{\bullet\bullet}$

5.4.1 Fundamentals of Magnetic Susceptibility[95]

A sample within an homogeneus magnetic field H acquires a magnetization M, that is related to H through the magnetic susceptibility χ:

$$M= \chi H$$

χ is the algebraic sum of two contributions: a diamagnetic (negative) and a paramagnetic (positive), χ_D and χ_P respectively:

$$\chi= \chi_D + \chi_P$$

When χ_D dominates, the sample is diamagnetic (it is repelled by the magnetic field); when χ_P is the leading contribution, the sample is paramagnetic (it is attracted by the applied field). Paramagnetic samples have always a χ_D part, due to the interaction of the magnetic field with the motion of the electrons in their orbits. Hence, the value of χ experimental obtained must be corrected. χ_D is independent of the temperature and the strength of the applied field and it is additive calculated from tabulated data, while, χ_P is dependent of the temperature. This dependence for magnetic moments without intermolecular interactions is described by Curie-Law:

$$\chi= C/T$$

where C is the Curie constant, $C= Ng^2\mu_B S(S+1)/3k_B$.

The temperature dependence for magnetic moments with a weak intermolecular interaction j, is described by Curie-Weiss-Law:

$$\chi= C/(T-\Theta)$$

where C is the Curie constant, Θ is the Weiss constant, $\Theta= zjS(S+1)/3k_B$, z is the number of interacting centers, S is the electronic spin, k_B is the Boltzmann constant.

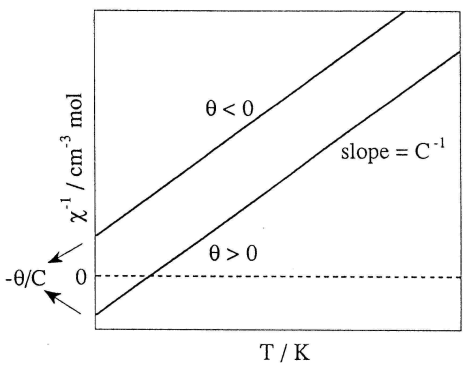

Fig. **35**: Plot of χ^{-1} versus T for an assembly of molecules obeying the Curie-Weiss law.[95]

A plot of χ^{-1} versus T[K] for a system obeying the Curie-Weiss-Law gives a straight line with slope= C^{-1}. The intercept with the T axis yields two possible values of Θ: a positive, that indicates ferromagnetic intermolecular interactions, and a negative, that indicates antiferromagnetic intermolecular interactions.

The temperature dependence for two magnetic equivalent centers with a strong intermolecular interaction J, is described by Bleaney-Bowers expression:

$$\chi = 2N_A g^2 \mu_B^2/(kT[3+\exp(-J/kT)])$$

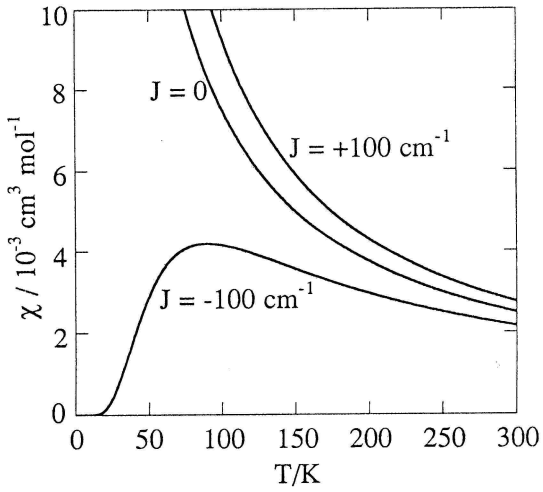

Fig. **36**: Calculated χ(T)-curves for J= 0 and ±100.[95]

A plot of χ versus T[K] shown that for J< 0, (the case of an antiferromagnetic interaction), the magnetic susceptibility presents a maximum, and then tends to zero when T approaches zero. Indeed, at low temperature only the diamagnetic ground state is thermally populated. The maximum of the susceptibility is characteristic for an antiferromagnetic interaction and fulfills approximately the relation:

$$|J|/kT_{max} = 1.599$$

When the interaction is ferromagnetic, a steeper rise of the susceptibility is observed than in a non interacting system. In this case, the progression of the curve reacts non sensitively to the changes of J. In fact, χT for J= 0 is only 75% as large as when J= ∝, because ¼ of the molecules are singlets that do not contribute to χT.[96]

The experimental values of the susceptibility are described by a modification of Bleaney-Bowers expression through the introduction of an "effective" temperature, (T/(T-Θ)):

$$\chi = 2N_A g^2 \mu_B^2/(k(T-\Theta)[3+\exp(-J/kT)])$$

5.4.2 Results

The magnetic susceptibility for **18••** was measured in the temperature range from 1.8 to 300 K at the constant magnetic field. The measurement was performed at different magnetic field strengths: 5 kG, 10 kG, 15 kG, and 30 kG. The temperature dependence of the susceptibility measured at 30 kG is shown in Fig. **37**. The values obtained for the exchange interaction and the parameters Θ, and ρ are shown in the capture.

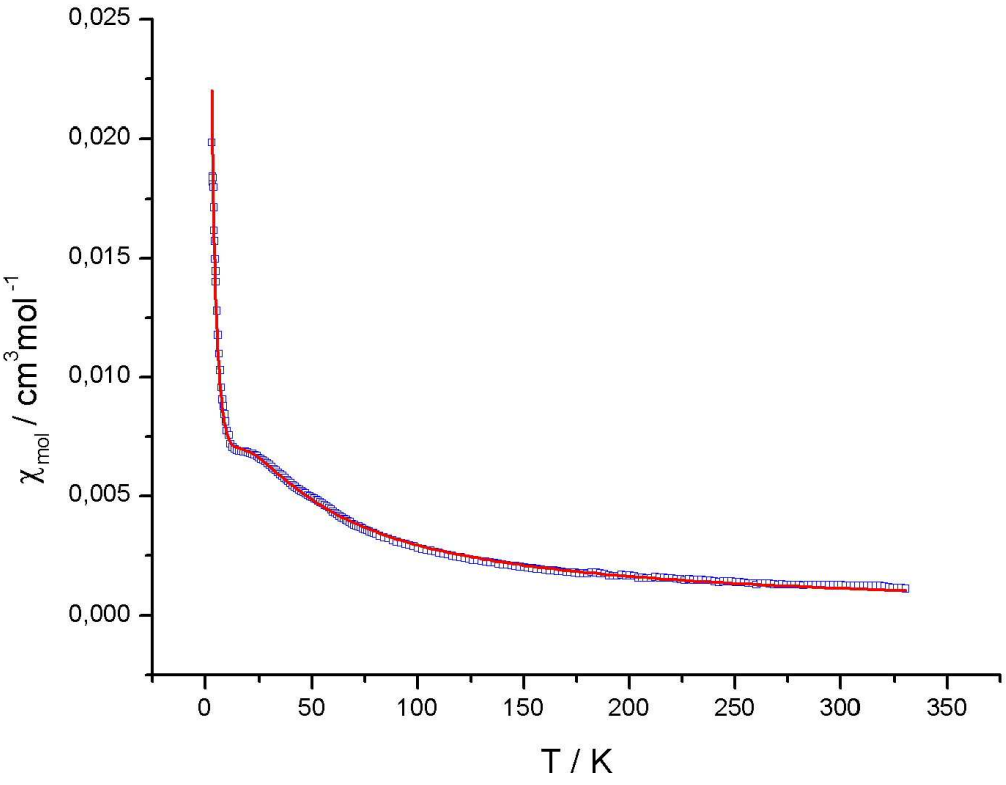

Fig. **37**: Experimental molare susceptibility data for **18••** at 30 kG in the temperature range 1.8-300 K. The solid line represents the best fit to the Bleaney-Bowers expression with J= -25.9 cm^{-1}, Θ= -14.2 K, and ρ= 0.0221.

The magnetic susceptibility, χ, passes through a slight bump at about 50 K, then to a second more pronounced bump at about 20 K, and rises to a maximum at 1.8 K. It must be noted the unexpected presence of a second bump at about 50 K, which may be attributable to the *cis* form of **18••**, even if in the case of McMurry coupling of aldeydes only the formation of the

trans isomer is documented. EPR spectroscopy can not help to determine the second species, because the two dimers give identical EPR spectra (J> 1.5 cm^{-1}, see Fig. **34**). Attempts of separation by column chromatography were unsuccessful.

The experimental data can be described by a modified Bleaney-Browers relation:[95]

$$\chi_m = \frac{2Ng^2\mu_B^2}{k(T-\Theta)[3+\exp(-J/kT)]}(1-\rho)+\frac{Ng^2\mu_B^2}{2kT}\rho$$

The modification accounts for intermolecular magnetic interactions by the parameter Θ and for traces of non coupled species in the sample, that cause an increase of the experimental susceptibility below T= 5 K, by their mole fraction ρ. The impurity is assumed to follow the Curie law, and to show the same g-value as the coupled species. Since each molecule of **18••** contains two vanadium centers, the Curie correction term must be multiplied by a factor of 2. The fraction of the non coupled component was determined to ρ= 0.0221. The value g= 1.9860 was taken from the EPR spectrum. Fit parameters to the experimental data using the modified Bleaney-Bowers relation for **18••** and [7-7]-bitrovacene,[51] **20••**, are shown in Table **18**.

	J/k [K]	**J [cm^{-1}]**	**Θ [K]**	**g**
18••	-37.2	-25.9	-14.2	1.9860
20••	-34.61	-24.05	-10.25	1.9832

Table **18**: Fit parameters to the experimental data using the modified Bleaney-Bowers relation for **18••** and **20••**.

Considering the magnetic data for all studied dimeric trovacene complexes, it is observed that the magnitude of the exchange coupling constant for the [7-7]-complexes (directly joined or linked through a spacer) exceeds the values found for the [5-5]-isomers. This finding demonstrates that the exchange interaction is much more effective in bis(cycloheptatrienyl)-ligands. The difference of the exchange interaction reflects the different spin density distribution on the ring protons depending on the ring size.[97]

A direct comparison was carried out for both [7-7]-linked compounds, **18••** and **20••**. The exchange interaction J is antiferromagnetic in both complexes (J< 0).

The value of J obtained by magnetic measurement corresponds to the sum of J (symmetric anisotropic), J (asymmetric anisotropic), and J (isotropic). The value of J (isotropic) can not be determined alone by magnetic measurements. In the EPR experiments the anisotropic values of J are cancelled due to the molecular motion. In addition, EPR measurements in dilute solutions are not disturbed by intermolecular interactions. In magnetic measurements in the solid state strong intermolecular interactions can be anticipated, because it is reasonable to believe that the crystal structure must be similar to those of **19$^{\bullet\bullet}$** and **20$^{\bullet\bullet}$**, in which the vanadium-vanadium intramolecular distance is comparable to the intermoleculare distance between adjacent molecules.[98] Unfortunately, J obtained by EPR spectroscopy are limited to values below 1.5 cm^{-1}.

In the case of the complex **18$^{\bullet\bullet}$** (in which the two monomer units are linked by a spacer), a lower value of J than for **20$^{\bullet\bullet}$** (in which the two monomer units directly linked) was expected. A possible reason for this result is the presence of the Cp* ligand, which posses amplified donor capacity in comparison to the Cp ligand. In the case of the dimer **18$^{\bullet\bullet}$** spin density is transfer into the spacer, resulting in a stronger overlap of orbitals, which finally leads to the unexpected high value of J.

6. Sila-trovacenophanes

Compounds in which carbon is bound to one of its higher homologues, such as silicon, form that particular branch of organometallic chemistry which has found the most extensive technical applications.

In 1872 Ladenburg obtained the first silicon oil, and in 1901 Kipping carried out the pioneering work concerning silicones proper. The large-scale production of silicones was triggered by the demand for new materials with special properties. The elucidations of the principles of polymerisation (Standinger, Nobel prize 1953), the development of a rational method to prepare the monomers (Rochov and Müller), and the silyleneferrocenylene polymers (Rosenberg, 1969)[99] started the interest in the formation and study of metallocene containing bridging elements of group 14. Dehalogenation of organochlororosilane affords organopolysilanes, that have been the focus of attention for technical applications. They have found use as precursors in the manufacture of ceramic fibres consisting of β-siliconcarbide.

Cyclic molecules attract considerable attention because of the questions they pose concerning structure, bonding, reactivity, and their function as precursors to solid-state materials and new polymer systems. Metallocenophanes are interesting, strained organometallic molecules, in which the presence of a single bridging atom connecting the two rings leads to a tilted structure.

The synthesis of 1,1'-ferrocenyldiphenylsilane, **23**, was the first example of a metallocenophane.[100] Since then, a considerable number of others ferrocenophanes has been prepared (e.g., with P, As, Ge, and Zr serving as bridging atoms).[101] Organosilane bis(arene) transition metal complexes have become an area of continued interest, due to their remarkable electronic properties, solvolytic lability, and potential precursors in inter- and intra-annularly bridged species.[102]

Short inter-annular bridges require deviation from the molecular geometry of the metallocene, such as ring tilt (α), and distortions of the bridging substituents from the ring plane (β). Hence, in metallocenophanes the rings are not planar and parallel as in simple metallocene molecules, but they are inclined towards each other and towards the bridging atom, and there is considerable bond angle distortion at the substituted carbon atoms of both rings.[103]

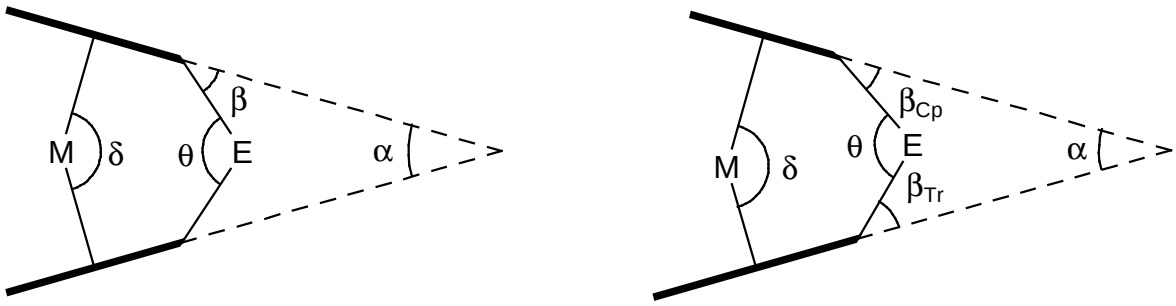

Fig. **38**: Molecular distortion in symmetrical and unsymmetrical metallocenophanes.[103]

Prewious works have shown that the strain present in [1]-silaferrocenophane profoundly influences the chemical reactivity observed for these molecules. Moreower, the discovery that [1]-silaferrocenophane undergoes spontaneous, exothermic, and quantitative thermally induced ROP reactions when heated above their meltinting points to yield poly(ferrocenylsilane), with an high molecular weight (M_w= 520.000, M_n= 340.000 according to gel permeation chromatography analysis) that corresponds to polymer chains with over 1200 repeated units.[104a]

6.1 Synthesis of [1,8-(Diphenylsilanediyl)(η^7-cycloheptatrienyl-η^5-cyclopentadienyl)vanadium], **24•**, and [1,8-(Tetramethyldisilane-1,2-diyl)(η^7-cycloheptatrienyl)(η^5-cyclopentadienyl)vanadium], **25•**

The accessibility of dilithiated trovacene allowed the synthesis of [1,8-(diphenylsilanediyl)(η^7-cycloheptatrienyl-η^5-cyclopentadienyl)vanadium], **24•**, and [1,8-(tetramethyldisilane-1,2-diyl)(η^7-cycloheptatrienyl)(η^5-cyclopentadienyl)vanadium], **25•**, by coupling reaction of 1,1'-dilithiotrovacene, with 1,2-dichlorodiphenylsilane and dichlorotetramethyldisilane, respectively (in analogy to reported examples in the chemistry of ferrocene and bis(benzene)chromium).[104,105]

The ring-tilt distortion observed is the sum of both types of distortion: ring-tilt using the vanadium atom as a fulcrum, and ring-tilt about the centroids of the rings.

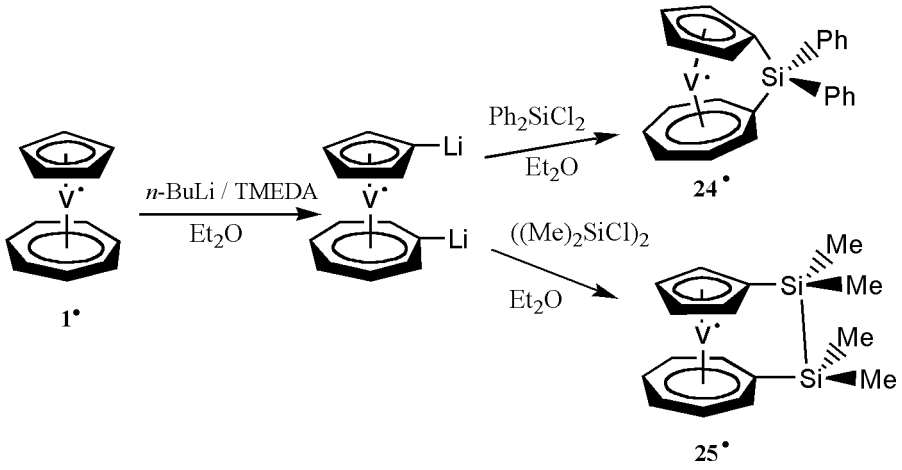

6.2 Structure of [1,8-(Diphenylsilanediyl)(η^7-cycloheptatrienyl-η^5-cyclopentadienyl)vanadium], 24•

[1,8-(Diphenylsilanediyl)(η^7-cycloheptatrienyl)(η^5-cyclopentadienyl)vanadium], **24•**, crystallizes from an ether solution at –20°C in form of violet needles.

Crystals are monoclinic with space group $P2_1/n$; lattice constants *a*= 1114.3(2) pm; *b*= 1527.0(2) pm; *c*= 1190.7(2) pm; with four molecules per unit cell. The molecular structure is shown in Fig. **39**, and important parameters are given in Table **20-21**.

The structure shows that the rings are planar and inclined at an angle of 17° (α), in analogy to the reported examples of μ-(1,1'-ferrocenyldiphenylsilane), **26**,[104] where the respective value is 19.2°, and of μ-(1,1',6,6'-tetraphenylsilanechromium), **27**,[105] where the tilting amounts to 14.6°. The C(1)–Si–C(8) bridging angle is 98.17(8)°, hence the silicon atom has a distorted tetrahedral coordination. The deviation β' of the exocyclic bonds from the plane of the five-membered ring amounts to 33°, and the respective deviation β'' from the plane of the seven-membered ring amounts to 45°. Hence, this considerable distortion at the substituted carbon atoms, C(1) and C(8), is the dominant parameter of the strain in bridged trovacene, more important than the tilt angle of the ring (α), and the bond-angle distortion at the bridging silicon atom.

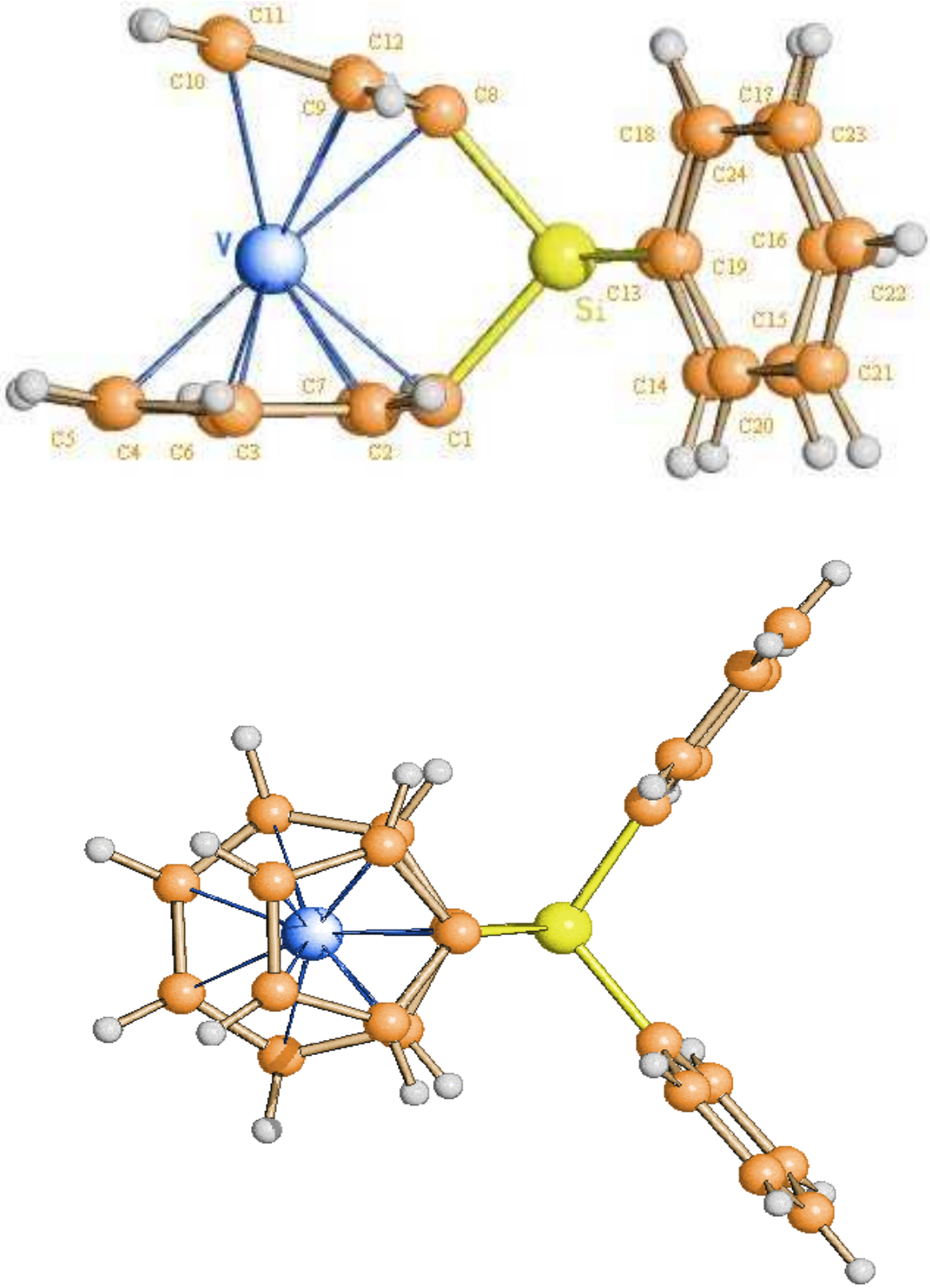

Fig. **39**: Molecular structure of **24**$^{\bullet}$ (a, top); alternative view of a molecule of **24**$^{\bullet}$ (b, bottom).

V(1)–Si(1)	2.880(7)	V(1)–C(1)	2.136(2)
V(1)–C(2)	2.163(2)	V(1)–C(3)	2.206(2)
V(1)–C(4)	2.210(2)	V(1)–C(5)	2.203(2)
V(1)–C(6)	2.203(2)	V(1)–C(7)	2.178(2)
V(1)–C(8)	2.216(2)	V(1)–C(9)	2.232(2)
V(1)–C(10)	2.273(2)	V(1)–C(11)	2.284(2)
V(1)–C(12)	2.240(2)	Si(1)–C(1)	1.988(2)
Si(1)–C(8)	1.877(2)	Si(1)–C(13)	1.866(2)
Si(1)–C(19)	1.863(2)	C(1)–C(2)	1.436(3)
C(1)–C(7)	1.435(3)	C(2)–C(3)	1.414(3)
C(3)–C(4)	1.409(3)	C(4)–C(5)	1.409(3)
C(5)–C(6)	1.410(3)	C(6)–C(7)	1.409(3)
C(8)–C(9)	1.436(3)	C(8)–C(12)	1.440(3)
C(9)–C(10)	1.410(3)	C(10)–C(11)	1.413(3)
C(11)–C(12)	1.411(3)	C(13)–C(14)	1.395(3)
C(13)–C(18)	1.392(3)	C(14)–C(15)	1.391(3)

Table **20**: Selected bond lengths (Å) for **24•**.

Si(1)–V(1)–C(1)	40.98(5)	Si(1)–V(1)–C(2)	64.57(6)
Si(1)–V(1)–C(3)	101.92(6)	Si(1)–V(1)–C(4)	134.62(6)
Si(1)–V(1)–C(5)	134.13(6)	Si(1)–V(1)–C(6)	100.73(6)
Si(1)–V(1)–C(7)	63.75(5)	Si(1)–V(1)–C(8)	40.67(5)
Si(1)–V(1)–C(9)	67.81(6)	Si(1)–V(1)–C(10)	100.97(6)
Si(1)–V(1)–C(11)	100.76(6)	Si(1)–V(1)–C(12)	67.41(5)

Table **21**: Selected bond angles (deg) for **24•**.

6.3 Structure of [1,8-(Tetramethyldisilane-1,2-diyl)(η^7-cycloheptatrienyl)(η^5-cyclopentadienyl)vanadium], 25•

[1,8-(Tetramethyldisilane-1,2-diyl)(η^7-cycloheptatrienyl)(η^5-cyclopentadienyl)vanadium], **25•**, crystallizes from an ether solution at –20°C in form of violet needles.

The crystals are monoclinic with space group $P2_1$; lattice constants *a*= 664.0(1) pm; *b*= 1310.9(1) pm; *c*= 944.8(1) pm; with four molecules per unit cell. The molecular structure is shown in Fig. **40**, and important parameters are given in Table **22-23**.

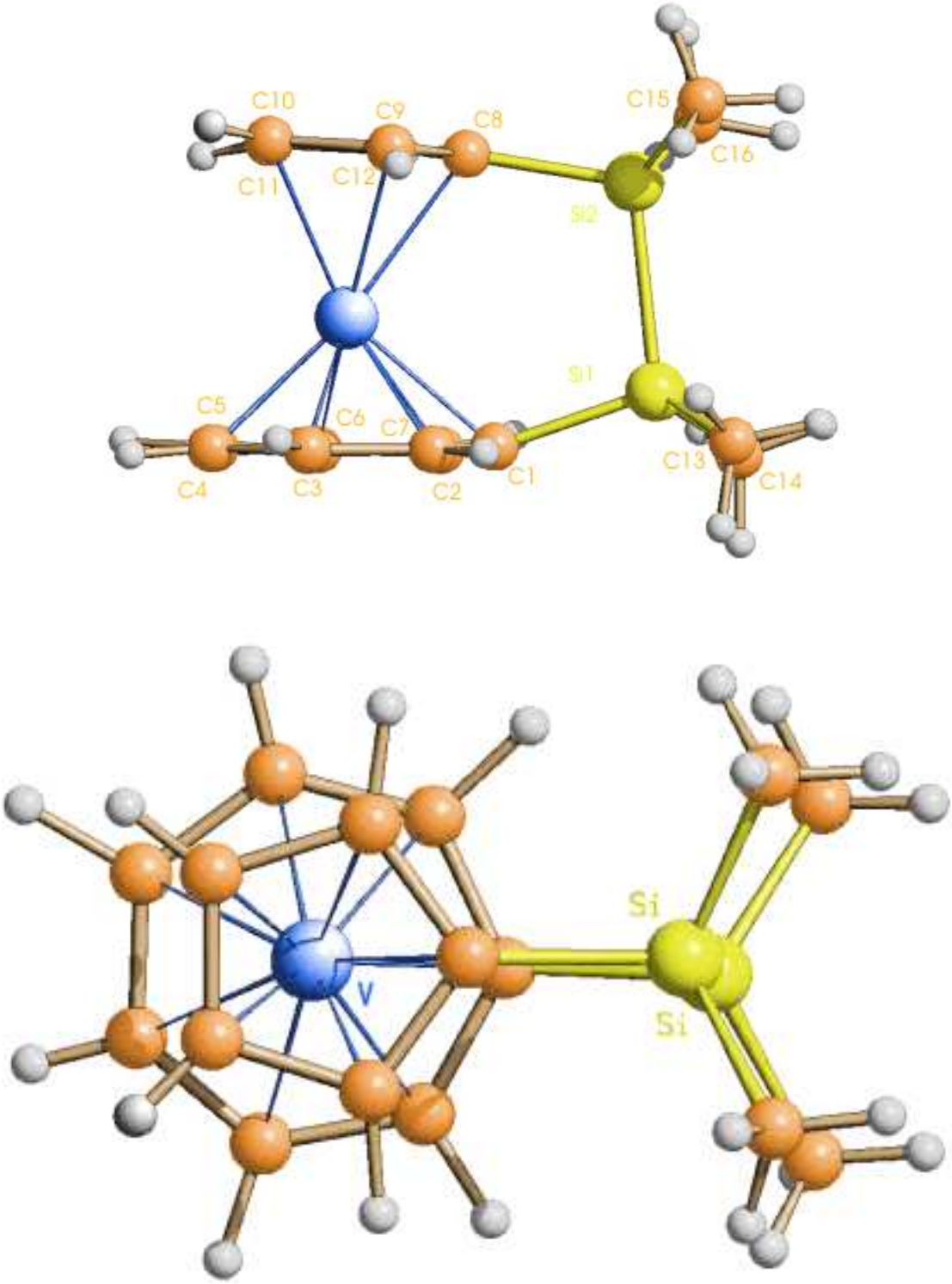

Fig. **40**: Molecular structure of **25**$^{\bullet}$ (a, top); alternative view of a molecule of **25**$^{\bullet}$ (b, bottom).

V(1)–C(1)	2.191(4)	V(1)–C(2)	2.191(5)
V(1)–C(3)	2.189(6)	V(1)–C(4)	2.196(6)
V(1)–C(5)	2.199(5)	V(1)–C(6)	2.194(5)
V(1)–C(7)	2.191(5)	V(1)–C(8)	2.262(6)
V(1)–C(9)	2.267(6)	V(1)–C(10)	2.267(6)
V(1)–C(11)	2.266(6)	V(1)–C(12)	2.255(6)
Si(1)–Si(2)	2.355(2)	Si(1)–C(1)	1.894(6)
Si(1)–C(13)	1.887(6)	Si(1)–C(14)	1.876(6)
Si(2)–C(8)	1.890(6)	Si(2)–C(15)	1.875(6)
Si(2)–C(16)	1.858(6)	C(1)–C(2)	1.433(7)
C(1)–C(7)	1.431(7)	C(2)–C(3)	1.410(8)
C(3)–C(4)	1.431(8)	C(4)–C(5)	1.405(9)
C(5)–C(6)	1.404(9)	C(6)–C(7)	1.416(8)
C(8)–C(9)	1.419(8)	C(8)–C(12)	1.414(8)
C(9)–C(10)	1.429(9)	C(10)–C(11)	1.42(1)
C(11)–C(12)	1.43(1)		

Table **24**: Selected bond lengths (Å) for **25**$^{\bullet}$.

Si(2)–Si(1)–C(1)	102.9(1)	Si(2)–Si(1)–C(13)	112.7(2)
Si(2)–Si(1)–C(14)	112.5(2)	C(1)–Si(1)–C(13)	111.0(2)
C(1)–Si(1)–C(14)	109.1(2)	C(13)–Si(1)–C(14)	108.5(3)
Si(1)–Si(2)–C(8)	105.4(2)	Si(1)–Si(2)–C(15)	113.2(2)
Si(1)–Si(2)–C(16)	112.4(2)	C(8)–Si(2)–C(15)	108.8(3)
C(8)–Si(2)–C(16)	108.3(3)	C(15)–Si(2)–C(16)	108.5(3)
V(1)–C(1)–Si(1)	120.0(2)	Si(1)–C(1)–C(2)	115.6(3)
Si(1)–C(1)–C(7)	116.3(3)	Si(2)–C(8)–C(9)	126.2(5)
V(1)–C(8)–Si(2)	116.7(3)	Si(2)–C(8)–C(12)	126.2(5)

Table **25**: Selected bond angles (deg) for **25**$^{\bullet}$.

The Si-Si and Si-C bonds show the manner in which the strain caused by bridging is relieved by bond elongation rather than by significant twisting, since the dihedral angle between the two rings is very low, 4°. The same applies to μ-(1,1'-ferrocenyltetramethyldisilanylene), **28**, where the respective angle measures 4.3°.[104] Overall, the larger silicon covalent radius, which governs the Si-Si and Si-C_{rings} bond lengths, permits the energetically more favourable parallel disposition of the rings in the structure. The eclipsed conformation of the Si_2Me_4 bridge is another reflection of the greater covalent radius of silicon compared to carbon. The C_{methyl}-Si-C_{methyl} bond angles (108.5(3)°) are larger than the $C_{5\text{-ring}}$-Si-Si angle (105.4(2)°) and $C_{7\text{-ring}}$-Si-Si angle, (102.9(1)°), reflecting the constraint within the bridging cycle.

6.4 Comparison of the two Structures

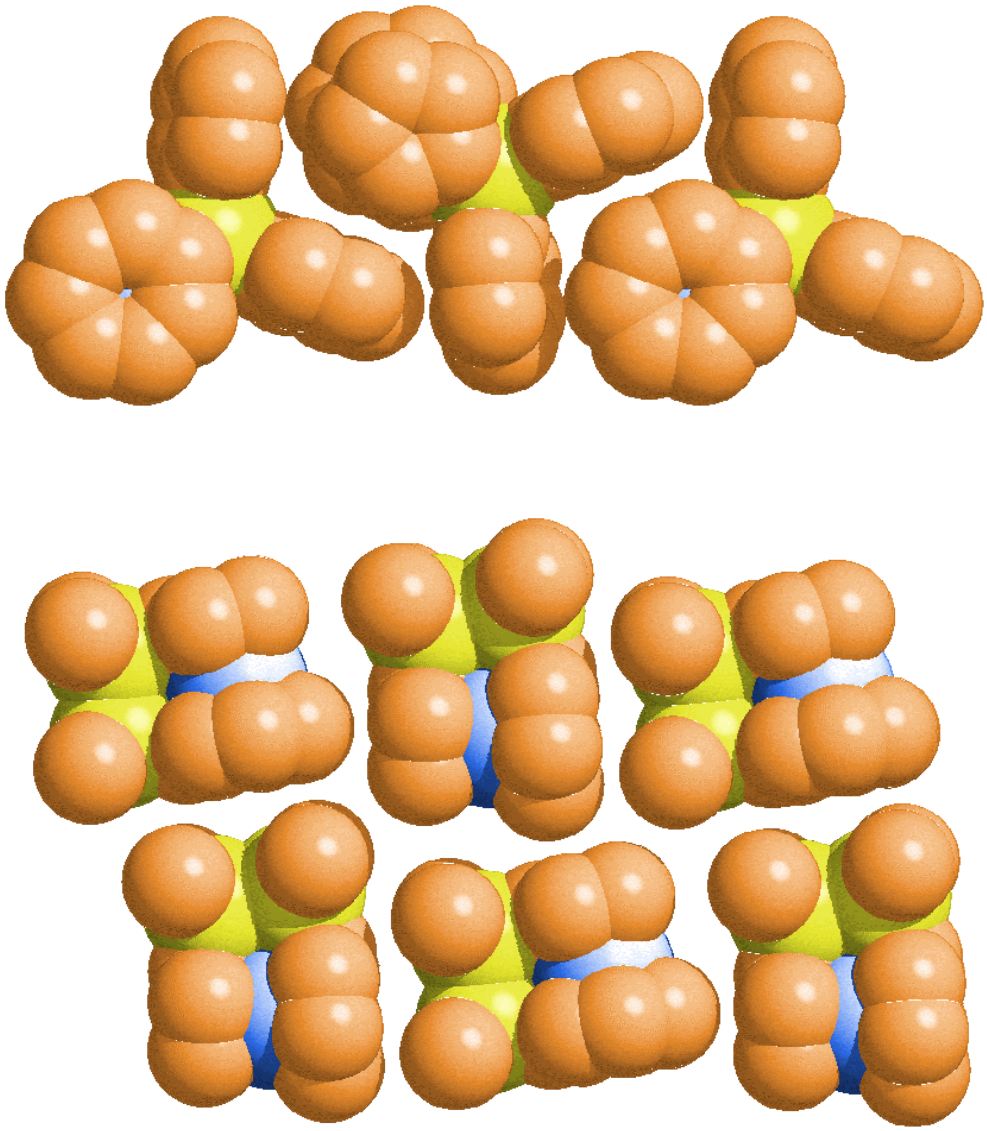

Fig. **41**: Molecular row of **24**$^{\bullet}$ along the *b*-axis (a, top); molecular layer of **25**$^{\bullet}$ (b, bottom).

The most significant difference between the two compounds is the tilt angle α between the planes of the cyclopentadienyl- and the cyloheptatrienyl-ring: 17° in μ-(1,1'-trovacenyldiphenylsilane) **24**$^{\bullet}$ and 4° in μ-(1,1'-trovacenyltetramethyldisilanylene) **25**$^{\bullet}$. The different degrees of ring tilting can also be appreciated by comparing the Cp-V-Tr angle δ: the detected angle δ= 81.64(7)° in compound **24**$^{\bullet}$ is indicative of greater tilting compared to compound **25**$^{\bullet}$, where the respective value is 94.9(2)°. The presence of additional strain in **24**$^{\bullet}$ is evidenced by the angles β_{Cp} and β_{Tr} (see Fig. **38**) between the planes of the

cyclopentadienyl- and the cyloheptatrienyl-ligands and the C(ring)-Si bonds: the observed values of β_{Tr}= 33° and β_{Cp}= 45° in **24•** are much greater compared to those of 4° and 18° in **25•**. This dramatic distortion from planarity at the ipso ring carbon atoms bonded to silicon is almost certainly the reason for the particular physical properties of the trovacenophane **24•**.

In **24•** the angle C(Cp)-Si-C(Tr), θ, is very small, 98.17(8)°, in comparison to an idealized value of 109.5° for an sp^3-hybridized silicon atom. The small θ angle in **24•** causes a minor widening of the C(Ph)-Si-C(Ph) angle to a value of 111.67(9)°, significantly greater than the corresponding angle found in **25•** (average 104.15(2)°). The bond lengths between the carbon atoms of the rings and the bridging silicon atom (in **24•**: 1.877(2) Å for C(Cp)-Si, and 1.889(2) Å for C(Tr)-Si; in **25•**: 1.890(6) Å for C(Cp)-Si, and 1.894(6) Å for C(Tr)-Si) differ very slightly between the two compounds. In addition, in the packing of molecule **24•** no strong C-H···π interactions between ring protons of a molecule and the phenyl groups of the adjacent molecule are present (value found for the nearest H_{Cp} to the phenyl groups: H···C_{Ph}(centroid) 3.21 Å), in contrast to [5]-trovacenol, **29•**, in which interactions of slightly positively charged hydrogen atoms of a Tr ligand with the electron-rich π-electron system of an adjacent Cp ligand is observed (value found: H···C_{Cp}(centroid) 2.700 Å) [strong interactions of this type have values in the range 2.5-3.0 Å, as can be deduced from an examination of the Cambridge Structural Database].[106]

6.5 Cyclic Voltammetry of $24^{\bullet}$ and $25^{\bullet}$

Among the multitude of electroanalytical techniques available to study electroactive species, cyclic voltammetry has proven to be most advantageous for evaluating the effects of ligands on the oxidation/reduction potential of the central metal. This advantage derives from the minimal quantities of substance necessary, and the capability of cyclic voltammetry to rapidly convey information concerning the redox behavior of a substance over a wide potential range. Trovacene has been the subject of previous cyclovoltammetric investigation,[107] and provides a basis for assessing the electrochemical effects of methyl-, and phenyl-silane bridging in the mono-, and di-sila-trovacenophanes. The interest in cyclovoltammetric investigation of the two sila-complexes is due to the pronunced electron-withdrawing character of the silyl-substituents. This should cause a substantial anodic shift in the oxidation potential (M^0/M^+), and in the reduction potential (M^0/M^-). Precise data will be useful for ascertaining changes in electronic structure, attributable to ring tilt in the two complexes (especially in mono-silyltrovacenophane).

Cyclovoltammetric data for the two organosilane-substituted trovacene complexes, and for the parent molecule trovacene, **1**$^{\bullet}$, are presented in Table **26**. Typical cyclovoltammetric traces for **24**$^{\bullet}$ and **25**$^{\bullet}$ are depicted in Figs. **42-43**.

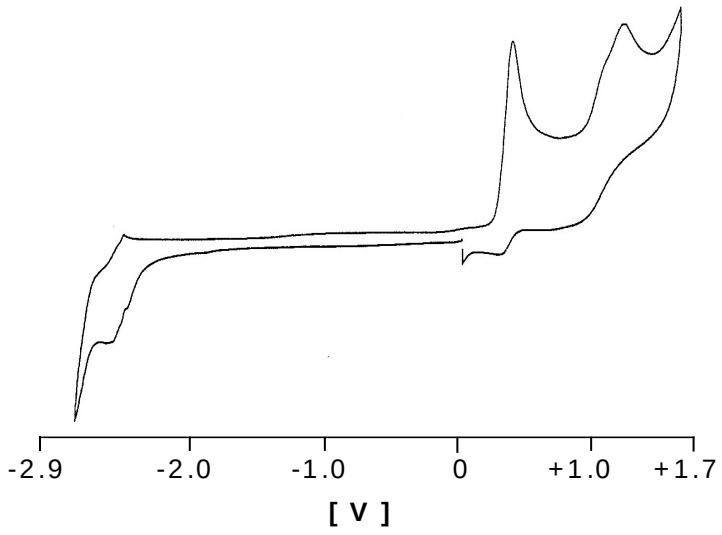

Fig. **42**: Cyclic voltammogram for **24**$^{\bullet}$.

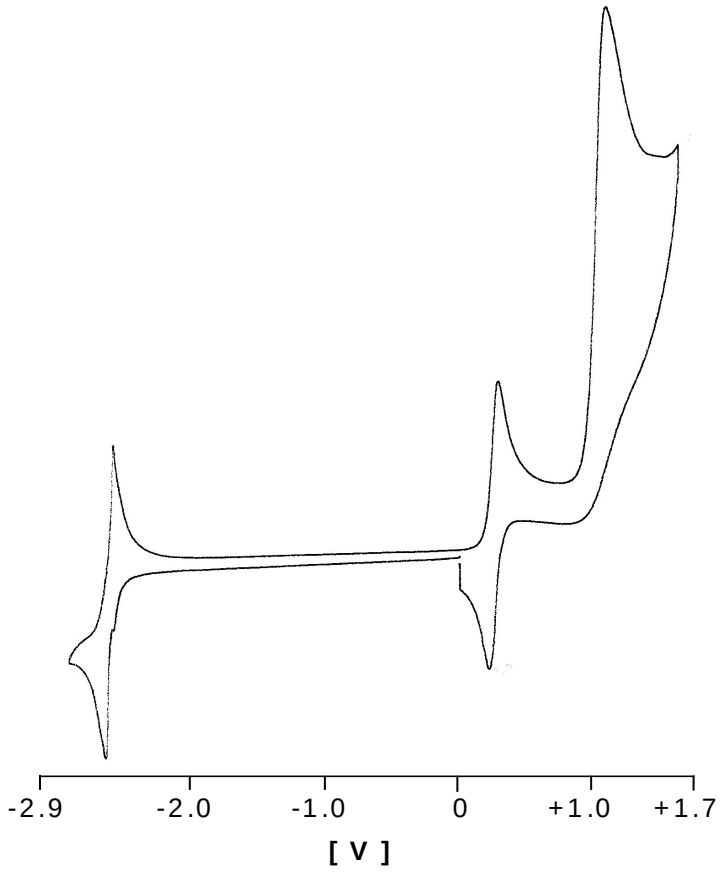

Fig. **43**: Cyclic voltammogram for **25•**.

	TVC(1)Si	**TVC(2)Si**	**TVC**
$E_{1/2}^{(0/+1)}$ [V]	E_{pa}= 376	0.248	0.260
	E_{pc}= 287		
ΔE_p[a] [mV]		76	64
$r=i_{pa}/i_{pc}$		1	0.93
E_{pa}[b] [mV]	1.025	1.066	1.03
$E_{1/2}^{(0/-1)}$ [V]	-2.473	–2.489	–2.55
ΔE_p[a] [mV]	41	66	66
$r=i_{pa}/i_{pc}$	1	1	1

[a] $\Delta Ep= (E_{pa} - E_{pc})$ [b] irreversible

Table **26**: Cyclovoltammetric data for **24•**, **25•** measured in DME/0.1 M TBAP, vs. SCE, ν= 0.1 V/s, T=-40°C.

The silatrovacenophane **25**$^{\bullet}$ displays an oxidation potential almost equal to that of the parent complex trovacene, **1**$^{\bullet}$. This finding may be rationalized in terms of electron donation from the silicon-silicon σ bond to the rings π orbitals (σ-π conjugation), and a withdrawal effect of ring electron density through silicon *d* orbital overlap. The sum of both effects gives no oxidation potential shift.

Due to the high sensitivity of the strained trovacenophane **24**$^{\bullet}$, bearing a single silicon atom bridge, the cyclic voltammogram is reproducible at the scan rates used in this study only for a few cycles. This cycling results in a gradual decomposition that produces a transient uncharacterized species. This fact reflects the aggregate action of silyl-substitution and bending of the sandwich structure. It may be postulated a ring opening induced by electron transfer. The same effect has been reported also for the corresponding ferrocenophane,[108] and for the respective bis(benzene)chromium derivative,[109] where a collection of data is prevented by its high sensitivity towards bridge cleavage. Oxidation of the metal center promotes bridge cleavage, thereby releasing the considerable structural strain inflicted by the bridging unit. In contrast, the reversibility noted for **25**$^{\bullet}$, reflects the lower degree of structural strain due to the -R_4Si_2- bridge. In this context, the data are in accordance with those collected for the analoguous bis(benzene)chromium derivative.

The quantum mechanical calculations of Hoffman and Lauher[110] for the titanocene molecule, Cp_2Ti, are helpful to explain the effect of deformation of the sandwich structure in bis(arene)metal-types, especially the tilting of the ring-metal-ring axis, on their redox potential. The authors studied the dependence of the energies of frontier orbitals on the tilting angle θ (see Figs. **44** and **45**). An important result is the destabilization of a_1-orbitals, that reflects itself in a cathodic shift of the redox potential of the tilted complex with respect to its undistorted analogue. The change in reactivity induced by tilting is based not only on the increased steric interaction between the rings and their substituents, but also on the modification of the nature and energy of the frontier orbitals. Hence, the illustrated results predict an easier oxidation of a tilted metallocene.

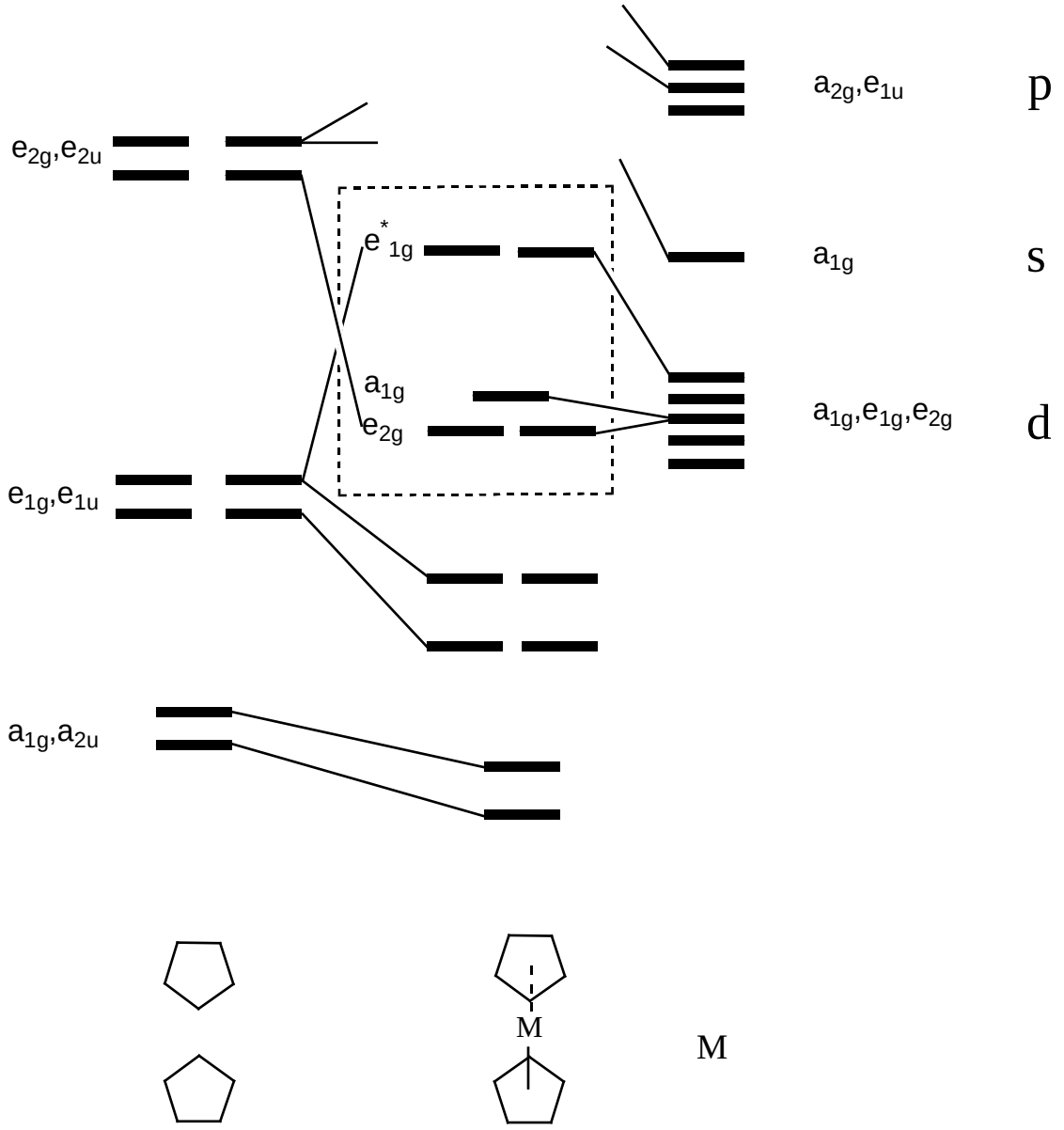

Fig. **44**: Interaction diagram for a D_{5d} metallocene (the frontier orbitals are in the box).[110]

As it is shown in Figs. **44** and **45**, in a D_{5d} metallocene the π orbitals of the two parallel Cp ligands yields three sets of nearly degenerate orbitals: a low-lying filled pair of a_{1g} and a_{2u} symmetry, a set of filled orbitals, e_{1g} and e_{1u}, and a high-lying empty set of anti-bonding orbitals of symmetry e_{2g} and e_{2u}. These orbitals interact with the orbitals of the metal yielding a strong interaction with the metal *s* and *p* orbitals and also a strong bonding interaction with the e_{1g} (d_{xz}, d_{yz}) set. The remaining *d* orbitals of the metal, the a_{1g} (d_z^2) and the e_{2g} ($d_{x^2-y^2}$) set remain essentially non-bonding.

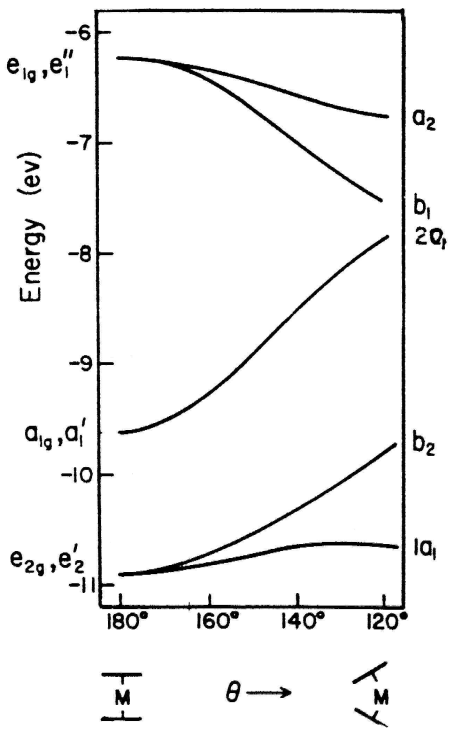

Fig. **45**: Cp_2M orbitals as a function of the bending angle.[110]

When there is a distortion of the Cp_2M moiety, an analysis focusing on the change in energy and shape of the Cp_2M fragment orbitals with θ (CpMCp angle),(Fig. **45**), it is noted that the b_2 and $2a_1$ orbitals rise in energy with increasing bending, decreasing θ. The basic trend noted in Fig. **45** is that the orbitals descended from e_{1g}^* are stabilized with bending and the orbitals derived from a_{1g} and e_{2g} are destabilized.

In the axially symmetric sandwich the a_{1g} orbital is predominantly metal d_z^2 in character; in the bent sandwich the HOMO $2a_1$ is allowed to mix with the sub-HOMO $1a_1$. Since the $1a_1$, being derived from e_{2g}, possesses a sizeable ligand contribution, $2a_1$ will also acquire some ligand character. Thus, a singly occupied HOMO $2a_1$ provides for spin transfer to the ligands, leading to diminished spin population on the central metal.

6.6 EPR of 24• and 25•

ESR spectra of the two silatrovacenophanes **24•**, **25•**, in fluid and in rigid solution are shown in Fig. **46**, and the parameters are collected in Table **27**.

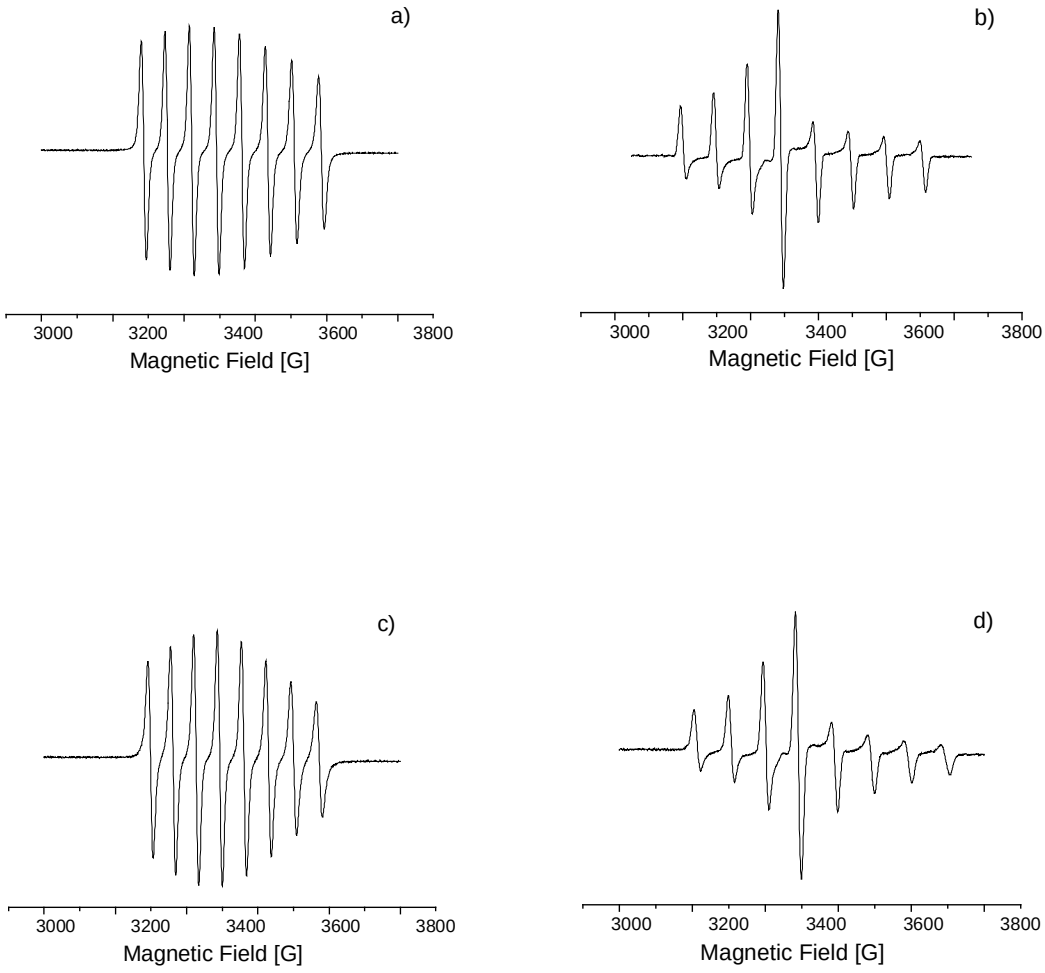

Fig. **46**: EPR spectra of **24•** in toluene: a) at 295 K, b) at 127 K, frequency 9.2688 GHz, and spectra of **25•** in toluene: c) at 295 K, d) at 121 K, frequency: 9.2688 GHz.

	TVC(1)Si	TVC(2)Si
<g>	1.984	1.984
g_1	1.974	1.976
g_2	1.973	1.977
g_3	1.996	1.999
a(^{1}H)/ [G]	2.49	3.04
a_{iso}/[G]	-67.6	-70.6
A_1/[G]	96.8	103.4
A_2/[G]	100.7	101.0
A_3/[G]	6.1	7.5

Table **27:** EPR parameters of the sila-complexes **24$^\bullet$**, and **25$^\bullet$**.

A comparison of the EPR parameters demonstrates that disila-, and mono-sila-trovacenophane form a homologous series, in which several trends are evident:

–substitution by silicon groups and tilting leaves the value of <g>, and its anisotropic components virtually unaffected;

–the vanadium hyperfine coupling constant a(^{51}V) decreases in the order TVC(2)Si>TVC(1)Si, indicating a greater degree of metal→ligand spin transfer in proceeding from **25$^\bullet$** (4°) (in which the rings are almost parallel) to **24$^\bullet$** (with a tilt angle between the rings of 17°). This decrease concords with the reduced ring tilt, in that in an untilted complex, the π-orbitals of the arene ligands lie in the nodal plane of the metal d_z^2-orbital, i.e., they are essentially non-interacting. Upon ring tilting, these orbitals become increasingly σ-antibonding, thereby rising in orbital energy, by increasing metal d_z^2-orbital-π-orbital mixing,[110] which in turn facilitates spin delocalisation from the metal center onto the ligands. Therefore a(^{1}H, **25$^\bullet$**)> a(^{1}H, **24$^\bullet$**);

–the line width dependence from the nuclear spin quantum number M_I(^{51}V) increases in the series: TVC(1)Si>TVC(2)Si, in line with the increase of effective molecular radius.

6.7 Poly(trovacenylsilane)

The incorporation of transition elements into a polymer main chain would be expected to allow access to processable materials with unusual and useful properties (i.e., electrical, magnetic, optical, catalytic).[111] This is particularly the case where the metal atoms are present in the main chain in close spatial proximity to one another so as to promote cooperative interactions.[112]

Organopolysilanes, although containing sp^3-hybridized Si atoms, display conjugation to a certain extent. Therefore, it appeared interesting to prepare organopolysilanes which also contain paramagnetic building blocks in order to investigate spin-spin interaction.[113]

Hence, it is of interest to see whether the reaction of α,ω dichlorosilanes with metalated trovacenes would lead to polymers, in addition to the expected sila-trovacenophanes:

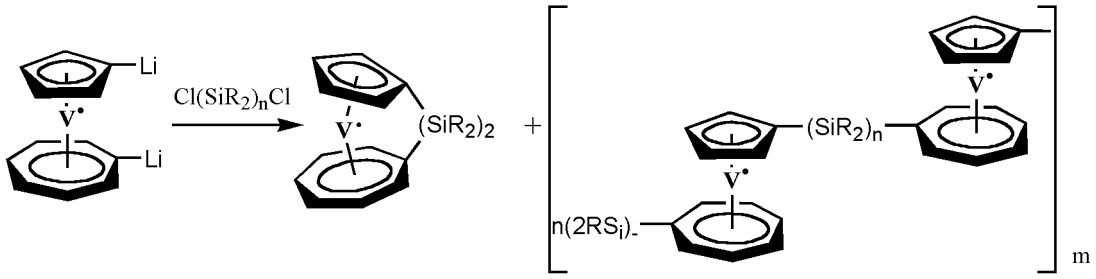

The study of organometallic polymers is become an area of growing interest, since such systems can be useful precursors to novel materials. Especially, the exploration of processable high molecular weight polymers with skeletal transition-metal atoms has generated interest for their large potential in applications such as materials with novel electrical, optical, or magnetic properties. The discovery that strained, ring-tilted metallocenophanes, such as the silicon-bridge 1,1-dimethyl-1-silaferrocenophane, **30**, undergo thermal ring-opening polymerisation (ROP) to afford poly(ferrocenylsilane), has provided access to a range of new transition metal-based polymers with intriguing properties.[104]

The corresponding sila-derivative of trovacene, [1,1-(dimethylsilandiyl)(η^7-cyclohepta-trienyl)(η^5-cyclopentadienyl)vanadium], **31$^\bullet$**, was synthesized as described below, and a ring-opening polymerization attempt was performed to obtain an organometallic polymer with paramagnetic properties.

Three different methods of polymerisation were tested:

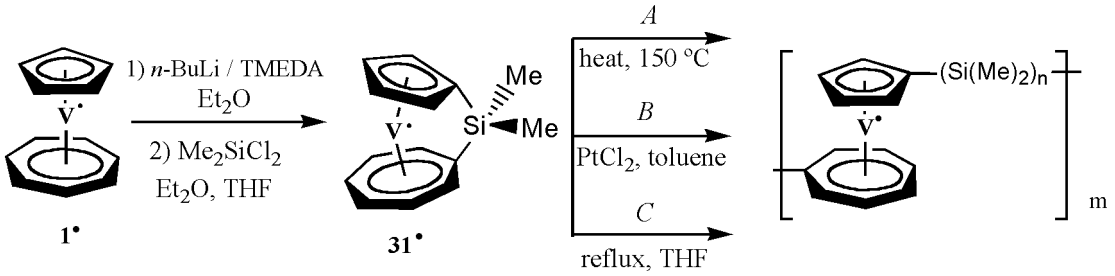

Since ring strain provides an important driving force for ring-opening polymerisation, **31•** would be an excellent candidate for polymerisation studies. The monomer **31•** was synthesised by slow addition of dimethyldichlorosilane to 1-1'-dilithiotrovacene, affording a violet oil. Unexpectedly, the elementary analysis of the product showed a nitrogen content of 2.6%, which may be attributed to an incorporation of TMEDA that was used as chelating agent in the dimetalation of trovacene. In the analysis of the fragmentation pattern of the mass spectrum, in addition to the molecular peak of the monomer (m/z= 264), an unexpected peak at m/z= 734, corresponding to a trimer after loss of a dimethylsilyl unit, was observed. This result shows that a successful polymerisation cannot be excluded.

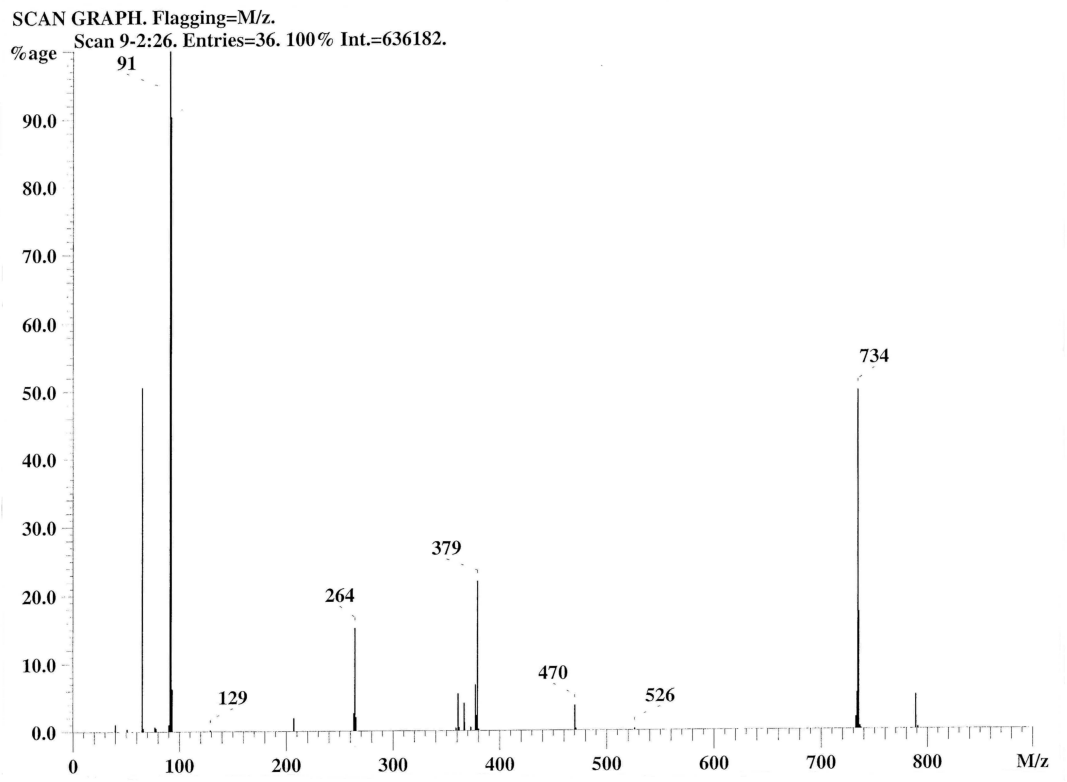

Fig. **47**: Fragmentation pattern in the mass spectrum of the product **31•**.

6.7.1 Polymerisation Attempts and Analysis of the Products

Method A[104]

When **31•** is heated in an evacuated, sealed Pyrex tube at 150 °C, the tube contents melt and then become gradually more viscous. After 20 minutes the tube content is completely immobile. Heating was continued for an additional 40 minutes at the same temperature. Finally, a dark violet solid was obtained, which is difficult soluble in diethyl ether, and soluble in toluene. Subsequent analysis of the product by mass spectroscopy indicates that a possible polymeric structure may be present. Elementary analysis values show the presence of ca. 5% of nitrogen, probably due to coordination of TMEDA.

Polymerisation of the phenylated trovacenophane **24•** was also attempted under the same conditions as chosen for **31•**. No changes were observed in the sealed tube upon heating up to 200°C. Another experiment was performed in solution (EPR-tube under nitrogen), under monitoring the progress of the reaction with increasing temperature by EPR spectroscopy. However, a change in the spectra was not observed. The failure of any polymerisation was also confirmed by the absence of peaks above the mass of the monomer in the mass spectrum of the sample after the heating.

Method B[114]

This method comprises ring-opening polymerisation of this species under employment of $PtCl_2$ as catalyst. The reaction of the crude **31•**, was performed in toluene solution at 80°C during 2 hours in presence of a trace of $PtCl_2$. The product, dark violet powder, was isolated by precipitation from toluene into an anti-solvent such as petroleum ether.
Mass spectroscopy analysis shows a peak of m/z= 943 (corresponding to a tetramer after loss of two dimethylsilyl units). Considering this result, a GPC measurement was undertaken to give a more accurate insight into the molecular mass distribution. The experiment was performed using THF as eluent, and polystyrene as standard. The weight average of the molecular mass, M_w, amounts to about 683, but in the plot is also noted that molecules with molar mass of about $2*10^3$ are present. Hence, the ring-opening polymerisation yielded mainly oligomers, but a small proportion of polymeric products was also formed.

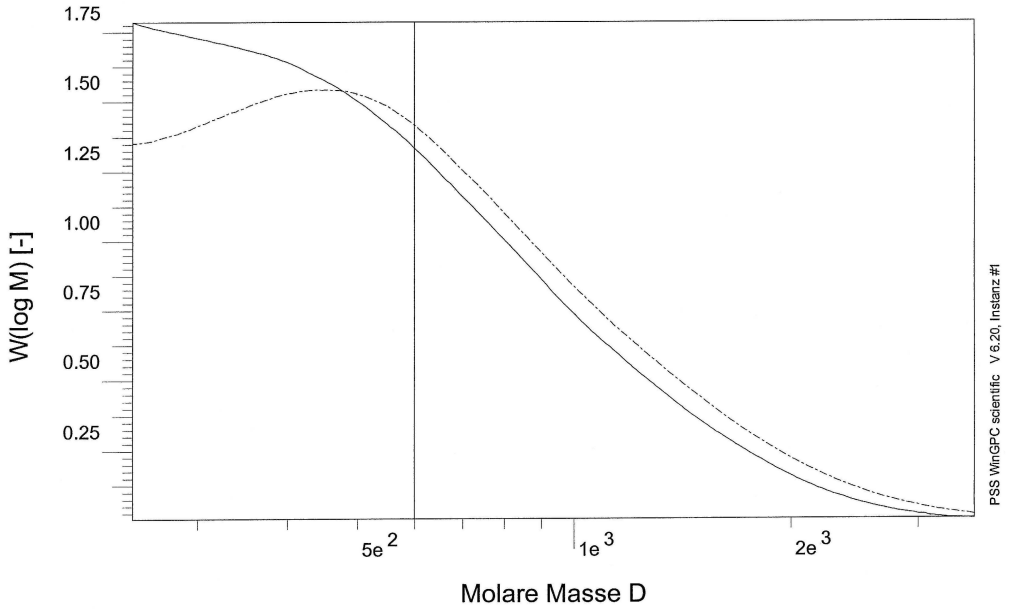

Fig. **48**: GPC experiment performed on the product of reaction obtained in accord to Method B. The dotted curve was obtained by UV-detection; the solid curve by index refraction-detection.

Method C[115]

The reaction between 1-1'-dilithiotrovacene and dimethyldichlorosilane was performed in refluxing THF during a period of 7 hours. After removal of the solvent, the residue was dissolved in toluene and precipitated by addition of petroleum ether to yield a brown-violet precipitate. Analysis of the products of repeated reactions under similar conditions by mass spectroscopy showed in one case the formation of a dimer, and in another case the formation of a trimer. In elemental analysis no nitrogen was found. Attempts to separate and/or purify the dimer and the trimer (by chromatographic column or crystallization) were unsuccessful. It was not possible to control the reaction conditions to yield selectively only one product.

EPR studies were undertaken in all three cases: the first two methods show an eight-line spectrum, with broad lines, corresponding to a big molecule that rotates slowly in solution (in each spectrum a high percentage of monomer is present). The reaction products obtained by method C show a superimposed fifteen-line spectrum and twenty two-line spectrum in

varying proportions. Hence, both spectra reveal a mixture of monomer and dimer as well as trimer, as already suggested by the results of mass spectroscopy. A simulation of the recorded EPR spectra was not possible, since the proportion of the monomer was too high, and since the structure of the oligomers was unknown. EPR spectra described above are shown in Fig. **49**.

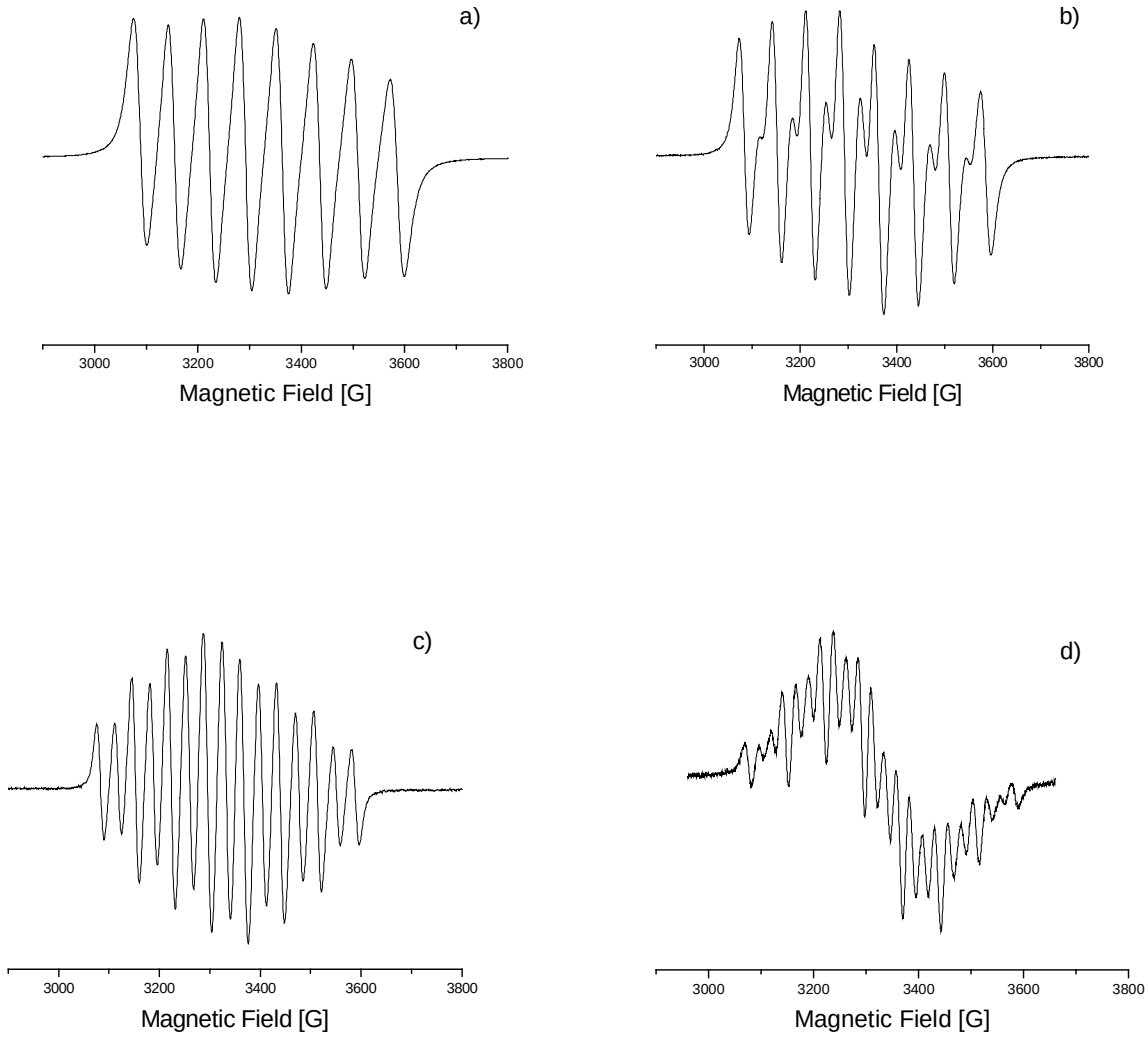

Fig. **49**: EPR spectra of the products of polymerization attempts: a) in toluene at 298 K, 9.2680 GHz; b) in toluene at 298 K, 9.2632 GHz; c) in toluene at 298 K, 9.2625 GHz; d) in toluene at 290 K, 9.2472 GHz.

In order to interpret the results obtained from EPR and mass spectrometry it is helpful to take account of the mechanisms proposed for the ROP of [1]ferrocenophanes, in which the presence of dimeric and trimeric species is postulated.

The mechanism for the polymerisation of sila-metallocenophanes is still under investigation. However, experiments have suggested that the bond cleavage during thermal ROP of silicon-bridged [1]ferrocenophanes occurs via heterolytic cleavage of the Si-Cp bond rather than a homolytic process.[116] Such cleavage might be initiated by minute traces of nucleophilic impurities (e.g. water). Alternatively, thermal heterolytic cleavage might afford a small population of zwitterionic, resonance stabilized species with positive charge at silicon and negative charge at the Cp ring, which could then initiate chain propagation by nucleophilic attack at the silicon atom of the initial monomer. However, a mechanism such as ring fusion via σ-bond metathesis is also possible.[117] In this case, the Si-C(Cp) bonds of the silaferrocenophane add to those of another molecule to yield a cyclic dimmers via a four-center transition state. The cyclic dimmer formed could than undergo the same reaction with monomer to yield a cyclic trimer, and these ring-fusion processes could continue until polymer is generated.

A mechanism proposed for the bond cleavage by metal halide catalyst (e.g. $PtCl_2$) involves initial oxidative-addition of a strained Si-C bond to the coordinatively unsatured metal center, chlorine transfer from the metal to silicon generating a growing chain and repetitive oxidative addition/reductive elimination steps for chain propagation.[118]

7. Benzoic Acid and Benzoate π-Complexes of Chromium

The concept of utilizing organometallic building blocks, which permits to introduce the characteristics of transition metals (such as redox processes, ionic charges and paramagnetism) into the crystals, are substantial to prepare novel materials.[22]

In this work, organometallic carboxylic acids, where use as units in the construction of crystal lattices. Aggregation is effect by means of hydrogen bonding which can be influenced by two oxidation states of the central metal atom as well as by the degree of protonation. The latter derives from the fact, that hydrogen bonding ability of -COOH and -COO^- groups obviously differ.

The neutral dicarboxylic acid $[Cr^0(\eta^6\text{-}C_6H_5COOH)_2]$ **4(H)$_2$** and its cation $[Cr^I(\eta^6\text{-}C_6H_5COOH)_2]^+$ **4(H)$_2^{+\bullet}$** have different magnetic properties: **4(H)$_2$** is diamagnetic, while **4(H)$_2^{+\bullet}$** is a 17-electron paramagnetic complex. These species offer a large number of combinations of hydrogen bonding donor/acceptor capacity together with different ionic charges. Removal of protons from neutral **4(H)$_2$** leads to sequential formation of a monoanion and of a dianion. Deprotonation of **4(H)$_2^{+\bullet}$** leads first to formation of the neutral sandwich zwitterion $[Cr^I(\eta^6\text{-}C_6H_5COOH)(\eta^6\text{-}C_6H_5COO^-)]$ **4(H)$^\bullet$**, with one -COOH and one -COO(-) system. Removal of protons from **4(H)$^\bullet$** leads to the dicarboxylate monoanion $[Cr^I(\eta^6\text{-}C_6H_5COO)_2]^-$ **4$^{-\bullet}$** with two -COO(-) groups.

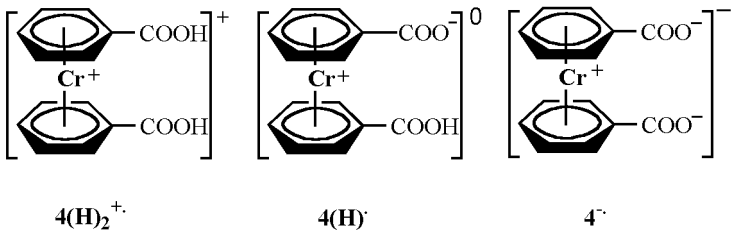

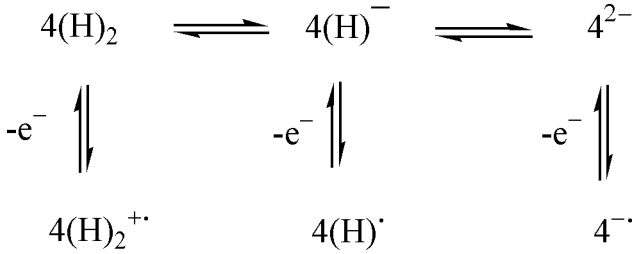

Hence, the fundamental building block "Cr(η^6-$C_6H_5COO)_2$" can participate, depending on the extent of protonation and on the metal atom oxidation state, in hydrogen bonding networks as a monocation, as a neutral species, and as a mono- and di-anion building block.

A comparison will be carried out with the almost isostructural complexes based on ferrocene, namely [Fe^{II}(η^5-$C_5H_4COOH)_2$], **32**,[119] (known in two polymorphic modifications), and on the cobaltocenium cation, namely [Co^{III}(η^5-$C_5H_4COOH)_2$]$^+$[PF_6]$^-$,[120] **33**$^+$, which are isoelectronic and diamagnetic.

7.1 Synthesis of 1,1'-Bis(carboxy-η^6-benzene)chromium, [(η^6-$C_6H_5COOH)_2Cr^0$], 4(H)$_2$

The neutral dicarboxylic acid **4(H)$_2$**, was synthesized by lithiation of bis(benzene)chromium in methylcyclohexane solution with *n*-BuLi and TMEDA, as it is described in literature[121] (a pioneer work concerned the synthesis of the correspondent ester).[122]

CO_2 was bubbled through the solution containing the 1,1'-dilithiated complex. Finally, the free dicarboxylic acid was obtained by hydrolysis with dilute aqueous HCl. The red powder obtained exposed to air produces immediately the cationic form (oxidation to chromium^I), recognizable by a turn of colour to orange. The complex is almost insoluble in organic solvents, but good soluble in hot water.

Its vanadium analogue, 1,1'-bis(carboxy-η^6-benzene)vanadium, [(η^6-$C_6H_5COOH)_2V^0$], **34**$^\bullet$, due to its radical character, offers the possibility to study electron-electron spin-spin interaction between the metal centers in molecules linked by hydrogen bonds.[50]

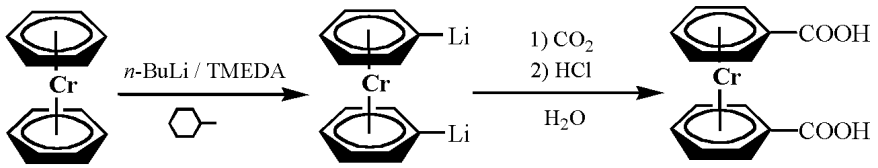

4 **4(H)$_2$**

7.2 Structure of 1,1'-Bis(carboxy-η^6-benzene)chromium, $4(H)_2$

1,1'-bis(carboxy-η^6-benzene)chromium, $4(H)_2$ forms a dimer in the crystal via a pair of typical hydrogen bonded eight membered rings involving the two -COOH groups of the acid. The molecular structure of **$4(H)_2$** is shown in Fig. **50**. Important parameters are given in Table **28-29**.

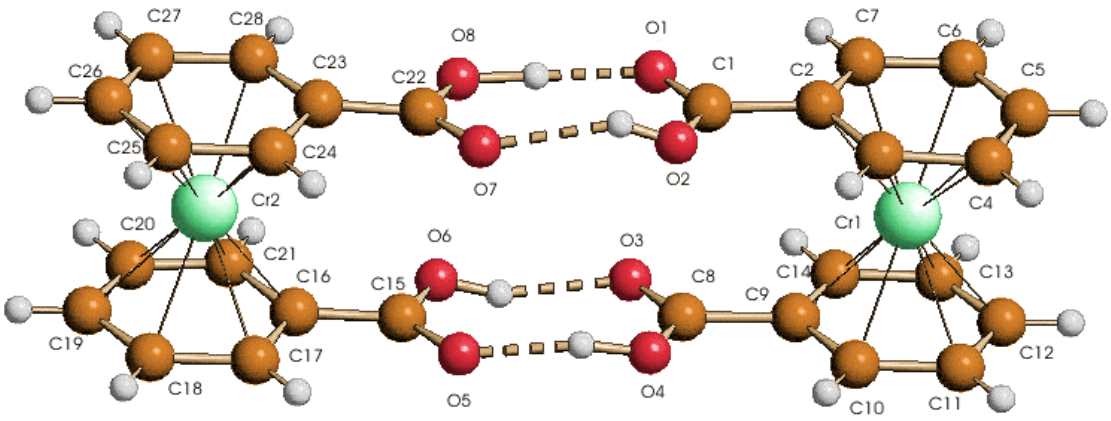

Fig. **50**: Representation of the dimers formed by molecules of **$4(H)_2$** in the solid state.

Twin intermolecular hydrogen bonding of the type are not very common because their formation requires a degree of structural flexibility that cannot be adopted by the sigma skeleton of the C-C–bonds in organic acids. In fact, it is observed that dicarboxylic organic acids tend to form chains in the solid state, rather than self-assemble in dimeric units. In contrast, compound **$4(H)_2$** can rotate around the coordination axis of the carbocyclic ligands to yield the eclipsed conformation of the -COOH groups required for the formation of the dimer. Indeed, a comparable situation can only be found in other organometallic sandwich molecules such as ferrocene dicarboxilic acid, **32**.

The dicarboxilic acid of ferrocene, **32** is known a monoclinic and a triclinic form, which contain exactly the same type of dimeric unit, although in different packings in the solid state. The three crystals are formed by layers of dimers arranged in continguous rows. The main difference between the packings of 1,1'-bis(carboxyl-η^6-benzene)chromium, **$4(H)_2$** and ferrocene dicarboxilic acid, **32** arises from the angles formed by the dimer long axes passing between two chromium or iron atoms (165° for **$4(H)_2$,** 90° and 100° for the two polymorphs

of. **32**, respectively) and for the dimer rotation around the same axes within the layer (90° for **4(H)$_2$**, 0° and 90° for the two polymorphs of **32**, respectively).

The hydrogen bonding parameters of the carboxylic acid dimers in the two neutral systems are very similar [O···O 2.558(2), 2.603(2), 2.638(2), 2.643(2) Å in **4(H)$_2$**; 2.593(2), 2.635(2) Å, and 2.620(2), 2.643(2), 2.625(2), 2.671(2) Å respectively in the two polymorphic modifications of **32**]. Both, **4(H)$_2$** and **32** crystals, show the presence of a web of intermolecular C-H---O interactions between the cyclopentadienyl or aryl hydrogen atoms and the oxygen atoms of the -COOH groups. In both crystals the dimers are aligned and the oxygen atoms of the same side interacts with the H atoms of the aromatic rings. Some of the values of (C)H---O distances and C-H---O angles, obtained for hydrogen positions normalized to neutron diffraction value of 1.08 Å, fall in the lower limit for this type of interactions, even if only organometallic molecules are considered.[123]

Cr(1)-C(11)	2.078(15)	Cr(1)-C(3)	2.122(8)
Cr(1)-C(9)	2.124(13)	Cr(1)-C(14)	2.132(11)
Cr(1)-C(10)	2.135(12)	Cr(1)-C(13)	2.133(13)
Cr(1)-C(7)	2.136(13)	Cr(1)-C(2)	2.141(13)
Cr(1)-C(4)	2.141(7)	Cr(1)-C(12)	2.149(13)
Cr(1)-C(5)	2.150(13)	Cr(1)-C(6)	2.177(13)
C(1)-O(1)	1.241(16)	C(1)-O(2)	1.272(18)
C(1)-C(2)	1.418(19)	O(2)-H(200)	1.0560
C(2)-C(3)	1.416(15)	C(2)-C(7)	1.486(19)
C(8)-O(4)	1.314(18)	C(8)-C(9)	1.45(2)
O(4)-H(400)	0.8627	C(9)-C(10)	1.417(18)
C(9)-C(14)	1.446(14)	C(10)-C(11)	1.35(2)
Cr(2)-C(18)	2.108(14)	Cr(2)-C(16)	2.115(11)
Cr(2)-C(17)	2.118(12)	Cr(2)-C(21)	2.127(10)
Cr(2)-C(19)	2.138(15)	Cr(2)-C(20)	2.142(10)
Cr(2)-C(28)	2.144(14)	Cr(2)-C(24)	2.147(10)
Cr(2)-C(23)	2.147(12)	Cr(2)-C(26)	2.168(13)
Cr(2)-C(25)	2.175(13)	Cr(2)-C(27)	2.215(14)
C(15)-O(6)	1.267(18)	C(15)-O(5)	1.276(17)
C(15)-C(16)	1.532(17)	O(2)-H(600)	0.0560
C(16)-C(17)	1.34(2)	C(16)-C(21)	1.489(16)
C(22)-O(7)	1.229(18)	C(22)-C(23)	1.520(16)
O(8)-H(800)	0.8097	C(23)-C(24)	1.376(17)
C(23)-C(28)	1.402(18)	C(24)-C(25)	1.379(18)

Table **28**: Selected bond lengths (Å) for **4(H)$_2$**.

O(1)-C(1)-O(2)	120.3(13)	O(1)-C(1)-C(2)	122.7(12)
O(2)-C(1)-C(1)	116.9(12)	C(1)-O(2)-H(200)	122.8
C(3)-C(2)-C(1)	123.1(11)	C(3)-C(2)-C(7)	119.0(12)
C(4)-C(3)-C(2)	119.8(6)	C(5)-C(4)-C(3)	121.8(6)
C(4)-C(5)-C(6)	121.9(11)	C(7)-C(6)-C(5)	118.9(13)
C(6)-C(7)-C(2)	119.7(13)	O(3)-C(8)-O(4)	121.8(14)
O(3)-C(8)-C(9)	123.2(14)	O(4)-C(8)-C(9)	115.0(12)
C(8)-O(4)-H(400)	112.3	C(10)-C(9)-C(14)	120.1(11)
C(10)-C(9)-C(8)	124.8(12)	C(14)-C(9)-C(8)	115.1(11)
C(11)-C(10)-C(9)	116.1(13)	C(10)-C(11)-C(12)	127.0(14)
C(13)-C(12)-C(11)	117.2(13)	C(12)-C(13)-C(14)	121.5(12)
C(13)-C(14)-C(9)	118.0(11)	O(6)-C(15)-O(5)	126.4(12)
O(6)-C(15)-C(16)	118.4(11)	O(5)-C(15)-C(16)	115.1(12)
C(15)-O(6)-H(600)	120.4	C(17)-C(16)-C(21)	122.3(12)
C(17)-C(16)-C(15)	121.1(11)	C(21)-C(16)-C(15)	116.6(12)
C(19)-C(18)-C(17)	122.4(13)	C(18)-C(19)-C(20)	118.7(12)
C(19)-C(20)-C(21)	119.0(9)	C(16)-C(21)-C(20)	118.6(10)
O(8)-C(22)-O(7)	125.4(11)	O(8)-C(22)-C(23)	120.0(11)
O(7)-C(22)-C(23)	114.6(12)	C(22)-O(8)-H(800)	111.1
C(24)-C(23)-C(28)	120.9(11)	C(24)-C(23)-C(22)	123.6(11)
C(28)-C(23)-C(22)	115.4(12)	C(25)-C(24)-C(23)	120.7(12)
C(24)-C(25)-C(26)	118.7(12)	C(27)-C(26)-C(25)	124.3(13)
C(26)-C(27)-C(28)	113.8(12)	C(23)-C(28)-C(27)	121.7(12)

Table **29**: Selected bond angles (deg) for **4(H)$_2$**.

7.3 Synthesis of [1,1'-Bis(carboxy-η^6-benzene)chromium^{I}][hexafluorophosphate], [(η^6-$C_6H_5COOH)_2Cr^{I}]^+[PF_6]^-$, $4(H)_2^{+\bullet}$ α and β Form, and [(Carboxy-η^6-benzene)(carboxylato-η^6-benzene)chromium^{I}][ammoniumhexafluorophosphate], $[Cr^1(\eta^6\text{-}C_6H_5COOH)(\eta^6\text{-}C_6H_5COO)]\bullet[NH_4][PF_6]$, $4(H)^{\bullet}$

The cationic form [1,1'-bis(carboxy-η^6-benzene)chromium][hexafluorophosphate], $4(H)_2^{+\bullet}$ **4(H)$_2^{+\bullet}$** α form and β form , and the zwitterionic form [(carboxy-η^6-benzene)(carboxylato-η^6-benzene)chromium^{I}][ammoniumhexafluorophosphate], **4(H)$^{\bullet}$**, were obtained by bubbling air through aqueous solutions of 1,1'-bis(carboxyl-η^6-benzene)chromium, **4(H)$_2$** and by adding a saturated solution of $[NH_4]^+[PF_6]^-$ under conditions (temperature, sequence of addition).

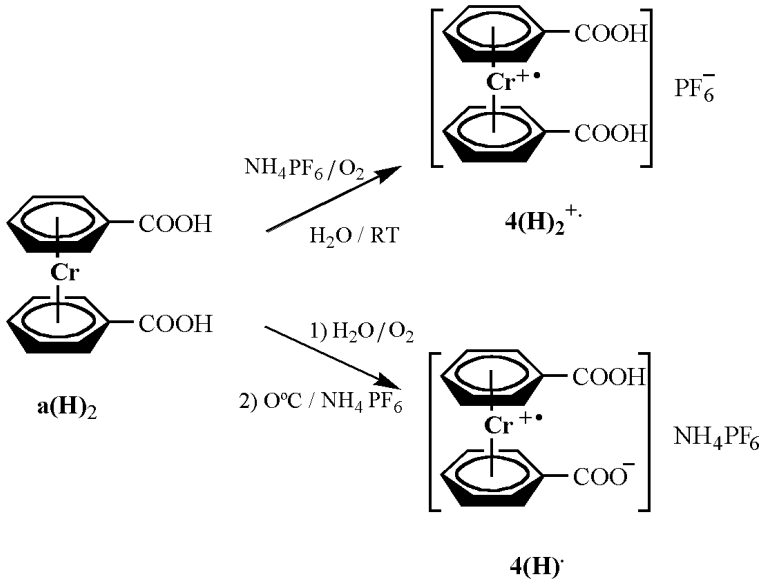

7.4 Polymorphic Modification of the Salt [1,1'-Bis(carboxy-η^6-benzene)chromium^{I}][hexafluorophosphate], $4(H)_2^{+\bullet}$

7.4.1 Fundamentals of Polymorphism[124]

Polymorphism is the property of a substance to exist in different crystalline phases resulting from different arrangements of the molecules in the solid state.

Many organometallic molecules are structurally non-rigid because of the two distinctive features of bonding between the metal center(s) and the ligands, and the delocalised bonding interactions between the π unsaturated systems and the metal(s). Structural flexibility plays a particularly important role in organometallic polymorphism. The consequence is that structurally non-rigid organometallic molecules are likely candidates for the formation of conformational polymorphs. Conformational polymorphism occurs when a molecule can adopt different shapes due to internal degrees of freedom or different relative dispositions of ligands in a metal-organic species.[125] With flexible organometallic systems, however, the bonding mode of the ligands may change in the course of reorientational or migrational (fluxional) processes.[126] Pseudo-polymorphism refers to cases in which a given substance is known to crystallize with different amounts or types of solvent molecules.[127] Crystals formed by structural isomers related by a low-energy interconversion pathway are referred to as crystal isomers.

Crystal polymorphs or isomers may (or may not) interconvert via a phase transition. The change in the crystal structure associated with a phase transition, in which intermolecular bonds are broken and formed, is the crystalline equivalent of an isomerization at the molecular level. The chemical and physical properties of the crystalline material can change dramatically in the course of the solid-state transformation.[128]

The characterization of polymorphs (often molecules co-crystallized with solvent molecules) requires solid-state techniques as X-ray diffraction, powder diffraction, differential scanning calorimetry (DSC), thermogravimetric analysis (TGA), IR and NMR spectroscopy in solid-state, optical and electronic microscopy.

Even though polymorphic modifications contain exactly the same substance, they differ in chemical and physical properties such as density, diffraction pattern, solid state spectrum, melting point, stability, reactivity, morphology, colour, but also mechanical properties, those relevant for comminution and tableting. Many drugs exist in polymorphic modifications which have different efficiencies of assimilation arising from the differences in solubility.[129] Hence, the existence of polymorphism in substances destined to pharmacological use has relevant commercial and biomedical implications.

7.4.2 Structures of [1,1'-Bis(carboxyl-η^6-benzene)chromium^{I}][hexafluorophosphate], $\mathbf{4(H)_2}^{+\bullet}$ α and β Form

The salt $\mathbf{4(H)_2}^{+\bullet}$ has been crystallized in two polymorphic modifications, α, and β form. The crystal packings are shown in Fig. **51, 52**. Important parameters are given in Table **30-33**.

Both crystals, $\mathbf{4(H)_2}^{+\bullet}$ α and β form, contain chains of complex cations held together by hydrogen bonds between the carboxylic groups, in which the O···O separations differ slightly (2.629(2), 2.634(2) Å in $\mathbf{4(H)_2}^{+\bullet}$ α form and 2.618(4) Å in $\mathbf{4(H)_2}^{+\bullet}$ β form) and are comparable to the value of 2.600(2) Å observed for the cationic [1,1'-Cobaltoceniumdicarboxylic acid][hexafluorophosphate], $\mathbf{33}^{+}$. The structure of [1,1'-bis(carboxyl-η^6-benzene)chromium][hexafluorophosphate], $\mathbf{4(H)_2}^{+\bullet}$ α and β form is shown in Fig. **53**.

These values are also very similar to those of the neutral species, thus confirming that the O···O separation is a rather "conservative" parameter which does not depend in any appreciable manner on the charged or neutral nature of the complex or on the metal involved.[130] Moreover, it must be noted that the different pK_S values attributable to $\mathbf{4(H)_2}$ and $\mathbf{4(H)_2}^{+\bullet}$ do not influence the strength of the hydrogen bridges.

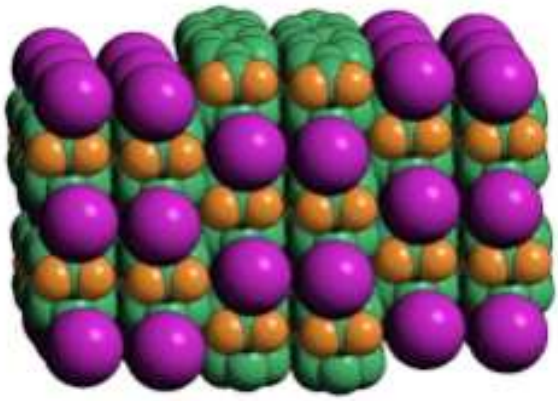

Fig.**51**: Packing projections along the cationic chains directions in **4(H)$_2^{+\bullet}$** α form (the largest spheres represent the orientationally disordered $[PF_6]^-$ anions).

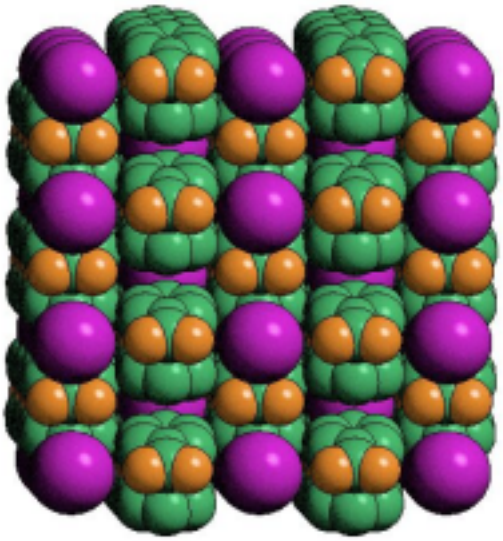

Fig.**52**: Packing projections along the cationic chains directions in **4(H)$_2^{+\bullet}$** β form (largest spheres represent the orientationally disordered $[PF_6]^-$ anions).

In both crystals, **4(H)$_2^{+\bullet}$** α and β form the cationic chains are placed side by side and form a stepladder superstructure with the $[PF_6]^-$ anions accommodated between the steps, as it is shown in Fig. **53**.

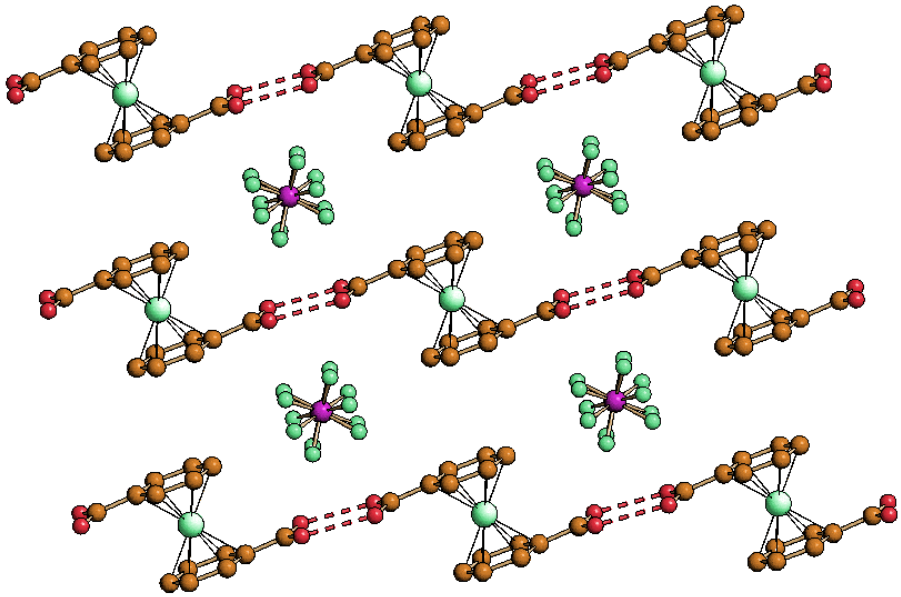

Fig.**53**: Stepladder hydrogen bonding superstructure formed by the cationic chains in crystalline **4(H)$_2$**$^{+\bullet}$ α and β form with $[PF_6]^-$ anions accommodated between the steps.

Cr(1)-C(6)	2.1251(16)	Cr(1)-C(6a)	2.1251(16)
Cr(1)-C(5)	2.1298(17)	Cr(1)-C(5a)	2.1298(17)
Cr(1)-C(1)	2.1350(17)	Cr(1)-C(1a)	2.1350(17)
Cr(1)-C(4)	2.1444(19)	Cr(1)-C(4a)	2.1444(19)
Cr(1)-C(2)	2.1496(18)	Cr(1)-C(2a)	2.1496(18)
Cr(1)-C(3)	2.154(2)	Cr(1)-C(3a)	2.154(2)
C(1)-C(2)	1.3900	C(1)-C(6)	1.3900
C(2)-C(3)	1.3900	C(3)-C(4)	1.3900
C(4)-C(5)	1.3900	C(5)-C(6)	1.3900
C(6)-C(7)	1.509(3)	C(7)-O(1)	1.260(3)
C(7)-O(2)	1.264(3)	P(1)-F(1)	1.569(4)
P(1)-F(2)	1.580(4)	P(1)-F(3)	1.575(4)
P(1)-F(4)	1.588(4)	P(1)-F(5)	1.547(4)
P(1)-F(6)	1.568(4)		

Table **30**: Selected bond lengths (Å) for **4(H)$_2$**$^{+\bullet}$ α form.

C(2)-C(1)-C(6)	120.0	C(3)-C(2)-C(1)	120.0
C(2)-C(3)-C(4)	120.0	C(5)-C(4)-C(3)	120.0
C(6)-C(5)-C(4)	120.0	C(5)-C(6)-C(1)	120.0
C(5)-C(6)-C(7)	120.00(13)	C(1)-C(6)-C(7)	119.89(13)
O(1)-C(7)-O(2)	125.2(2)	O(1)-C(7)-C(6)	117.31(19)
O(2)-C(7)-C(6)	117.50(19)	F(5)-P(1)-F(6)	178.3(5)
F(5)-P(1)-F(1)	88.6(4)	F(6)-P(1)-F(1)	93.0(4)
F(5)-P(1)-F(3)	91.6(4)	F(6)-P(1)-F(3)	83.0(3)
F(1)-P(1)-F(3)	93.1(3)	F(5)-P(1)-F(2)	90.6(4)
F(6)-P(1)-F(2)	88.8(4)	F(1)-P(1)-F(2)	87.5(3)
F(3)-P(1)-F(2)	177.8(3)	F(5)-P(1)-F(4)	91.6(4)
F(6)-P(1)-F(4)	86.8(4)	F(1)-P(1)-F(4)	179.7(4)
F(2)-P(1)-F(4)	92.3(3)		

Table **31**: Selected bond angles (deg) for **4(H)$_2^{+\bullet}$** α form.

Cr(1)-C(6)	2.131(8)	Cr(1)-C(6a)	2.131(8)
Cr(1)-C(5)	2.132(9)	Cr(1)-C(5a)	2.132(9)
Cr(1)-C(1)	2.145(9)	Cr(1)-C(1a)	2.145(9)
Cr(1)-C(4)	2.147(9)	Cr(1)-C(4a)	2.147(9)
Cr(1)-C(2)	2.160(9)	Cr(1)-C(2a)	2.160(9)
Cr(1)-C(3)	2.161(9)	O(2)-C(7)	2.161(9)
O(1)-C(7)	1.137(14)	O(1)-C(7)	1.223(14)
C(1)-C(2)	1.3900	C(1)-C(6)	1.3900
C(2)-C(3)	1.3900	C(3)-C(4)	1.3900
C(4)-C(5)	1.3900	C(5)-C(6)	1.3900
C(6)-C(7)	1.505(14)	P(1)-F(3a)	1.50(2)
P(1)-F(3b)	1.57(2)	P(1)-F(2a)	1.563(19)
P(1)-F(2b)	1.544(16)	P(1)-F(1a)	1.544(19)
P(1)-F(1b)	1.598(17)		

Table **32**: Selected bond lengths (Å) for **4(H)$_2^{+\bullet}$** β form.

C(1)-C(2)-C(3)	120.0	C(2)-C(1)-C(6)	120.0
C(4)-C(3)-C(2)	120.0	C(3)-C(4)-C(5)	120.0
C(6)-C(5)-C(4)	120.0	C(5)-C(6)-C(1)	120.0
C(5)-C(6)-C(7)	117.2(7)	C(1)-C(6)-C(7)	122.7(7)
O(2)-C(7)-O(1)	124.8(11)	O(2)-C(7)-C(6)	121.9(10)
O(1)-C(7)-C(6)	113.3(11)	F(3a)-P(1)-F(3b)	54.2(12)
F(3a)-P(1)-F(2a)	93.2(13)	F(3b)-P(1)-F(2a)	135.3(12)
F(3a)-P(1)-F(1a)	91.1(13)	F(3b)-P(1)-F(1a)	91.1(13)
F(3b)-P(1)-F(1a)	63.7(12)	F(2a)-P(1)-F(1a)	91.0(16)
F(3a)-P(1)-F(1b)	69.2(12)	F(3b)-P(1)-F(1b)	93.1(12)
F(2a)-P(1)-F(1b)	43.3(11)	F(3a)-P(1)-F(2b)	131.0(13)
F(3b)-P(1)-F(2b)	86.4(13)	F(2a)-P(1)-F(2b)	98.2(11)
F(1a)-P(1)-F(2b)	41.4(12)	F(1b)-P(1)-F(2b)	87.5(14)

Table **33**: Selected bond angles (deg) for **4(H)$_2^{+\bullet}$** β form.

The structure of **4(H)$_2^{+\bullet}$** α form.can be ideally converted into that of **4(H)$_2^{+\bullet}$** β form by sliding in opposite directions two of every four layers formed by cationic chains and anions: this is the main difference between the two forms. This is inferred by comparing the packing projections (see Fig. **52-53**) along the cationic chains in both crystals (the cationic chains extend along the c-axis in **4(H)$_2^{+\bullet}$** α form and along the (1-1-1) diagonal in **4(H)$_2^{+\bullet}$** β form). The ion arrangement in **4(H)$_2^{+\bullet}$** β form is almost the same as that observed in the isostructural salt [1,1'-Cobaltoceniumdicarboxylic acid][hexafluorophosphate], $[Co^{III}(\eta^5\text{-}C_5H_4COOH)_2]^+$-$[PF_6]^-$, **33**$^+$.[35]

In **4(H)$_2^{+\bullet}$** α form the arrangement is such that pairs of cationic chains of $\{[Cr^I(\eta^6\text{-}C_6H_5COOH)_2]^+\}_n$ (as well as pairs of rows of anions) are placed next to each other and extend along the c-axis.

Comparing the ion distributions in the two crystals, it can be noted that, while **4(H)$_2^{+\bullet}$** β form adopts a nearly cubic NaCl-like structure, **4(H)$_2^{+\bullet}$** α form shows presence of twin rows of cations and anions.

7.5 Structure of the Zwitterion [(Carboxy-η^6-benzene)(carboxylato-η^6-benzene)chromium^I][ammoniumhexafluorophosphate], 4(H)$^\bullet$ as Co-crystal with [NH$_4$][PF$_6$], 4(H)$^\bullet$

[(Carboxy-η^6-benzene)(carboxylato-η^6-benzene)chromium^I][ammoniumhexafluoro-phosphate], **4(H)$^\bullet$**, the zwitterionic form of compound **4(H)$_2^{+\bullet}$,** was obtained as a co-crystal with ammonium hexafluorophosphate. The chromium organometallic zwitterion in **4(H)$^\bullet$** forms dimers joined together by two short hydrogen bonding interactions [2.477(2) Å], as it is shown in Fig. **54**.

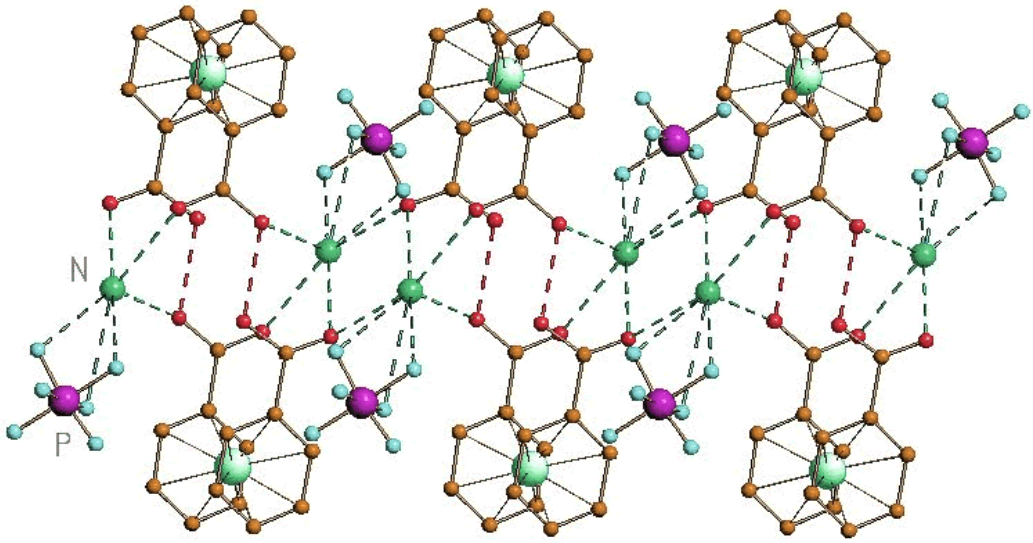

Fig.**54**: Stepladder hydrogen bonding superstructure formed by the zwitterionic chains of **4(H)•**.

Cr(1)-C(3)	2.101(10)	Cr(1)-C(2)	2.113(11)
Cr(1)-C(11)	2.121(11)	Cr(1)-C(12)	2.142(10)
Cr(1)-C(4)	2.113(10)	Cr(1)-C(1)	2.137(11)
Cr(1)-C(10)	2.108(11)	Cr(1)-C(13)	2.150(10)
Cr(1)-C(5)	2.116(11)	Cr(1)-C(6)	2.137(11)
Cr(1)-C(9)	2.150(11)	Cr(1)-C(8)	2.177(10)
C(1)-C(2)	1.3900	C(1)-C(6)	1.3900
C(2)-C(3)	1.3900	C(3)-C(4)	1.3900
C(4)-C(5)	1.3900	C(5)-C(6)	1.3900
C(6)-C(7)	1.51(2)	C(8)-C(9)	1.3900
C(7)-O(2)	1.202(19)	C(7)-O(2)	1.26(2)
C(9)-C(10)	1.3900	C(8)-C(13)	1.3900
C(10)-C(11)	1.3900	C(11)-C(12)	1.3900
C(12)-C(13)	1.3900	C(13)-C(14)	1.509(17)
C(14)-O(4)	1.232(19)	C(14)-O(3)	1.262(18)
N(1)-H(100)	0.8259	N(1)-H(101)	0.9488
P(1)-F(4a)	1.545(16)	P(1)-F(1)	1.539(14)
P(1)-F(6a)	1.555(17)	P(1)-F(2)	1.534(16)
P(1)-F(5a)	1.581(16)	P(1)-F(3a)	1.579(15)

Table **34**: Selected bond lengths (Å) for **4(H)•**.

C(1)-C(2)-C(3)	120.0	C(2)-C(1)-C(6)	120.0
C(4)-C(3)-C(2)	120.0	C(3)-C(4)-C(5)	120.0
C(6)-C(5)-C(4)	120.0	C(5)-C(6)-C(1)	120.0
C(5)-C(6)-C(7)	119.9(10)	C(1)-C(6)-C(7)	120.1(10)
O(2)-C(7)-O(1)	124.9(18)	O(2)-C(7)-C(6)	119.8(16)
O(1)-C(7)-C(6)	115.3(15)	C(9)-C(8)-C(13)	120.0
C(8)-C(9)-C(10)	120.0	C(11)-C(10)-C(9)	120.0
C(12)-C(11)-C(10)	120.0	C(11)-C(12)-C(13)	120.0
C(12)-C(13)-C(8)	120.0	C(12)-C(13)-C(14)	119.3(10)
C(8)-C(13)-C(14)	120.7(10)	O(4)-C(14)-O(3)	123.5(15)
O(4)-C(14)-C(13)	117.6(14)	O(3)-C(14)-C(13)	118.9(15)
H(100)-C(1)-H(101)	111.0	F(4a)-P(1)-F(1)	95.1(12)
F(4a)-P(1)-F(6a)	97.8(17)	F(1)-P(1)-F(6a)	111.5(14)
F(4a)-P(1)-F(2)	84.8(13)	F(1)-P(1)-F(2)	178.9(12)
F(6a)-P(1)-F(2)	69.6(14)	F(4a)-P(1)-F(5a)	86.1(14)
F(1)-P(1)-F(5a)	78.1(12)	F(6a)-P(1)-F(5a)	169.1(16)
F(2)-P(1)-F(5a)	100.8(14)	F(4a)-P(1)-F(3a)	175.4(14)
F(6a)-P(1)-F(3a)	80.7(11)	F(6a)-P(1)-F(3a)	85.6(15)
F(2)-P(1)-F(3a)	99.4(13)	F(5a)-P(1)-F(3a)	91.1(13)

Table **35**: Selected bond angles (deg) for **4(H)$^{\bullet}$**.

The neutral dimers formed by **4(H)$_2$** and **4(H)$^{\bullet}$** differ with regard to the chromium oxidation states, besides involving twice as many hydrogen bonding interactions in the dimer formation in the case of **4(H)$^{\bullet}$**.

The O···O separation in **4(H)$^{\bullet}$** is comparable with the value of 2.470(5) Å observed in cobalticinium salt **35**$^{+}$,[35] but, while in **35**$^{+}$ the ammonium cation is completely encapsulated within a cage formed by four molecules of zwitterion, in **4(H)$^{\bullet}$** the ammonium cation interacts both with the organometallic dimer and with the $[PF_6]^-$ anion. The ammonium cation forms two distinct types of hydrogen bonding interactions: one with the oxygen atoms of the carboxylic/carboxylate groups [N-H---O 2.818-2.909(2) Å] and the other with the PF_6^- anions [N-H---F of 2.208-2.517(2) Å].

The different organization in **4(H)$^{\bullet}$** and in **33**$^{+}$ may reflect a subtle difference in size between the two zwitterions (i.e., a hypothetical cage formed by the chromium complex units would be "too large" to accommodate conveniently the $[NH_4]^+$ cation), but may also indicate the potential existence of an alternative packing available for these complexes (i.e., the existence of polymorphic arrangements).

Crystals of zwitterionic molecules are formally molecular in nature: they do not contain ions carrying charges of opposite sign.

7.6 Hydrogen Bonding Interaction in the three Species

A comparison between the hydrogen bonding parameters for the four complexes is shown in Table **36**.

In terms of hydrogen bonding interaction it has been noted that the neutral species **4(H)$_2$** and the cationic species **4(H)$_2^{+\bullet}$** α and β form hydrogen bonding interactions that are strictly comparable in length, while the respective bond in neutral zwitterionic dimer **4(H)$^\bullet$** is much shorter. The presence of shorter O···O distances in the cases of **4(H)$_2^{+\bullet}$** α and β form and **4(H)$_2$** with respect to **4(H)$^\bullet$** may suggest that, at least in the solid state, proton removal from –COOH groups, leaves the negative charge essentially localized on the deprotonated group, whose hydrogen bonding behaviour in the solid state appears to be unaffected by the electronic nature of the metal center. A possible explanation may be that the electron localization allows full advantage to be taken of the stabilizing contribution arising from the electrostatic (δ+)-(δ–) component of the interaction, even in the case of building blocks carrying the same charge.[131]

By comparing the O-H···O interactions in the neutral dimer (average value 2.630(2) Å) with the chain formed by the neutral zwitterions (2.447(2) Å), **4(H)$^\bullet$**, and the cationic chain in **4(H)$_2^{+\bullet}$** α form (average value 2.621 Å) and **4(H)$_2^{+\bullet}$** β form (2.618 Å), it can be observed that the acids in their fully protonated forms, whether neutral or cationic, show long O···O separations. Hence, the difference in O···O separations between [COOH]···[COOH] and [COOH]···[COO$^-$] interactions does not depend on the neutral or ionic nature of the complex, but on the acceptor group.

Parameter type	$4(H)_2$	$4(H)_2^{+\bullet}$ α	$4(H)_2^{+\bullet}$ $\beta^{+\bullet}$	$4(H)^{\bullet}$
O---O	2.638 2.643	2.629 2.634	2.618	2.447
	2.558 2.603			
O---N				2.909 2.860
				2.818 2.841
(O)H---O, O-H---O	1.60 170	1.71 161		
	1.77 162			
	1.63 164			
	1.90 152			
(C)H---O, C-H---O	2.47 142	2.59 135		2.48 138
	2.52 155			
	2.40 148			
	2.46 155			
	2.50 139			
	2.52 155			
(N)H---F				2.45 128
				2.52 112
				2.21 130
(C)H---F, C-H---F		2.56 151	2.42 140	2.36 120
		2.36 153	2.48 128	2.47 135
		2.49 142	2.41 136	2.42 135
		2.42 162	2.43 128	2.33 163
		2.42 127	2.39 149	2.59 125
		2.51 137	2.42 148	2.54 134
		2.59 145	2.48 158	2.59 118
		2.55 126	2.55 156	2.55 120
			2.52 137	
			2.54 127	
			2.39 142	
			2.57 127	

Table **36**: Relevant hydrogen bonding interactions [(C)H--O, (C)H--F, and (N)H—F< 2.600 Å] in crystalline $4(H)_2$, $4(H)_2^{+\bullet}$ α and β form, $4(H)^{\bullet}$.

8. Summary

The strategy followed in this work is based on the utilization of hydrogen bonds, master key interaction in crystal engineering, between adequately functionalised organometallic molecules. Exchange interactions mediated by hydrogen bridges, i.e. O-H---O, in paramagnetic complexes can be studied employing EPR spectroscopy.

Hence, a study of selective metalation of trovacene, **1**•, in the five-membered ring, in both rings, and in the seven-membered ring obtained employing (η^7-cyclo-heptatrienyl)(η^5-pentamethylcyclopentadienyl)vanadium, **2**•, was undertaken and subsequent reactions of carboxylation and formylation were performed.

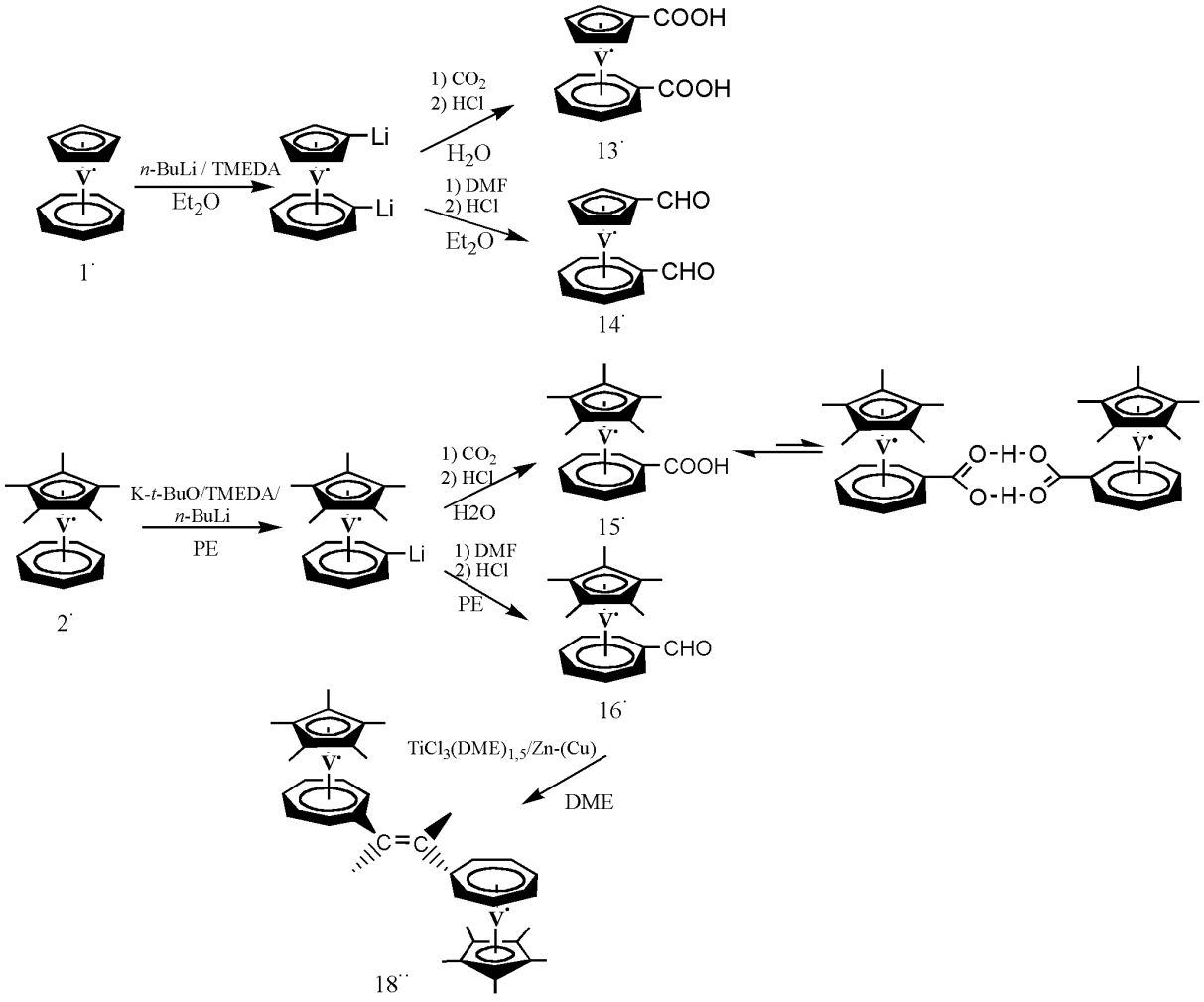

The crystal structure of **13**• shows the formation of dimeric units, while in the case of **16**• no hydrogen bond between two formyl groups was found. EPR studies confirm the absence also in solution of hydrogen bonds between two formyl groups in both cases, **14**• and **16**•. In

general, it is observed that formyl groups form weaker hydrogen bonds than carboxylic groups.

The electronic changes caused by the Cp* ligand on the trovacene moiety are evident in EPR and cyclic voltammetry studies. The EPR spectrum of **15•** shows the presence of a dimeric species (due to the formation of intermolecular hydrogen bonds) with a ratio dimer/monomer much lower than in the case of (η^7-cycloheptatrienyl)(carboxy-η^5-cyclopentadienyl)-vanadium, **6•**. This may be traced to the inductive effect of the five methyl groups of the Cp*, ligand which will reduce the strength of the hydrogen bonds in **15•**. Moreover, the EPR measurements of **15•** and **16•** show a marked decrease of the hyperfine coupling a(^{51}V) in comparison to **6•** and (η^7-cycloheptatrienyl)(formyl-η^5-cyclopentadienyl)vanadium, **17•**, confirming the superior electron donor capacity of Cp* compared to Cp, which is stronger than the electron withdrawing effect of the formyl and carboxylic groups.

In cyclic voltammetry measurements of **2•**, **15•** and **16•** the effect of the methyl groups is demonstrated by a decrease of the oxidation potential in direct comparison to non-methylated trovacenes. A shift of the redox potential by -0.180 V due to the replacement of Cp by Cp* was determined.

On the other side, the introduction of a second electron acceptor group on the trovacene moiety also causes changes. In fact, in EPR studies of **13•** and **14•** is noted that the two acceptor groups do not exercise an additive effect, but rather a contrary effect, yielding lower a(^{51}V) values than in the cases of the corresponding mono-substituted complexes.

Furthemore, in cyclic voltammetry experiments on derivates of **13•** and **14•** more anodic oxidation potentials are obtained, which is in line with the fact that the new derivatives are stable to air (contrary, trovacene is stable to air only for a few minutes).

A dinuclear species, **18••**, was synthesized by McMurry coupling of **16•**. The observation of the half-field signal in the EPR spectrum of **18••** indicates a strong exchange interaction between the two vanadium centers. The half-field signal could not be detected in any other [5-5]-trovacene dinuclear complex linked by a bridge. This observation indicates that electron spin dipolar coupling in [7-7] linked dimers markedly exceeds that exhibited by its [5-5] isomers. In addition, the intensified electron donor capacity of the Cp* influences the results of the magnetic measurements, in which the value of the exchange interaction J of **18••** exceeds that of the directed linked [7-7]-bitrovacene **20••**.

Distortion of the molecular geometry, such as ring tilting or deviations of the individual rings from the planarity can be studied spectroscopically to furnish understanding of the bonding in tilted sandwich complexes. Strained, ring-tilted sila-metallocenophanes are of interest because of the fact that these species readily undergo thermally induced ring-opening polymerisation (ROP). For this purpose, via dilithiation of trovacene, monosila- and disila-trovacenophanes were synthesized, and, thermal or catalytic ring-opening polymerisation was attempted.

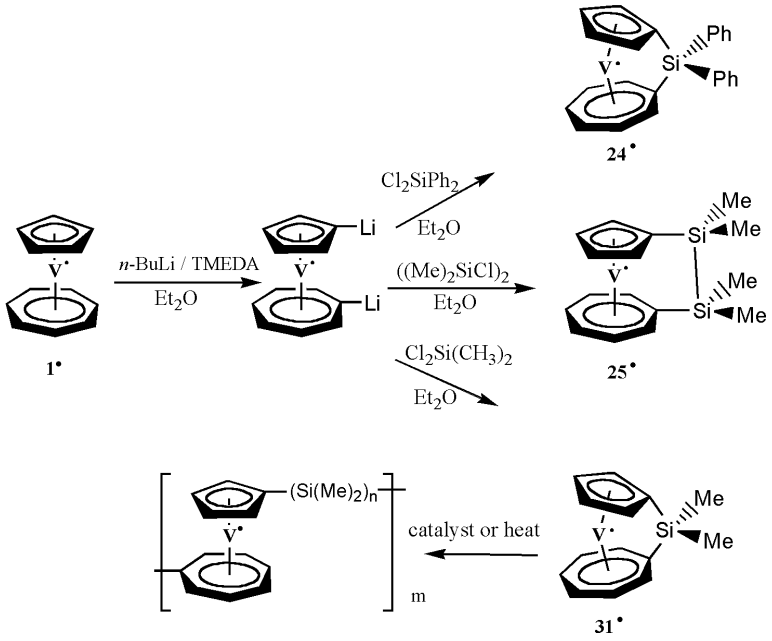

The effect of the strain is demonstrated in the EPR studies by the decrease of the vanadium hyperfine coupling constant in the order **25**$^{\bullet}$>**24**$^{\bullet}$, indicating an increase of metal→ligand spin transfer in proceeding from **25**$^{\bullet}$ (in which the rings are almost parallel, tilt angle amounts to 4°) to **24**$^{\bullet}$ (with a tilt angle between the rings of 17°). In addition, in cyclic voltammetry experiments the oxidation potentials display electron donation from the silicon-silicon σ bond to the ring π orbitals.

Gel permeation chromatography (GPC) studies of the ring-opening polymerisation of **31**$^{\bullet}$ show that the reaction yielded mainly oligomers, but a small amount of polymeric products was also formed.

In organometallic carboxylic acids the hydrogen bonding capacity of the –COOH groups can be combined with the topology of the ligand coordination about the metal centers. In this study the chromium sandwich complex of benzoic acid, $[Cr(\eta^6\text{-}C_6H_5COOH)_2]$ **4(H)$_2$**, was used as such as well as in the oxidized form **4(H)$_2^{+\bullet}$**, containing Cr^I as the central metal and in the deprotonated, zwitterionic form **4(H)$^\bullet$**. The different packing modes, governed by hydrogen bonding, have been elucidated by means of X-ray diffraction.

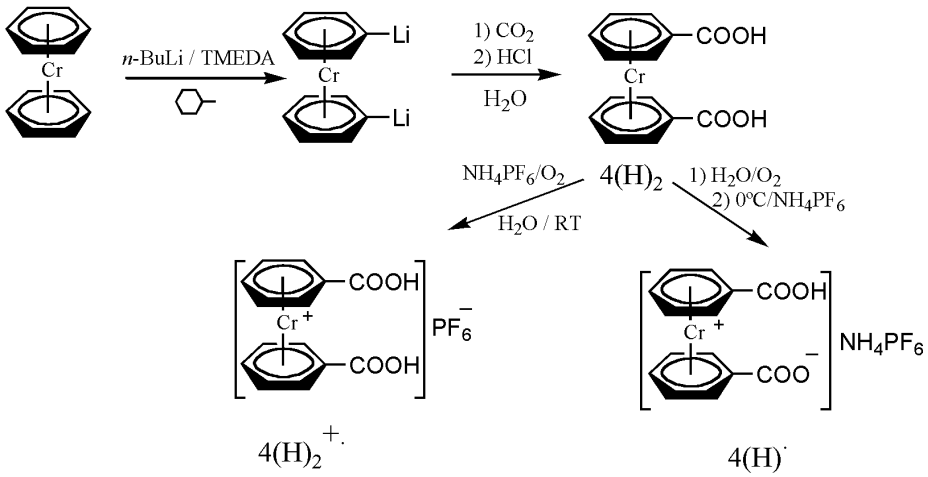

Analysing the structures of the neutral, **4(H)$_2$**, and the cationic form, **4(H)$_2^{+\bullet}$**, (this last known in two polymorphic modifications) it was interesting to note that the hydrogen bond lengths between the carboxylic groups in both species are almost identical. Moreover, the zwitterionic form, **4(H)$^\bullet$**, obtained as a co-crystal with NH_4PF_6, forms two types of hydrogen bonding interactions: one with the oxygen atoms of the carboxylic/carboxylate groups, and the other with the PF_6^- anions. A comparison between the hydrogen bonding parameters for all the complexes leads to the conclusion that the difference in O···O separations between [COOH]···[COOH] and [COOH]···[COO^-] interactions does not depend on the neutral or ionic nature of the complex, but on the respective acceptor group.

9. Zusammenfassung

Die Strategie, die in dieser Arbeit verfolgt wurde, basiert auf der Ausnutzung von Wasserstoffbrückenbindungen, der Schlüsselwechselwirkung im Crystal Engineering, zwischen entsprechend funktionalisierten metallorganischen Molekülen. Durch Wasserstoffbrücken, d.h. O-H---O, vermittelte Austauschwechselwirkungen in paramagnetischen Komplexen können mittels EPR-Spektroskopie untersucht werden.

Hierzu wurde eine Untersuchung zur regioselektiven Metallierung von Trovacen, **1•**, am Fünfring, an beiden Ringen und am Siebenring, letzteres unter Verwendung von (η^7-cycloheptatrienyl)(η^5-pentamethylcyclopentadienyl)vanadium, **2•**, sowie anschließender Carboxylierungs- bzw. Formylierungsreaktionen durchgeführt.

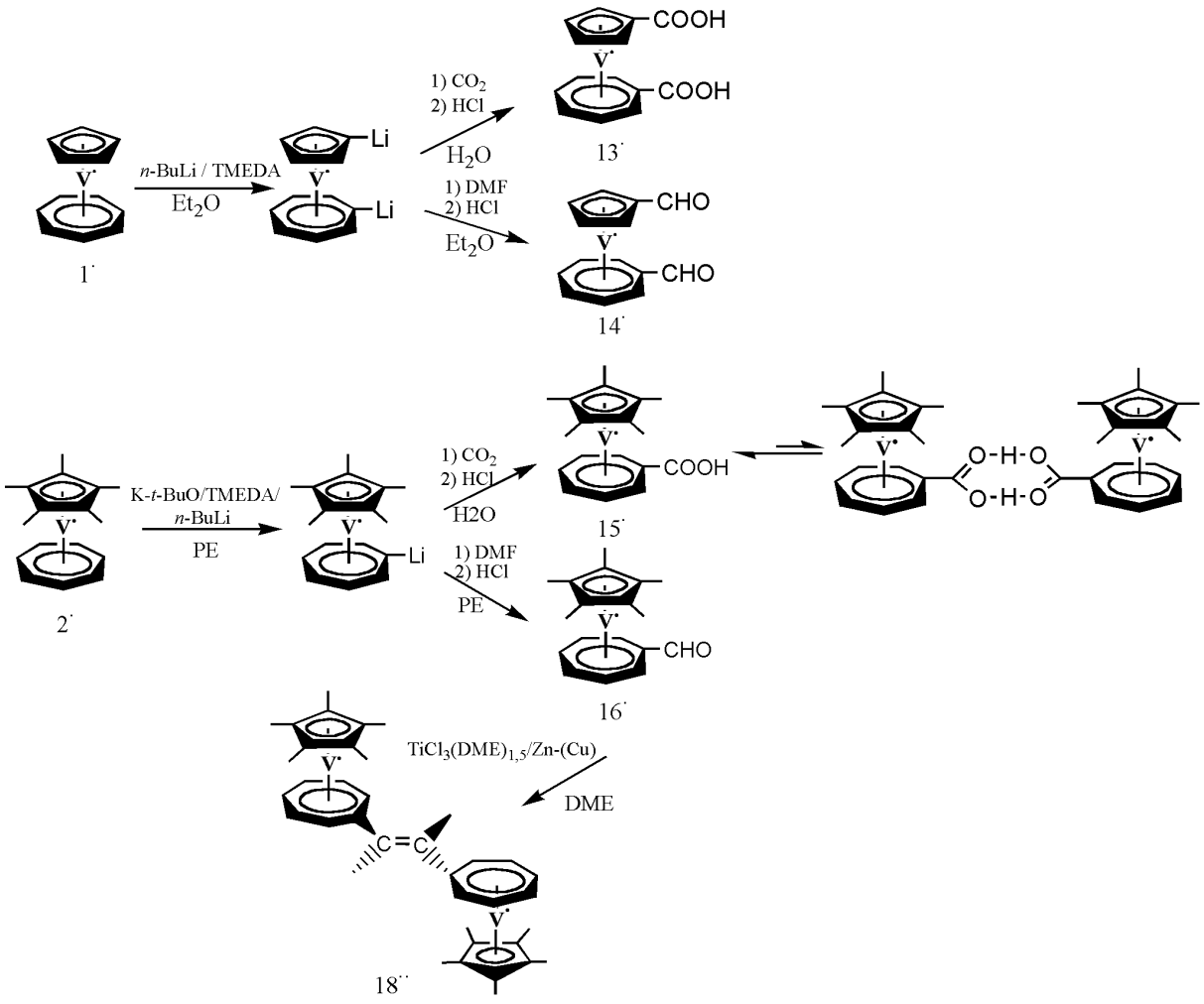

Die Kristallstruktur von **13•** belegt die Bildung von Dimeren, während im Fall von **16•** keine Wasserstoffbrücken zwischen zwei Formylgruppen gefunden wurden. EPR Untersuchungen bestätigen die Abwesenheit von Wasserstoffbrücken-Wechselwirkungen zwischen

Formylgruppen sowohl in Lösungen von **14**$^{\bullet}$ als auch von **16**$^{\bullet}$. Dabei ist zu berücksichtigen, daß Formylgruppen im Allgemeinen schwächere Wasserstoffbrücken bilden als Carboxylgruppen.

Die elektronischen Veränderungen, die der Cp* Ligand im Trovacengerüst bewirkt, werden in EPR- und cyclovoltammetrischen Untersuchungen deutlich. Das EPR-Spektrum von **15**$^{\bullet}$ zeigt die Bildung einer dimeren Spezies (durch Bildung intermolekularer Wasserstoffbrücken) mit einem viel geringeren Dimer/Monomer-Verhältnis als im Falle von (η^7-Cycloheptatrienyl)-(carboxy-η^5-cyclopentadienyl)vanadium, **6**$^{\bullet}$. Dies läßt sich auf den induktiven Effekt der fünf Methylgruppen des Cp*-Liganden zurückführen, der die Wasserstoffbrücken in **15**$^{\bullet}$ schwächt. Darüber hinaus zeigen die EPR-Messungen von **15**$^{\bullet}$ und **16**$^{\bullet}$ eine im Vergleich zu **6**$^{\bullet}$ und **17**$^{\bullet}$ deutliche Verminderung der Hyperfeinkopplung a(^{51}V), was beweist, daß zum einen Cp* weitaus stärkere Elektronendonoreigenschaften besitzt als Cp und daß zum anderen diese Donoreigenschaften stärker sind als der elektronenziehende Effekt der Formyl- und Carboxylgruppen.

In cyclovoltammetrischen Messungen von **2**$^{\bullet}$, **15**$^{\bullet}$ und **16**$^{\bullet}$ äußert sich der Effekt der Methylgruppen in einer kathodischen Verschiebung des Oxidationspotentials um –0.180 V im direkten Vergleich mit nicht-methylierten Trovacenen.

Zudem führt auch die Einführung eines zweiten Elektronenakzeptors in das Trovacengerüst zu Veränderungen. EPR-Untersuchungen von **13**$^{\bullet}$ und **14**$^{\bullet}$ ergaben, daß die beiden Akzeptorgruppen keinen additiven, sondern vielmehr einen entgegengesetzten Effekt ausüben, woraus geringere a(^{51}V)-Werte als im Fall der entsprechenden monosubstitutierten Verbindungen resultieren.

Außerdem wurden in cyclovoltammetrischen Experimenten der Derivate **13**$^{\bullet}$ und **14**$^{\bullet}$ anodischere Oxidationspotentiale bestimmt, was in Übereinstimmung mit der Beobachtung ist, daß diese neuen Derivate an Luft unbegrenzt stabil sind (Trovacen hingegen ist an Luft nur wenige Minuten stabil).

Durch McMurry-Kopplung von **16**$^{\bullet}$ wurde die zweikernige Spezies **18**$^{\bullet\bullet}$ synthetisiert. Die Intensität des Halbfeldsignals im EPR-Spektrum von **18**$^{\bullet\bullet}$ zeigt eine starke Austauschwechselwirkung zwischen den beiden Vanadiumzentren an. Ein Halbfeldsignal konnte bisher in keinem der an den Fünfringen über eine Trenngruppe verbrückten Trovacen-Dimere festgestellt werden. Diese Beobachtung deutet darauf hin, daß die dipolare Elektronenspinkopplung in [7-7] verbundenen Dimeren diejenige in [5-5]-verknüpften Analoga deutlich übersteigt. Außerdem beeinflußt das höhere Elektronendonorvermögen des

Cp* das Ergebnis der magnetischen Suszeptometrie, in der für **18**$^{\bullet\bullet}$eine Austauschkopplung J bestimmt wurde, die diejenige des direkt verbundenen [7-7]-Bitrovacens **20**$^{\bullet\bullet}$ übersteigt.

Verzerrungen der molekularen Geometrie in gekippten Sandwichkomplexen, wie beispielsweise Ringkippung oder Abweichungen der einzelnen Ringe aus der Planarität, können spektroskopisch untersucht werden und zum Verständnis der Bindungsverhältnisse beitragen. Gespannte Sila-Metallocenophane mit gekippten Ringen sind insbesondere von Interesse, da sie sehr leicht thermisch induzierte, ringöffnende Polymerisation (ring-opening polymerisation, ROP) eingehen. Mittels Dilithiierung von Trovacen wurden zunächst Monosila- und Disila-trovacenophane synthetisiert, mit denen anschließend thermisch oder katalytisch induzierte, ringöffnende Polymerisationen versucht wurden.

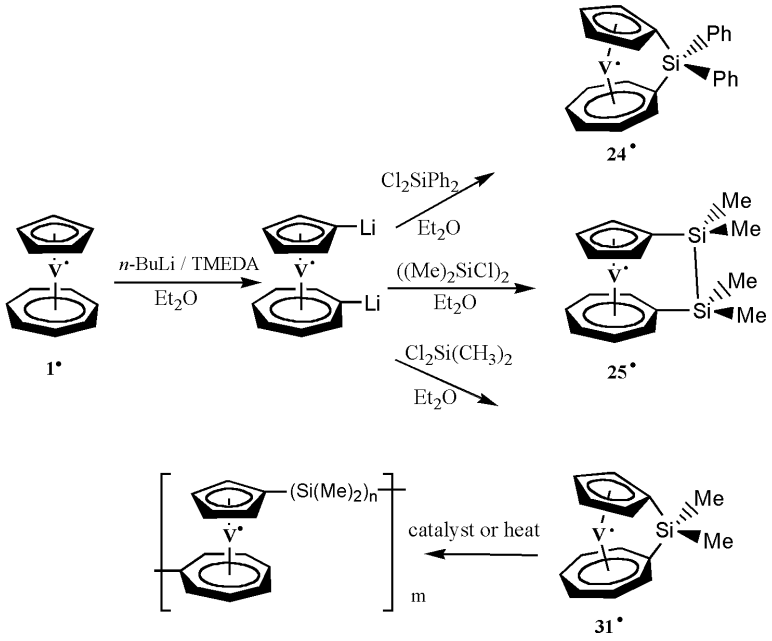

Der Effekt der Spannung zeigt sich in EPR-Untersuchungen in einer Verminderung der Vanadium-Hyperfeinkopplungskonstante von **25**$^{\bullet}$ zu **24**$^{\bullet}$, was auf eine Zunahme des Metall→Ligand Spintransfers beim Übergang von **25**$^{\bullet}$ (worin die beiden Ringe annähernd parallel sind, der Neigungswinkel beträgt lediglich 4°) zu **24**$^{\bullet}$ (mit einem Neigungswinkel von 17° zwischen den Ringen) hindeutet. Darüber hinaus weisen die in cyclovoltammetrischen Experimenten bestimmten Oxidationspotentiale auf eine Elektronendonation aus der Si-Si- σ-Bindung in die π-Orbitale der Ringe hin.

Gelpermeationschromatographische Untersuchungen (GPC) an Produkten der ringöffnenden Polymerisation von **31**$^{\bullet}$ ergaben, daß die Reaktion im wesentlichen Oligomere liefert, jedoch auch einen geringen Anteil polymeren Produkts.

In metallorganischen Carbonsäuren kann die Fähigkeit der -COOH-Gruppen, Wasserstoffbrückenbindungen zu bilden, mit der Topologie der Ligandenkoordination bezüglich des Metallzentrums kombiniert werden. In dieser Arbeit wurde der Chrom-Sandwichkomplex von Benzoësäure, $[Cr(\eta^6\text{-}C_6H_5COOH)_2]$ **4(H)$_2$**, sowohl als Neutralkomplex als auch in der oxidierten Form **4(H)$_2^{+\bullet}$**, mit Cr^I als Zentralmetall, sowie in der deprotonierten, zwitterionischen Form **4(H)**$^{\bullet}$ studiert. Die durch Wasserstoffbrückenwechselwirkungen bestimmten unterschiedlichen Packungsarten wurden mittels Röntgenbeugung aufgeklärt.

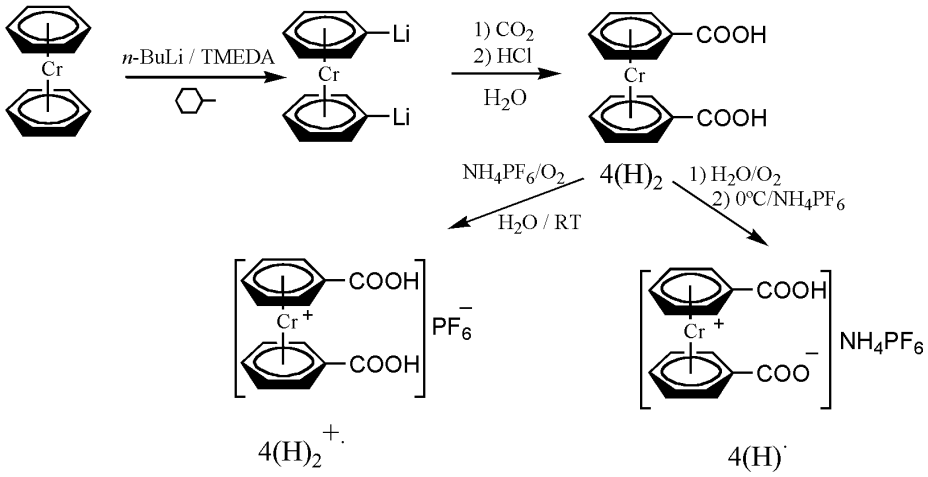

Die Kristallstrukturanalyse der neutralen, **4(H)$_2$**, und der kationischen Form, **4(H)$_2^{+\bullet}$**, (letztere ist in zwei polymorphen Modifikationen bekannt) ergab interessanterweise, daß die Längen der Wasserstoffbrücken zwischen den Carboxylgruppen in beiden Spezies kaum voneinander abweichen. Die zwitterionische Form, **4(H)**$^{\bullet}$, wird als Cokristall mit NH_4PF_6 isoliert, wobei die eingelagerten Ammoniumionen zwei Arten von Wasserstoffbrückenwechselwirkungen eingehen: eine mit den Sauerstoffatomen der Carboxyl/Carboxylat-Gruppen und die andere mit den PF_6^- -Anionen. Ein Vergleich der H-Brückenparameter aller Komplexe führt zu der Schlußfolgerung, daß die Unterschiede in den O···O Abständen der [COOH]···[COOH] und der [COOH]···[COO^-] Wechselwirkungen nicht von der Ladung oder der Natur des Komplexes, sondern von der jeweiligen Akzeptorgruppe abhängen.

10. Experimental Section

10.1 Materials

All experimental manipulations involving the syntheses and crystallizations were carried out under dry-oxygen free nitrogen by employing Schlenk techniques.
All the solvents were dried by refluxing over drying agents (see table) then distilled under nitrogen atmosphere.

SOLVENTS	DRYING AGENTS
Toluene	Potassium
Diethyl ether	Sodium/Potassium
Tetrahydrofuran	1.CaH_2 2.Potassium
Petroleum ether(40-60°C)	Sodium/Potassium
Methylcyclohexane	Potassium
Dimethoxyethane	Potassium
Methanol	Magnesium
Acetone	P_2O_5

Table **37**: Drying agents for the used solvents.

The aqueous solutions (H_2O, HCl 2 M, NaOH 0.1 M) were made oxygen-free by passing through nitrogen for 2 days and stored under nitrogen. Extra dry toluene for EPR experiments was dried over potassium followed by distillation over $LiAlH_4$; DME for cyclovoltammetric experiments was purchased from Aldrich (>99%) and distilled over sodium.
Aluminum oxide and silanized silica gel 60 were used for column chromatography. The stationary phases were dried at 120°C in vacuum for 2 days and stored under nitrogen.
The following compounds were purchased from commercial sources and eventually purified (distillation, recrystallization) prior to use:
n-Butyllithium (solution 1.6 M in hexane), N,N,N',N'-tetramethylethylenediamine (distilled over CaH_2), potassium-*tert*-butoxide, HBF_4 (solution 54% in diethyl ether), dimethylformamide (distilled over CaH_2), ($TiCl_3(DME)_{1,5}$ + Zn/Cu),[83] dichlorodiphenylsilane, 1,2-dichlorotetramethyldisilane, dichlorodimethylsilane, platinum(II)chloride, NH_4PF_6.
The starting materials were prepared according to literature procedures: (η^7-cyclo-heptadienyl)(η^5-cyclopentadienyl)vanadium[132], **1**$^\bullet$ (η^7-cycloheptadienyl)(η^5-penta-methyl-cyclopentadienyl)vanadium[133], **2**$^\bullet$, bis(benzene)chromium[134], **3**.

10.2 Instrumental Analysis

Mass Spectrometry: mass spectra samples were prepared in special glass equipment under nitrogen and measured on a CH7 (EI-MS) (70 eV) Spectrometer, (Varian MAT).

Elemental Analysis (C, H, N): the tin-crucibles (filled in special devise under nitrogen atmosphere) containing the substance were burned in a oxygen-stream. The analytical measurements were made employing Elementar Analyser (Vario EL).
In the elementary analyses of vanadium sandwich complexes is noted that value found for carbon is often lower than calculated. This is due to the formation of stable carbides of vanadium. The effect is more pronounced in the case of (η^7-cycloheptatrienyl)(η^5-pentamethylcyclopentadienyl)vanadium and its derivates, because of the presence of the additional five methyl groups. The combustion of the carbon atoms is not complete. Combustion would be complete at temperatures higher than those accessible with the analyse available.

Infrared Spectroscopy: the samples were prepared as KBr-pellets and the spectra were recorded on Interferometer IFS 88, (Bruker), from 4000 to 400 cm^{-1}.

Gel Permeation Chromatography: samples with concentration of ca. 1 mg/mL were measured in THF relative to polystyrene standards. A column (600 x 8 mm, Type SDV linear, 10 µL, PSS) were used. Detection was performed employing a refractive index detector K731 (Knauer), and a UV/VIS-detector UV 3071 (Knauer). The evaluation of the measured data was carried out by the computer program WinGPC Version 4.01 (PSS).

^{1}H NMR Spectroscopy: the spectra were measured on a AM-500 Spectrometer (Bruker), 500 MHz. d_8-THF δ= 1.73, 3.58 ppm was used as solvent. Sample solutions were submitted in sealed tubes; the solutions were tempered (at 60°C for 12 hours) prior to recording the spectra in order to destroy Cr^I complex radical cations adventitiously present.

Electron Paramagnetic Resonance: all measurements were performed in solution 10^{-5}-10^{-4} molar of the complexes on a X-Band Spectrometer ESP 300 (Bruker). The sample were prepared in inert atmosphere in quartz or glass tubes (∅ 4 mm) and flame-sealed under

vacuum. A modified TE 102 Square-Pulse Resonator (Varian) was employed as cavity. The frequency was determined using the Frequency-Counter Mod. TR 5214 (Advantest).

ENDOR: ^{1}H ENDOR spectra were recorded on a ESP 300 spectrometer (Bruker) with EN 200 S/E/T ENDOR-Triple accessory. The sample were prepared in inert atmosphere in glass tube (∅ 5 mm) and flame-sealed under vacuum.

Cyclic Voltammetry: the measurements were made in a special cell containing unstirred millimolar solution of the complex in DME in the presence of $(n\text{-}Bu)_4NClO_4$ (0.1 M) as supporting electrolyte at –40°C and with sweep rate (v= dE/dt) 0.1 V/s. Working electrode: 2 mm glassy carbon electrode (EG & G); counter electrode: platinum wire (Amel); reference electrode: mercury/calomel electrode (Amel). The equipment consisted of the potentiostat (Amel, Mod. 522), function generator (Amel, Mod. 560), multipurpose unit (Amel, Mod. 563). The voltammogramms were registered by a digital storage oscilloscope (Nicolet, Mod. 3091) and X-Y-recorder (Kipp and Zonen, Mod. BD 90). Cyclovoltammetry was performed under argon protection. Dimethoxyethane was dried over calcium hydride.

Crystal Structure Analysis: X-ray diffraction data were collected on a NONIUS CAD-4 diffractometer equipped with a liquid nitrogen Oxford-Cryostream device. Crystal date and details of measurements are summarized in Tables. Common to all compounds: MoKα radiation, λ= 0.71073 Å, monochromator graphite, psi-scan absorption correction.
SHELXL97[135] was used for structure solution and refinement based on F^2.
SCHAKAL97[136] was used for all graphical representations.
Correspondence between the structures determined by X-ray diffraction and the bulk material was confirmed by powder diffraction. Powder spectra were measured on an automated PW 1100 Powder Diffractometer with monochromatic Cu-Kα radiation.

Magnetic Susceptibility: magnetic susceptibility was studied with a SQUID Magnetometer (Quantum Design) in the temperature range 1.8-300 K. The samples for magnetic measurements were prepared in special sealed teflon-crucibles (filled under nitrogen atmosphere). The samples contained ca. 10 mg of substance. The data were corrected for magnetization of the sample holder (KLF), and diamagnetic corrections were applied to the data based on Pascal's constant.

10.3 Preparations

Synthesis of (Carboxy-η^7-cycloheptatrienyl)(carboxy-η^5-cyclopentadienyl)vanadium, [(η^7-C_7H_6COOH)(η^5-C_5H_4COOH)V^0], 13$^\bullet$. A 100 mL flask equipped with a magnetic stirring bar was charged with (η^7-cycloheptatrienyl)(η^5-cyclopentadienyl)vanadium (0.70 g, 3.38 mmol), diethyl ether (40 mL), and TMEDA (2.04 mL, 13.52 mmol). Then *n*-BuLi (8.34 mL, 13.52 mmol, solution 1.6 M in hexane) was added dropwise and the mixture was refluxed for 4 hours. After cooling to room temperature, CO_2 was bubbled through the solution containing the dark-violet suspension for 3 hours. The colour turned immediately to green. The solvent was removed in vacuum and the residue was dissolved in water. After filtration, HCl (12 mL, 2 M) was added to the filtrate, yielding a clear green precipitate, which was collected by filtration and dried under vacuum. Suitable crystal for X-ray diffraction were obtained by suspending 0.10 g of crude product in water, followed by addition of NaOH (2 mL, 0.1 M). The solution was then layered with 10 mL of diethyl ether containing HBF_4 (3 drops, solution 58% in diethyl ether).

Yield: 0.83 g, 83%.

MS, m/e: 295 (75%, M^+), 251 (38%, M^+-COOH), 175 (25%, $VC_6H_6COOH^+$), 159 (92%, $VCpCOOH^+$), 129 (21%,$C_6H_6V^+$), 91 (98%,$C_7H_7^+$), 51 (14%,V^+).

Anal. Calculated for $C_{14}H_{12}O_4V$ (295.19): C, 56.97; H, 4.11. Found: C, 56.56, H, 4.39.

IR (KBr): ν_{O-H} 2653 cm^{-1}, $\nu_{C=O}$ 1678 cm^{-1}, $\nu_{C=C}$ 1498, 1476 cm^{-1}, ν_{C-O} 1308 cm^{-1}, $\delta_{C-H,ring}$ 795 cm^{-1}.

Synthesis of (Formyl-η^7-cycloheptatrienyl)(formyl-η^5-cyclopentadienyl)vanadium, [(η^7-C_7H_6CHO)(η^5-C_5H_4CHO)V^0], 14$^\bullet$. A 100 mL flask equipped with a magnetic stirring bar was charged with (η^7-cycloheptatrienyl)(η^5-cyclopentadienyl)vanadium (0.70 g, 3.38 mmol), diethyl ether (50 mL), and TMEDA (2.04 mL, 13.52 mmol). Then *n*-BuLi (8.34 mL, 13.52 mmol, solution 1.6 M in hexane) was added dropwise and the mixture was refluxed for 4 hours. After cooling to room temperature, dimethylformamide (2.70 mL, 27.04 mmol) was added to the dark-violet suspension at –60 °C. The resulting violet mixture was stirred at –60 °C for 1 hour and at room temperature for additional 2 hours. HCl (1.75 mL, 2 M) was added at –5 °C and the green suspension was stirred at room temperature for 1 hour, then the solvent was removed in vacuum. The residue was dissolved in toluene and dried over $MgSO_4$. The product was chromatographed on aluminium oxide (neutral, 0% water). The first fraction, eluted with toluene, contained unreacted trovacene, the second, eluted with toluene/THF

(20:1), consisted of (η^7-cycloheptatrienyl)(formyl-η^5-cyclopentadienyl)vanadium, the last, eluted with THF/toluene (3:1), contained the title compound. The solvent was removed under vacuum to yield a dark green powder.

Yield: 0.52 g, 58%.

MS, m/e: 263 (100%, M^+), 235 (8%, M^+-CHO), 207 (25%, TVC^+), 157 (6%, $VC_6H_6CO^+$), 144 (8%, $VCpCO^+$), 141 (1%, $VC_6H_6C^+$), 128 (3%, $VCpC^+$), 129 (16%, $C_6H_6V^+$), 116 (40%, CpV^+), 91 (85%,$C_7H_7^+$), 51 (22%,V^+).

Anal. Calculated for $C_{14}H_{12}O_2V$ (263.19): C, 63.89; H, 4.60. Found: C, 63.46, H, 4.59.

IR (KBr): $\nu_{C(O)-H}$ 2961 cm^{-1}, $\nu_{C=O}$ 1682 cm^{-1}, $\nu_{C=C}$ 1497, 1463 cm^{-1}, $\delta_{C-H,ring}$ 799 cm^{-1}.

Synthesis of (Carboxy-η^7-cycloheptatrienyl)(η^5-pentamethylcyclopentadienyl)vanadium, [(η^7-C_7H_6COOH)(η^5-C_5Me_5)V^0], 15•. A 100 mL flask equipped with a magnetic stirring bar was charged with (η^7-cycloheptatrienyl)(η^5-pentamethylcyclopentadienyl)vanadium (0.15 g, 0.50 mmol), and petroleum ether (20 mL). At –50°C, TMEDA (0.2 mL, 1.0 mmol), potassium-*tert*-butoxide (0.13 g, 1.0 mmol) was added and the solution was stirred for 10 minutes. Then, at -20°C, *n*-BuLi (0.9 mL, 1.0 mmol, solution 1.6 M in hexane) was added dropwise and the mixture was stirred at this temperature for 1 hour. Then, at room temperature, CO_2 was bubbled through the solution containing the brown suspension for 3 hours. The colour turned immediately to clear green. The solvent was removed in vacuum and the residue was dissolved in water. After filtration of the unreacted (η^7-cycloheptatrienyl)(η^5-pentamethylcyclopentadienyl)vanadium, HCl (4 mL, 2 M) was added to the filtrate, yielding a clear green precipitate, which was collected by filtration and dried under vacuum.

Yield: 0.034 g, 20%.

MS, m/e: 321 (50%, M^+), 277 (74%, M^+-COOH), 136 (100%, $C_5(CH_3)_5^+$), 91 (31%,$C_7H_7^+$), 51 (1%,V^+).

Anal. Calculated for $C_{18}H_{22}O_2V$ (321.31): C, 67.29; H, 6.90. Found: C, 63.96, H, 6.69.

IR (KBr): ν_{C-CH_3} 2909 cm^{-1}, $\nu_{O-H,\ free}$ 2627 cm^{-1}, $\nu_{O-H,\ bonded}$ 2542 cm^{-1}, $\nu_{C=O}$ 1651 cm^{-1}, $\nu_{C=C}$ 1496, 1466 cm^{-1}, δ_{as-CH_3} 1430 cm^{-1}, δ_{s-CH_3} 1375 cm^{-1}, ν_{C-O} 1319 cm^{-1}.

Synthesis of (Formyl-η^7-cycloheptatrienyl)(η^5-pentamethylcyclopentadienyl)vanadium, [(η^7-C_7H_6CHO)(η^5-C_5Me_5)V^0], 16•. A 100 mL flask equipped with a magnetic stirring bar was charged with (η^7-cycloheptatrienyl)(η^5-pentamethylcyclopentadienyl)vanadium (0.20 g, 0.72 mmol), and petroleum ether (20 mL). At –50°C TMEDA (0.3 mL, 1.44 mmol), and potassium-*tert*-butoxide (0.18 g, 1.44 mmol) were added and the solution was stirred for 10

minutes. Then, at -20°C, *n*-BuLi (1.2 mL, 1.44 mmol, solution 1.6 M in hexane) was added dropwise and the mixture was stirred at this temperature for 1 hour. Dimethylformamide (0.2 mL, 2.88 mmol) was added to the brown suspension at –60 °C. The resulting red-violet mixture was stirred at –60 °C for 1 hour and at room temperature for an additional 2 hours. HCl 2 M (0.3 mL) was added at –5 °C and the green suspension was stirred at room temperature for 1 hour. After filtration, the solution was dried over $MgSO_4$. The product was chromatographed on silica gel. The first fraction, eluted with petroleum ether, contained unreacted (η^7-cycloheptatrienyl)(η^5-pentamethylcyclopentadienyl)vanadium, the second, eluted with petroleum ether/diethyl ether (10:1), contained the product. The solvent was removed under vacuum to yield green-brown crystals.

Yield: 0.044 g, 20%.

MS, m/e: 305 (100%, M^+), 277 (29%, M^+-CHO), 91 (85%,$C_7H_7^+$).

Anal. Calculated for $C_{18}H_{22}OV$ (263.19): C, 70.81; H, 7.26. Found: C, 68.98; H, 7.54.

IR (KBr): $\nu_{C\text{-}CH_3}$ 2961 cm^{-1}, $\nu_{C(O)\text{-}H}$ 2771 cm^{-1}, $\delta_{H\text{-}C=O}$ 2717 cm^{-1}, $\nu_{C=O}$ 1674 cm^{-1}, $\nu_{C=C}$ 1491, $\delta_{as\text{-}CH_3}$ 1426 cm^{-1}, $\delta_{s\text{-}CH_3}$ 1374 cm^{-1}, $\nu_{C\text{-}O}$ 1306 cm^{-1}.

Synthesis of E-1,2-Bis[(η^7-cycloheptatrienyl)(η^5-pentamethylcyclopentadienyl)-vanadium]ethene, 18$^{\bullet\bullet}$. A 100 mL flask equipped with a magnetic stirring bar was charged with $TiCl_3(DME)_{1,5}$ (1.14 g, 3.94 mmol) and zinc-copper couple (3.80 g, 58.10 mmol) in 50 mL of DME. The mixture was heated at 80°C for 2 hours to form the active titanium reagent. After cooling to room-temperature, 1-formyl(η^7-cycloheptatrienyl)(η^5-pentamethyl-cyclopentadienyl)vanadium, (0.28 g, 0.90 mmol) in 10 mL of DME was added by a syringe, and the mixture was heated for 20 hours. The reaction slurry was cooled to room temperature and petroleum ether was added. The mixture was filtered through a small layer of silica gel to remove inorganic salts. The filtrate was concentrate under vacuum and dissolved in petroleum ether. From the solution a clear-green powder precipitated, which was collected, washed with petroleum ether/diethyl ether and dried under vacuum to give 0.3 g (Yield= 58 %) of pure **E-18$^{\bullet\bullet}$** isomer. The solution was concentrated to 5 mL and chromatographed on silicagel. A first clear-green fraction was eluted with petroleum ether. This contains a few milligrams of **E** isomer. A second dark-green fraction eluted with petroleum ether/toluene contained unreacted (formyl-η^7-cycloheptatrienyl)(η^5-pentamethylcyclopentadienyl)vanadium.

MS, m/e: 578 (100%, M^+), 290 (6%, M^{++}), 277 (39%, TVC^*), 185 (1%, Cp^*V).

Anal. Calculated for $C_{36}H_{44}V_2$ (578.63): C, 74.73; H, 7.66. Found: C, 70.39, H, 7.39.

IR (KBr): $\nu_{C\text{-}CH_3}$ 2961 cm^{-1}, $\nu_{C=C}$ 1629, 1692, $\delta_{as\text{-}CH_3}$ 1449 cm^{-1}, $\delta_{s\text{-}CH_3}$ 1375 cm^{-1}.

Synthesis of [1,8-(Diphenylsilanediyl)(η^7-cycloheptatrienyl)(η^5-cyclopentadienyl) vanadium], [$(Ph_2Si\text{-}\eta^7\text{-}C_7H_6)(\eta^5\text{-}C_5H_4)V^0$], 24•. A 100 mL flask equipped with a magnetic stirring bar was charged with (η^7-cycloheptatrienyl)(η^5-cyclopentadienyl)vanadium (0.20 g, 0.97 mmol), diethyl ether (30 mL), and TMEDA (0.58 mL, 3.83 mmol). Then, *n*-BuLi (2.41 mL, 3.83 mmol, solution 1.6 M in hexane) was added dropwise and the mixture was refluxed for 4 hours. After cooling to room temperature, dichlorodiphenylsilane (0.2 mL, 0.97 mmol) dissolved in 10 mL petroleum ether was added slowly (2 h) to the dark-violet suspension at –20°C. The colour of the mixture turned from dark-brown to violet and LiCl precipitated. The mixture was stirred at room temperature overnight. Then, LiCl was filtered off. Violet crystals suitable for X-ray diffraction were obtained by storing the solution at –20°C.

Yield: 0.24 g, 64%.

MS, m/e: 387 (100%, M^+), 309 (14%, M^+-Ph), 232 (14%, M^+-2Ph), 205 (3%, M^+-$Si(Ph)_2$).

Anal. Calculated for $C_{24}H_{20}SiV$ (387.45): C, 74.40; H, 5.20. Found: C, 73.14, H, 5.78.

Synthesis of [1,8-(Tetramethyldisilane-1,2-diyl)(η^7-cycloheptatrienyl)(η^5-cyclopentadienyl)-vanadium], [$(Me_2SiSiMe_2\text{-}\eta^7\text{-}C_7H_6)(\eta^5\text{-}C_5H_4)V^0$], 25•. A 100 mL flask equipped with a magnetic stirring bar was charged with (η^7-cycloheptatrienyl)(η^5-cyclopentadienyl)vanadium (0.15 g, 0.72 mmol), diethyl ether (30 mL), and TMEDA (0.43 mL, 2.88 mmol). Then, *n*-BuLi (1.81 mL, 2.88 mmol, solution 1.6 M in hexane) was added dropwise and the mixture was refluxed for 4 hours. After cooling to room temperature, 1,2-dichlorotetramethyldisilane (0.13 mL, 0.72 mmol) dissolved in 10 mL petroleum ether was added slowly (2 h) to the dark-violet suspension at –20°C. The colour of the mixture turned from dark-brown to clear violet and LiCl precipitated. The mixture was stirred at room temperature overnight. Then, LiCl was filtered off. Violet crystals suitable for X-ray diffraction were obtained by storing the solution at –20°C.

Yield: 0.10 g, 45%.

MS, m/e: 321 (9%, M^+), 205 (37%, M^+-$Si(CH_3)_2$-$Si(CH_3)_2$), 116 (54%, CpV^+), 91 (20%,$C_7H_7^+$).

Anal. Calculated for $C_{24}H_{22}Si_2V$ (321.46): C, 59.78; H, 6.90. Found: C, 56.83, H, 7.04.

Attempted Synthesis of Poly(trovacenylsilane), [-Si(CH$_3$)$_2$(η^7-C$_7$H$_6$)V^0(η^7-C$_5$H$_4$)-]$_n$.

Synthesis of [1,8-(Dimethylsilanediyl)(η^7-cycloheptatrienyl)(η^5-cyclopentadienyl) vanadium], [(Me$_2$Si-η^7-C$_7$H$_6$)(η^5-C$_5$H$_4$)V^0], 31$^\bullet$. A 100 mL flask equipped with a magnetic stirring bar was charged with (η^7-cycloheptatrienyl)(η^5-cyclopentadienyl)vanadium (0.20 g, 0.97 mmol), diethyl ether (30 mL), and TMEDA (0.58 mL, 3.83 mmol). Then, *n*-BuLi (2.41 mL, 3.83 mmol, solution 1.6 M in hexane) was added dropwise and the mixture was refluxed for 4 hours. After cooling to room temperature, dichlorodimethylsilane (0.12 mL, 0.97 mmol) dissolved in 10 mL petroleum ether was added slowly (2 h) to the dark-violet suspension at –20°C. The colour of the mixture turned from dark-brown to violet and LiCl precipitated. The mixture was stirred at room temperature overnight. Then, LiCl was filtered off, and the solution was evaporated under vacuum to yield **31$^\bullet$** as violet oil.

MS, m/e: 734 (50%, (TVC-Si(CH$_3$))$_3^+$-Si(CH$_3$)), 264 (15%, M$^+$), 207 (2%, TVC$^+$), 91 (100%,C$_7$H$_7^+$).

Anal. Calculated for C$_{14}$H$_{16}$SiV (263.31): C, 63.86; H, 6.12. Found: C, 58.55, H, 6.82, N 2.57.

Method A: [1,8-(Dimethylsilanediyl)(η^7-cycloheptatrienyl)(η^5-cyclopentadienyl)vanadium] was sealed in an evacuated Pyrex tube and heated at 150 °C for 1 hour. The content was dissolved in THF, filtered and precipitated by addition of petroleum ether. The dark-violet solid was collected by filtration, washed with additional petroleum ether and dried under vacuum.

MS, m/e: 470 (100%, (TVC)$_2$Si$_2^+$), 207 (13%, TVC$^+$), 91 (3%,C$_7$H$_7^+$), 51 (1%,V$^+$).

Anal. Calculated for C$_{14}$H$_{16}$SiV (263.31): C, 63.86; H, 6.12. Found: C, 58.18, H, 7.73, N 3.28 (calculated on the monomer unit).

Method B: [1,8-(Dimethylsilanediyl)(η^7-cycloheptatrienyl)(η^5-cyclopentadienyl)vanadium] was dissolved in 15 mL of toluene, and a few milligrams of PtCl$_2$ were added. The flask was placed in an oil bath maintained at 80-90°C on a hot plate. The solution was stirred vigorously at this temperature for ca. 2 hours, during which time the violet suspension faded to brown-violet. After cooling to room temperature, the suspension was filtered. Then, the filtrate was added dropwise by a syringe to a flask containing petroleum ether (100 mL), or petroleum ether/toluene (80:20) with rapid stirring. A brown-violet precipitate was formed, which was collected by filtration, washed with additional petroleum ether and dried under vacuum.

MS, m/e: 943 (3%, (TVC-Si(CH$_3$))$_4^+$-2Si(CH$_3$)), 759 (100%, (TVC)$_3$Si$_5^+$), 497 (9%, (TVC)$_2$Si$_3^+$), 235 (2%, TVC-Si$^+$), 207 (3%, TVC$^+$), 91 (5%,C$_7$H$_7^+$), 51 (3%,V$^+$).

Anal. Calculated for $C_{14}H_{16}SiV$ (263.31): C, 63.86; H, 6.12. Found: C, 44.94, H, 6.00, N 4.77 (calculated on the monomer unit).
GPC: M_w: 682.59, M_n: 499.77, M_w/M_n: 1.3658.

Method C: A 100 mL flask equipped with a magnetic stirring bar was charged with (η^7-cycloheptatrienyl)(η^5-cyclopentadienyl)vanadium (0.20 g, 0.97 mmol), diethyl ether (30 mL), and TMEDA (0.58 mL, 3.83 mmol). Then, *n*-BuLi (2.41 mL, 3.83 mmol, solution 1.6 M in hexane) was added dropwise and the mixture was refluxed for 4 hours. After cooling to room temperature, the solvent was evaporated under vacuum and the residue was dissolved in THF. Slow addition of dichlorodimethylsilane (0.12 mL, 0.97 mmol) dissolved in 10 mL of THF to the refluxing THF solution of 1,1'-dilithiotrovacene-TMEDA was followed by refluxing for 7 hours. After removal of the solvent, the residue was dissolved in toluene and precipitated by addition of petroleum ether. A brown-violet precipitate was formed, which was collected by filtration, washed with additional petroleum ether and dried under vacuum.
MS, m/e: 470 (9%, $(TVC)_2Si_2^+$), 264 (11%, $TVC\text{-}Si(CH_3)_2^+$), 207 (25%, TVC^+), 91 (17%,$C_7H_7^+$), 51 (7%,V^+).
Anal. Calculated for $C_{14}H_{16}SiV$ (263.31): C, 63.86; H, 6.12. Found: C, 62.27, H, 9.56 (calculated on the monomer unit).

Synthesis of 1,1'-Bis(carboxy-η^6-benzene)chromium, [(η^6-$C_6H_5COOH)_2Cr^0$], 4. A 100 mL flask equipped with a magnetic stirring bar was charged with bis(benzene)chromium (1.0 g, 4.80 mmol), methylcyclohexane (60 mL), and TMEDA (1.54 mL, 10.2 mmol). *n*-BuLi (6.25 mL, 10.2 mmol, solution 1.6 M in hexane) was added dropwise and the mixture was refluxed for 4 hours. Then at room temperature, CO_2 was fed through the brown suspension for 1 hour. The colour turned immediately to orange-red. The solvent was removed in vacuum and the residue was dissolved in water. After filtration of the unreacted bis(benzene)chromium, HCl (20 mL, 2 M) was added to the filtrate, yielding a red precipitate, which was collected by filtration and dried under vacuum.
Bis(carboxy-η^6-benzene)chromium, **4** (0.10 g, 0.34 mmol) was dissolved in hot water, followed by addition of NaOH (0.5 mL, 0.1 M). The solution was layered with 10 mL of diethyl ether containing HBF_4 (0.1 mL, solution 58% in diethyl ether). Red block crystals were obtained after one week.
Yield: 1.1 g, 80%.

MS, m/e: 122 (100%, $C_6H_5COOH^+$), 105 (93%, $C_6H_5CO^+$), 77 (95%, $C_6H_7^+$), 51 (35%, $C_4H_3^+$).

^{1}H NMR (300 MHz, THF-d8): 11.18 (s, 2H), 5.13 (d, 4H), 4.54 (m, 6H).

Anal. Calculated for $C_{14}H_{12}O_4Cr$ (296.24): C, 56.76; H, 4.08. Found: C, 56.74, H, 4.10.

IR (KBr): ν_{C-H} 3085 cm^{-1}, ν_{O-H} 2653 cm^{-1}, $\nu_{C=O}$ 1680 cm^{-1}, $\nu_{C=C}$ 1499, 1468 cm^{-1}, ν_{C-O} 1311 cm^{-1}, $\delta_{C-H,ring}$ 727 cm^{-1}.

Synthesis of [1,1'-Bis(carboxy-η^6-benzene)chromium][hexafluorophosphate],[(η^6-$C_6H_5COOH)_2Cr^I$]$^+$[PF_6]$^-$,31$^{+\bullet}\alpha$ and 31$^{+\bullet}\beta$. A 50 mL flask equipped with a magnetic stirring bar was charged with bis(carboxy-η^6-benzene)chromium (0.05 g, 0.17 mmol). A saturated solution of NH_4PF_6 in water (15 mL) was added, and air was fed through the mixture overnight at room temperature. Then, the solution was dried under vacuum. Yellow crystals of **31$^{+\bullet}\alpha$** suitable for X-ray diffraction were obtained by diethyl ether diffusion into an acetone solution of the salt, while slow evaporation of an acetone solution of the salt yielded yellow crystals of **31$^{+\bullet}\beta$**.

Synthesis of [1,1'-Bis(carboxyl-η^6-benzene)chromium][ammoniumhexafluoro-phosphate], [Cr^1(η^6-C_6H_5COOH)(η^6-C_6H_5COO)][NH_4][PF_6], 32$^{\bullet}$. A 50 mL flask equipped with a magnetic stirring bar was charged with bis(carboxy-η^6-benzene)chromium (0.10 g, 0.34 mmol), and water (15 mL). Then, air was fed through the mixture overnight at room temperature. The yellow solution obtained was cooled at 0°C, and NH_4PF_6 (0.01 g) was added. The precipitate obtained was filtered and dried under vacuum. Yellow crystals suitable for X-ray diffraction were obtained by recrystallization from methanol.

11. Literature

1) a) J. T. Kealy, P. L. Pauson; *Nature*, **1951**, *168*, 1039; b) S. A. Miller, J. A. L. Tebbboth, J. F. Tremaine, *J. Chem. Soc.*, **1952**, 632; c) G. Wilkinson, M. Rosemblum, M. C. Whiting, R. B. Woodward, *J. Amer. Chem. Soc.*, **1952**, *74*, 2125; d) E. O. Fischer, W. Pfab, *Z. Naturforsch.*, **1952**, *7B*, 377.

2) E. O. Fischer, W. Hafner; *Z. Naturforsch.*, **1955**, *10B*, 665.

3) Ch. Elschenbroich, *J. Organomet. Chem.*, **1968**, *14*, 157.

4) a) P. L. Timms, *J. Chem. Soc. Chem. Comm.*, **1969**, 1033; b) P. L. Timms, *J. Chem Ed.*, **1972**, *49*, 789; b) P. L. Timms, T. W. Turney, *Adv. Organomet. Chem.*, **1977**, *15*, 53; c) J. R. Blackborrow, D. Young, *Metal Vapour Synthesis in Organometallic Chemistry*, Springer Verlag Berlin, Heidelberg, New York, **1979**.

5) T. Hayashi, , *Acc. Chem. Res.*, **2000**, *33*, 354.

6) P. D. Beer, *Adv. Inorg. Chem.*, **1992**, *39*, 79.

7) H. Köpf, P. Köpf-Maier, , *Angew. Chem. Int. Ed. Engl.*, **1979**, *91*, 477.

8) J. S. Miller, J. C. Calabrese, H. Rommelmann, S. R. Chittipeddi, J. H. Zhang, W. M. Reiff, A. J. Epstein, *J. Amer. Chem. Soc.*, **1987**, *109*, 769.

9) M. L. H. Green, S. R. Marder, M. E. Thompson, J. A. Bandy, D. Bloor, P. V. Kolinsky, R. J. Jones, *Nature*, **1987**, *330*, 360.

10) D. Braga, F. Grepioni, G. R. Desiraju, *Chem. Rev.*, **1998**, *98*, 1375.

11) D. Rabinowich, G. M. J. Schmidt, *J. Chem. Soc.* (B), **1964**, 144.

12) G. R. Desiraju, *Chem. Commun.*, **1997**, 1475.

13) a) M. C. Etter, *Acc. Chem. Res.*, **1990**, *23*, 120; b) G. R. Desiraju, *Angew. Chem. Int. Ed. Engl.*, **1995**, *34*, 2311; c) D. Braga, F. Grepioni, *Chem. Comm.*, **1996**, 571; d) M. J. Zaworotko, *Nature*, **1997**, *386*, 220; e) M. Yaghi, L. Guangming, H. Li, *Nature*, **1995**, *378*, 703; f) P. Ball, *Nature*, **1996**, *381*, 648.

14) J. D. Dunitz, L. E. Orgen, *Nature*, **1953**, *171*, 121; J. D. Dunitz, L. E. Orgen, A. Rich, *Acta Crystallogr.*, **1956**, *9*, 373.

15) a) V. G. Albano, D. Braga, *Accurate Molecular Structures*; A. Domenicano, I. Hargittai, Eds., Oxford University Press: Oxford, U. K., **1991**; b) E. Sappa, A. Tiripicchio, P. Braunstein, *Chem. Rev.*, **1983**, *83*, 203; c) D. Imhof, L. M. Venanzi, *Chem. Soc. Rev.*, **1994**, 185.

16) E. L. Muetterties, J. R. bleeke, E. J. Wucherer, *Chem. Rev.*, **1982**, *82*, 499.

17) a) D. Braga, F. Grepioni, *Acc. Chem. Res.*, **1994**, *27*, 51; b) D. Braga, F. Grepioni, *Chem. Comm.*, **1996**, 571.

18) a) M. C. Etter, *Acc. Chem. Res.*, **1990**, *23*, 120; b) C. B. Aakeröy, K. R. Seddon, *Chem. Soc. Rev.*, **1993**, 397; c) S. Subramanian, M. J. Zaworotko, *Coord. Chem. Rev.*, **1994**, *137*, 557; d) M. J. Zaworotko, *Nature*, **1997**, *386*, 220.

19) D. Braga, F. Grepioni, P. Milne, E. Parigini, *J. Am. Chem. Soc.*, **1993**, *115*, 5115.

20) a) A. I. Kitaigorodsky, *Molecular Crystals and Molecules*; Accademic Press: New York, **1973**; b) J. Dunitz, *Acc. Chem. Res.*, **1995**, *28*, 193.

21) a) A. D. Burrows, C. V. Chan, M. M. Chowdry, J. E. McGrady, D. M. P. Mingos, *Chem. Soc. Rev.*, **1995**, 329; b) S. Subramanian, M. J. Zaworotsko, *Coord. Chem. Rev.*, **1994**, *137*, 357; c) L. Brammer, D. Zhao, F. T. Ladipo, J. Braddock-Wilking, *Acta Cryst. Sect. B*, **1995**, *B51*, 632.

22) a) D. J. Williams, *Angew. Chem. Int. Ed. Engl.*, **1984**, *23*, 690; b) N. J. Long, *Angew. Chem. Int. Ed. Engl.*, **1995**, *34*, 21; c) J. S. Miller, A. J. Epstain, *Chem. Commun.*, **1998**, 1319; d) A. Muller, F. Peters, M. T. Pope, D. Gatteschi, *Chem. Rev.*, **1998**, *98*, 239.

23) D. Braga, F. Grepioni, *J. Chem. Soc. Dalton Trans.*, **1999**, 1.

24) a) D. Braga, F. Grepioni, *Acc. Chem. Res.*, **1997**, *30*, 81; b) D. Braga, F. Grepioni, *Coord. Chem. Rev.*, **1999**, *183*, 19.

25) Ch. Elschenbroich, O. Schiemann, O. Burghaus, K. Harms, *J. Am. Chem. Soc.*, **1997**, *115*, 7452.

26) J. A. McCleverty, M. D. Ward, *Acc. Chem. Res.*, **1998**, *31*, 842.

27) a) T. Hayashi, H. Ogoshi, *Chem. Soc. Rew.*, **1997**, *26*, 355; b) J. L. Sessler, B. Wang, E. Harriman, *J. Am. Chem. Soc.*, **1993**, *115*, 10418; c) J. A. Roberts, J. B. Kirby, D. G. Nocera, *J. Am. Chem. Soc.*, **1995**, *117*, 8051; d) A. Harriman, Y. Kubo, J. L. Sessler, *J. Am. Chem. Soc.*, **1992**, *114*, 388; e) A. Berman, E. S. Izraeli, H. Levanon, B. Wang, J. L. Sessler, *J. Am. Chem. Soc.*, **1995**, *117*, 8252; f) T. Hayashi, T. Miyahara, S. Kumazaki, H. Ogoshi, K. Yoshihara, *Angew. Chem. Int. Engl. Ed.*, **1996**, *35*, 1964.

28) a) C. B. Aakeroy, K. R. Seddon, *Chem. Soc. Rev.*, **1993**, 397; b) D. Braga, F. Grepioni, G. R. Desiraju, *J. Organomet. Chem.*, **1997**, *548*, 33.

29) M. C. Etter, *Acc. Chem. Res.*, **1990**, *23*, 120.

30) M. S. Gordon, J. H. Jensen, *Acc. Chem. Res.*, **1996**, *26*, 536.

31) a) P. A. Kollmann, L. C. Allen, *Chem Rev.*, **1972**, *72*, 283; b) L. A. Curtis, M. Blander, *Chem. Rev.*, **1988**, *88*, 827.

32) D. Braga, F. Grepioni, *New J. Chem.*, **1998**, *22*, 1159.

33) a) M. Meot-Ner, *J. Am. Chem. Soc.*, **1984**, *106*, 1257; b) M. Meot-Ner, L. W. Sieck, *J. Am. Chem. Soc.*, **1986**, *108*, 7525.

34) G. A Jeffrey, *An Introduction to Hydrogen Bonding*, Oxford University Press, New York, **1997**.

35) D. Braga, L. Maini, L. Prodi, A. Caneschi, R. Sessoli, F. Grepioni, *Chem. Eur. J.*, **2000**, *6*, 1310.

36) Ch. Elschenbroich, *Organometallchemie*, B.G. Teubner, Stuttgart, **2003**.

37) a) G. G. Eberhard, W. A. Butte, *J. Org. Chem.*, **1964**, *29*, 2928; b) A. W. Langer Jr, *Trans. N. Y. Acad. Sci.*, **1965**, *27*, 741.

38) a) A. N. Nesmeyanov, E. G. Perevalova, R. V. Golovnya, O. A. Nesmeyanova, *Dokl. Akad. Nauk. SSSR*, **1954**, *97*, 459; b) R. A. Benkeser, D. Goggin, G. Schroll, *J. Am. Chem Soc.*, **1954**, *76*, 4025.

39) C. J. Groeneboom, H. J. de Liefde Meijer, F. Jellinek, *J. Organomet. Chem.*, **1974**, *69*, 235.

40) M. D. Rausch, M. Ogasa, R. D. Rogers, A. N. Rollin, *Organometallic*, **1991**, *10*, 2084.

41) M. Vliek, C. J. Groeneboom, H. J. de Liefde Meijer, F. Jellinek, *J. Organomet. Chem.*, **1975**, *97*, 67.

42) E.O. Fischer, S. Beitschaft, *Chem. Ber.*, **1966**, *99*, 2905.

43) H. Basch, A. Viste, H. B. Gray, *J. Chem. Phys.*, **1966**, *44*, 10.

44)R. D. Fischer, *Theoret. Chim. Acta*, **1963**, *1*, 418.

45) M. F. Rettig, C.D. Stout, A. Klug, P. Farnham, *J. Am. Chem. Soc.*, **1970**, *92*, 5100.

46) J. D. Zeinstra, J. L. de Boer, *J. Organomet. Chem.*, **1973**, *54*, 207.

47) J. Müller, B. Mertschenk, *J. Organomet. Chem.*, **1972**, *34*, 165.

48) C. J. Groenenboom, H. J. de Liefde Meijer, F. Jellinek, *Recl. Trav. Chim. Pays-Bas.*, **1974**, *93*, 6.

49) J. Plackmeyer, *Diplomarbeit*, Universität-Marburg, **1997**.

50) O. Schiemann, *Diplomarbeit*, Universität-Marburg, **1995**.

51) J. Plackmeyer, *Dissertation*, Universität-Marburg, **2001**.

52) B. Ibrahim, *Diplomarbeit*, Universität-Marburg, **1999**.

53) A. Behrendt, *Dissertation*, Universität-Marburg, **1995**.

54) M. Wolf, *Dissertation*, Universität-Marburg, **1999**.

55) R. Sanders, U. T. Mueller-Westerhoff, *J. Organomet. Chem.*, **1996**, *512*, 219.

56) D. W. Slocum, T. R. Engelmann, C. Ernst, C. A. Jennings, W. Jones, B. Koonsvitsky, J. Lewis, P. Shenkin, *J. Chem. Ed.*, **1969**, *46*, 144.

57) M. F. Rettig, C. D. Stout, A. Kleng, P. Farnham, *J. Am. Chem. Soc.*, **1970**, *92*, 5100.

58) L. Kevan, L. D. Kispert, *Electron Spin Double Resonance*, J. Wiley and Sons, New York, **1976**.

59) G. Feher, *Phys. Rev.*, **1956**, *103*, 834.

60) M. F. Retting, C. D. Stout, A. Klug, P. Farnahm, *J. Am. Chem. Soc.*, **1970**, 5100.

61) G. Engebretson, R. E. Rundle, *J. Am. Chem. Soc.*, **1963**, *85*, 481.

62) E. Keulen, F. Jellinek, *J. Organomet. Chem.*, **1966**, *5*, 490.

63) a) J. C. Green, M. L. H. Green, N. Kaltsoyannis, P. Mountford, P. Scott, *Organometallics*, **1992**, *11*, 3353; b) M. L. H. Green, D. K. P. Ng, *Chem. Rev.*, **1995**, *95*, 439.

64) a) R. Ramasami, J. F. Endicott, *J. Am. Chem. Soc.*, **1985**, *107*, 389; b) P. Bertrand, *Chem. Phys. Lett.*, **1985**, *113*, 104; c) G. Blondin, J. Girerd, *Chem. Rev.*, **1990**, *90*, 1359; d) M. D. E. Forbes, J. D. Ball, N. I. Avdievich, *J. Am. Chem. Soc.*, **1996**, *118*, 4707; e) R. E. Coffmann, G. R. Buettner, *J. Phys. Chem.*, **1979**, *83*, 2387.

65) a) D. Braga, F. Grepioni, E. Tedesco, K. Biradha, G. Desiraju, *Organometallics*, **1996**, *15*, 2692; b) P. D. Beer, M. G. B. Drew, A. R. Graydon, D. K. Smith, S. E. Stokes, *J. Chem. Soc. Dalton Trans.*, **1995**, 403; c) S. Shubina, N. V. Belkova, A. N. Krylov, E. V. Vorontsov, L. M. Epstein, D. G. Gusev, M. Niedermann, H. Berke, *J. Am. Chem. Soc.*, **1996**, *118*, 1105.

66) a) P. Caubère, *Chem. Rew.*, **1993**, *93*, 2317; b) M. Schlosser, *Pure Appl. Chem.*, **1988**, *60*, 1627; c) L. Lochmann, J. Trekoval, *J. Organomet. Chem.*, **1987**, *326*, 1; d) L. Lochmann, M. Fossatelli, L. Brandsma, *Recl. Trav. Chim. Pays-Bas.*, **1990**, *109*, 529.

67) a) D. H. Evans, K. M. O'Connell, R. A. Peterson, M. J. Kelly, *J. Chem. Educ.*, **1986**, *60*, 291; b) G. A. Mabot; *J. Chem. Educ.*, **1986**, *60*, 697; c) P. T. Kissinger, W. R. Heinemann; *J. Chem. Educ.*, **1986**, *60*, 702.

68) Ch. Elschenbroich, E. Bilger, B. Metz, *Organometallics*, **1991**, *10*, 2823.

69) a) J. C. Green, N. Kaltsoyannis, K. H. Sze, M. MacDonald, *J. Am. Chem. Soc.*, **1994**, *116*, 1994.

70) a) S. Evans, J. C. Green, S. E. Jackson, E. Higginson, *J. Chem. Soc. Dalton. Trans.*, **1974**, 304; b) D. W. Clack., K. D. Warren, *Inorg. Chim. Acta*, **1978**, *30*, 251; c) V. M. Rayón, G. Frenking, *Organometallics*, **2003**, *22*, 3304.

71) D. R. Kanis, M. A. Ratner, T. J. Marks, *J. Am. Chem. Soc.*, **1992**, *114*, 10338.

72) J. L. Robbins, N. Edelstein, B. Spencer, J. C. Smart, *J. Am Chem. Soc.*, **1982**, 104, 1882.

73) a) B. Bildstein, A. Hradsky, H. Kopacka, R. Malleier, K. H. Ongania, *J. Organomet. Chem.*, **1997**, *540*, 135; b) Ch. Elschenbroich, E. Bilger, R. D. Ernst, D. R. Wilson, M.S. Kralik, *Organometallics*, **1985**, *4*, 2068.

74) J. H. Wertz, J. R. Bolton, *Electron spin Resonance: Elementary Theory and Practical Application*; Mc Graw-Hill, New York, **1972**.

75) D. W. Clack, K. D. Warren, *Theoret. Chim. Acta*, **1978**, *30*, 291.

76) J. D. Zeinstra, W. C. Nieuwpoort, *Inorg. Chim. Acta*, **1978**, *30*, 103.

77) a) R. Wilson, D. Kivelson, *J. Chem. Phys.*, **1966**, *44*, 154; b) R. Wilson, D. Kivelson, *J. Chem. Phys.*, **1960**, *33*, 1094; c) A. Hudson, G. R. Luckhurst, *Chem. Rew.*, **1968**, *69*, 191.

78) B. A. Goodman, J. B. Raynor, *Adv. Inorg. Radoichem.*, **1970**, *13*, 136.

79) R. Wolf, A. Schweiger, H. H. Günthard, *Molecular. Phys.*, **1984**, 53, 585.

80) D. O. Cowan, C. Le Vanda, J. Park, F. Kaufman, *Acc. Chem. Res.*, **1973**, *6*, 1.

81) K. Deuchert, S. Hüning, *Angew. Chem. Int. Ed. Engl.*, **1978**, *17*, 875.

82) O. Schiemann, *Dissertation*, Universität-Marburg, **1998**.

83) J. E. McMurry, T. Lectka, J. G. Rico, *J. Org. Chem.*, **1989**, *54*, 3748.

84) T. Mukaiyama, T. Sato, T. Hanna, *Chem. Lett.*, **1973**, 1041.

85) J. E. McMurry, M. P. Fleming, *J. Am. Chem. Soc.*, **1974**, *96*, 4708.

86) D. Lenoir, H. Burghard, *J. Chem. Res.*, **1980**, 396.

87) S. Barlow, D. O'Hara, *Chem. Rev.*, **1997**, 637.

88) J. B. Flanagan, S. Margel, A. J. Bard, F. C. Anson, *J. Am. Chem. Soc.*, **1978**, *100*, 4248.

89) R. J. Cruchley, *Adv. Inorg. Chem.*, **1994**, *41*, 273.

90) Bencini, D. Matteschi, *EPR of Exchange Coupled Systems*, Springer, Berlin, **1990**.

91) F. E. Mabbs, *Chem. Soc. Rev.*, **1993**, *22*, 313.

92) S. H. Glarum, J. H. Marshall, *J. Chem. Phys.*, **1967**, *47*, 1347.

93) O. Burghaus, *unpublished results*.

94) L. R. Belford, N. D. Chasteen, *Inorg. Chem.*, **1970**, *9*, 169.

95) O. Kahn, *Molecular Magnetism*, VCH, Weinheim, **1993**.

96) K. Matzuda, H. Iwamura, *J. Chem. Soc. Perkin Tran.2*, **1998**, 1023.

97) a) Ch. Elschenbroich, F. Gerson, *J. Organomet. Chem.*, **1973**, *49*, 445; b) Ch. Elschenbroich, F. Gerson, *J. Am. Chem. Soc.*, **1973**, *95*, 6956.

98) a) Ch. Elschenbroich, O. Schiemann, O. Burghaus, K. Harms, J. Pebler, *Organometallics*, **1999**, *18*, 3273; b) Ch. Elschenbroich, J. Plackmeyer, K. Harms, O. Burghaus, J. Pebler, *Organometallics*, **2003**, *22*, 3367.

99) H. Rosenberg, U. S. Patent 3,426,053, filed August 31, 1966, patented February 4, 1969.

100) A. G. Osborne, R. H. Whiteley, *J. Organomet. Chem.*, **1975**, *101*, C27.

101) a) A. G. Osborne, R. H. Whiteley, *J. Organomet. Chem.*, **1980**, *193*, 345; b) D. Seyferth, H. P. Withers, *Organometallics*, **1982**, *1*, 1275; c) A. B. Fisher, J. B. Kinney, R. H. Staley,

M. S. Wrighton, *J. Am. Chem. Soc.*, **1979**, *101*, 6501; d) A. Darold, Y. Mugnier, R. Broussier, B. Gautheron, E. Lavirou, *J. Organomet. Chem.*, **1989**, *362*, C27.

102) a) Ch. Elschenbroich, J. Koch, *J. Organomet. Chem.*, **1982**, *229*, 139; b) Ch. Elschenbroich, J. Koch, J. Kroker, M. Wünsch, W. Massa, G. Baum, G. Stork, *Chem. Ber.*, **1988**, *121*, 1983; c) C. G. Francis, P. L. Timms, *J. Chem. Soc. Dalton Trans.*, **1980**, 1401; d) M. L. H. Green, I. Treurnicht, J. A. Bandy, A. Gourdon, K. Prout, , *J. Organomet. Chem.*, **1986**, *306*, 145.

103) A. G. Osborne, R. H. Whiteley, R. E. Meads, *J. Organomet. Chem.*, **1980**, *193*, 345.

104) a) D. A. Foucher, B.-Z. Tang, I. Manners, *J. Am. Chem. Soc.*, **1992**, *114*, 626; b) V. Dement'ev, F. Cervantes-Lee, C. Parkanyi, H. Sharma, K. H. Pannel, *Organometallics*, **1993**, *12*, 1983; c) W. Finckh, B. Tang, D. A. Foucher, D. B. Zamble, R. Ziembinski, A. Lough, I. Manners, *Organometallics*, **1993**, *11*, 823.

105) Ch. Elschenbroich, J. Hurley, W. Massa, *Organometallics*, **1990**, *9*, 889.

106) Ch. Elschenbroich, F. Lu, K. Harms, *Organometallics*, **2002**, *21*, 5152.

107) Ch. Elschenbroich, E. Bilger, B. Metz, *Organometallics,* **1991**, *10*, 2823.

108) E. Fujita, B. Gordon, M. Hillman, A. G. Nagy, *J. Organomet. Chem.*, **1981**, *218*, 105.

109) J. Hurley, *Dissertation*, Universtät-Marburg, **1989**.

110) J. W. Lauher, R. Hoffmann, *J. Am. Chem. Soc.*, **1976**, *98*, 1729.

111) E. W. Neuse, H. Rosenberg, *J. Macromol. Sci. Rev. Chem.*, **1970**, *44*, 1.

112) M. Peuckert, T. Vaahs, M. Brück, *Adv. Mater.*, **1990**, *2*, 398.

113) R. West, *J.Organomet. Chem.*, **1986**, *300*, 327.

114) D. A. Foucher, B. Z. Tang, I. Manners, *J. Am. Chem. Soc.*, **1992**, 114, 6246.

115) K. H. Pannell, H. K. Sharma, *Organometallics*, **1997**, *16*, 3077.

116) J. K. Pudelski, I. Manners, *J. Am. Chem. Soc.*, **1995**, *117*, 7265.

117) A. Clearfield, C. J. Simmons, H. P. Wither, D. Seyferth, *Inorg. Chim. Acta*, **1983**, *75*, 139.

118) H. Yamashita, M. Tanaka, K. Honda, *J. Am. Chem. Soc.*, **1995**, *117*, 8873.

119) F. Takusagawa, T. F. Koetzle, *Acta Crystallogr. Sect. B*,**1979**, *35*, 2888.

120) D. Braga, L. Maini, M. Polito, M. Rossini, F. Grepioni, *Chem. Eur. J.*, **2000**, *6*, 4227.

121) D. Braga, L. Maini, F. Grepioni, Ch. Elschenbroich, F. Paganelli, O. Schiemann, *Organometallics*, **2001**, *21*, 1875.

122) a) E. O. Fischer, H. Brunner, *Chem. Ber.*, **1962**, *95*, 1999; b) E. O. Fischer, H. Brunner, *Chem. Ber.*, **1965**, *98*, 175.

123) D. Braga, F. Grepioni, K. Biradha, V. R. Pediretti, G. R. Desiraju, *J. Am. Chem. Soc.*, **1995**, *117*, 3156.

124) W. C. McCrone, *Polymorphism in Physic and Chemistry of the Organic Solid State*; Ed. D. Fox, M. M. Labes, A. Wissemberg, Interscience: New York, **1965**.

125) J. Bernstein, *Organic Solid State Chemistry*; Ed. G. R. Desiraju, Amsterdam, **1987**.

126) a) F. A. Cotton, *Inorg. Chem.*, **1965**, *5*, 1083; b) G. J. Bullit, F. A. Cotton, T. J. Marksl, *J. Am. Chem. Soc.*, **1970**, *92*, 2155; c) F. A. Cotton, B. E. Hanson, *Rearrangements in Ground and Excited State*; Ed. P. De Mayo, Accademic Press: New York, **1980**.

127) A. Burger, *Topics in Pharmaceutical Sciences*; Ed. D. D. Breimer, P. Meenan, ACS Proceedings Series, Washington, DC, **1996**.

128) D. Braga, *Chem. Rev.*, **1992**, *92*, 633.

129) S. R. Birn, *Solid State Chemistry of Drugs*; Accademic Press: New York, **1982**.

130) D: Braga, F. Grepioni, J. J. Novoa, *New J. Chem.*, **2001**, *2*, 226.

131) D. Braga, F. Grepioni, *Acc. Chem. Res.*, **2000**, *33*, 601.

132) a) F. H. Köhler, W. Prösdorf, *Z. Naturforsch.*, **1977**, *32B*, 1026; b) C. Floriani, *J. Chem. Soc. Dalton Trans.*, **1976**, 1046; c) R. B. King, *J. Am. Chem Soc.*, **1959**, *81*, 5263.

133) a) C. M. Fendrick, L. D. Schertz, E. A. Mintz, T. J. Marks, *Inorg. Synth.*, **1992**, *29*, 193; b) D. Feitler, G. M. Whitesides, *Inorg. Chem.*, **1976**, *15*, 466; c) Brauer, *Handbuch der Präparativen Anorganischen Chemie*, III Ed., Vol. 3, pag. 1814; d)M. Hoch, A. Duch, D. Rehder, *Inorg. Chem.*, **1986**, *25*, 2907; e) M. Herberhold, W. Kremnitz, M. Kuhnlein, *Z. Naturforsch.*, **1987**, *42B*, 1520; f) M. Herberhold, S. Köppl, W. Milius, *Z. Naturforsch.*, **1999**, *54B*, 899.

134) E. O. Fischer, W. Hafner, *Z. Naturforsch.*, **1955**, *10B*, 665.

135) G. M. Sheldrick **SHELIX97**, *Program for Crystal Structure Determination*; University of Gottingen: Gottingen, Germany, **1997**.

136) E. Keller **SHAKAL97**, *Graphical Rapresentation of Molecular Models*; University of Freiburg: Freiburg, Germany, **1999**.

Appendix A: IR Spectra

Trovacene, $1^{\bullet}$

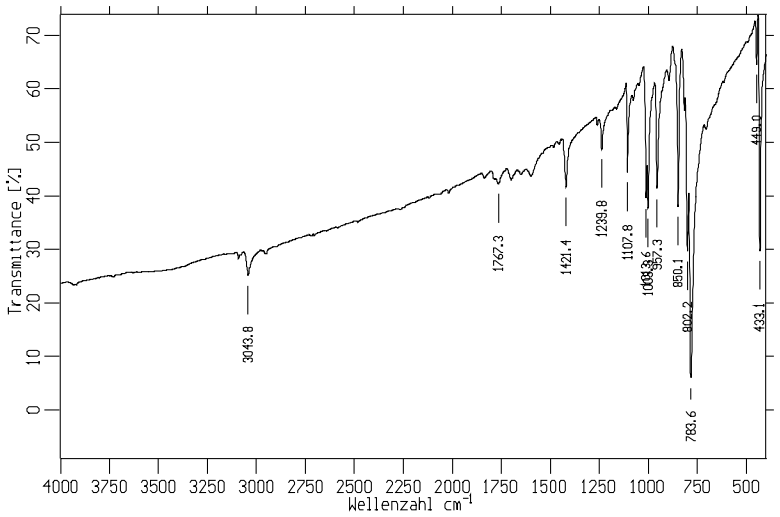

(Carboxy-η^7-cycloheptatrienyl)(carboxy-η^5-cyclopentadienyl) vanadium, $13^{\bullet}$

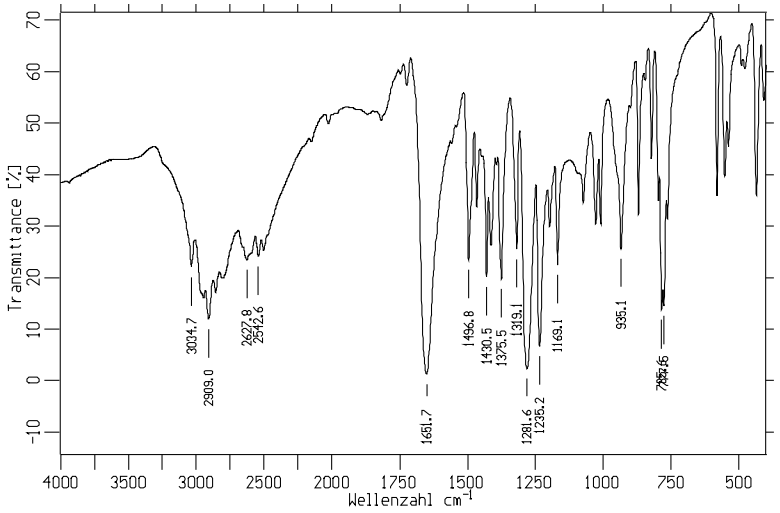

(Formyl-η^7-cycloheptatrienyl)(formyl-η^5-cyclopentadienyl)vanadium, 14$^\bullet$

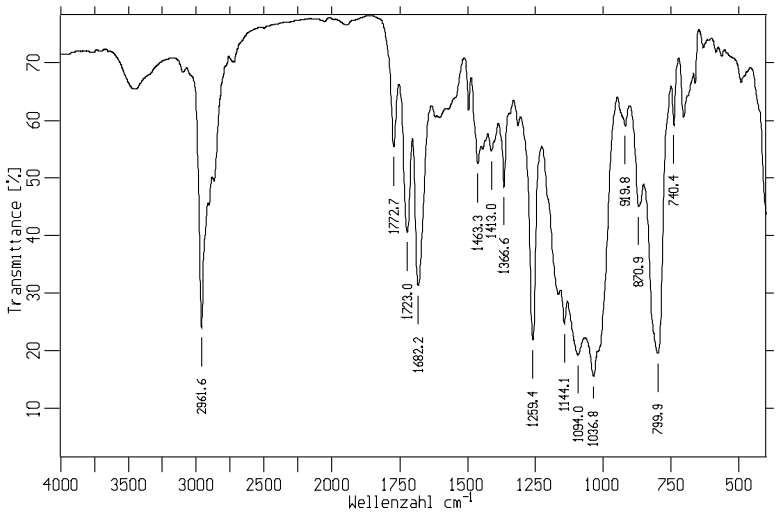

(η^7-cycloheptatrienyl)(η^5-pentametylcyclopentadienyl)vanadium, 2$^\bullet$

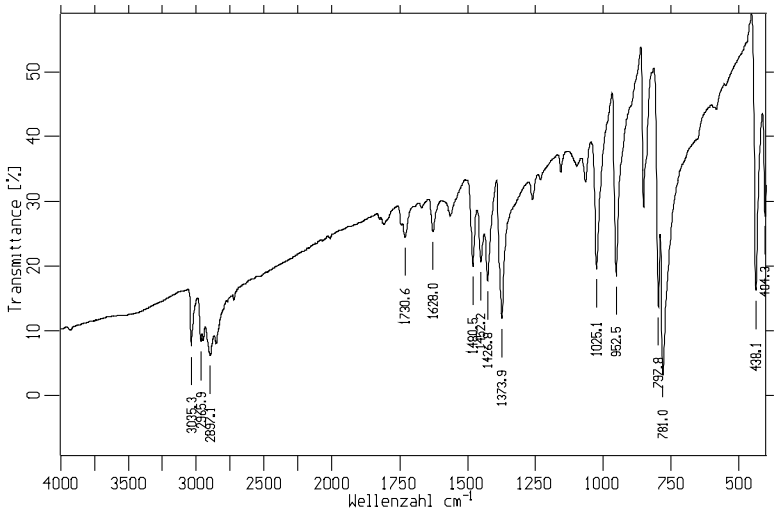

(Carboxy-η^7-cycloheptatrienyl)(η^5-pentamethylcyclopentadienyl)vanadium, 15$^\bullet$

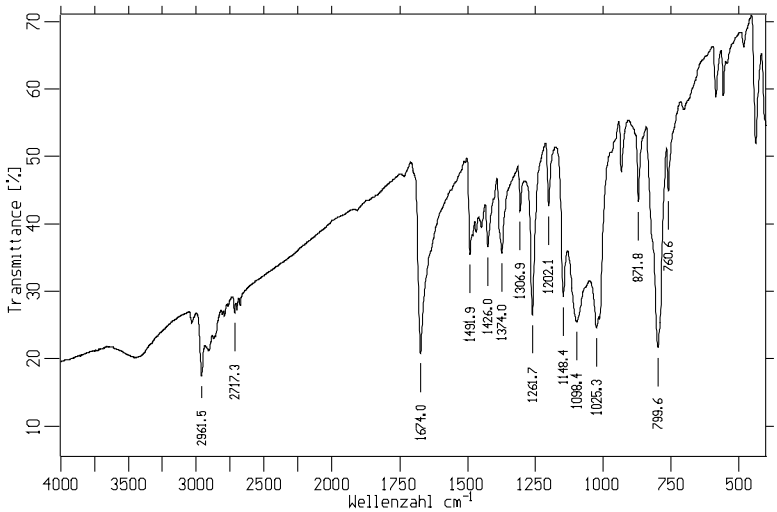

(Formyl-η^7-cycloheptatrienyl)(η^5-pentamethylcyclopentadienyl)vanadium, 16$^\bullet$

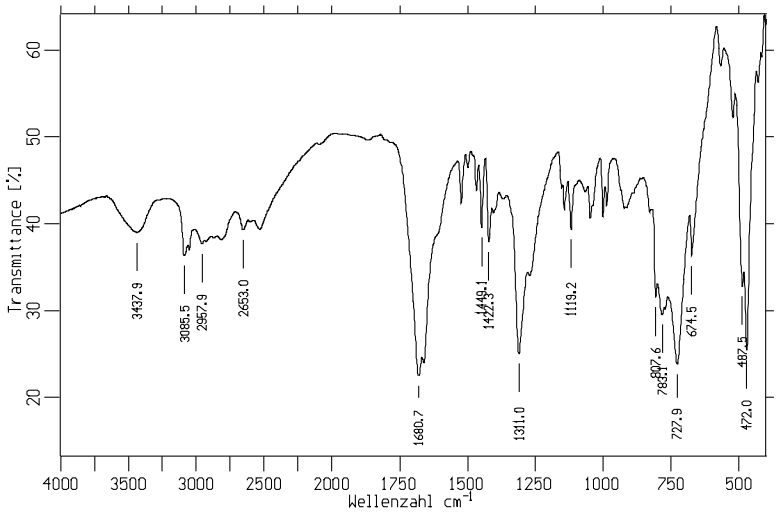

E-1,2-bis[(η^7-cycloheptatrienyl)(η^5-pentamethylcyclopentadienyl)vanadium]ethene, 18$^{\bullet\bullet}$

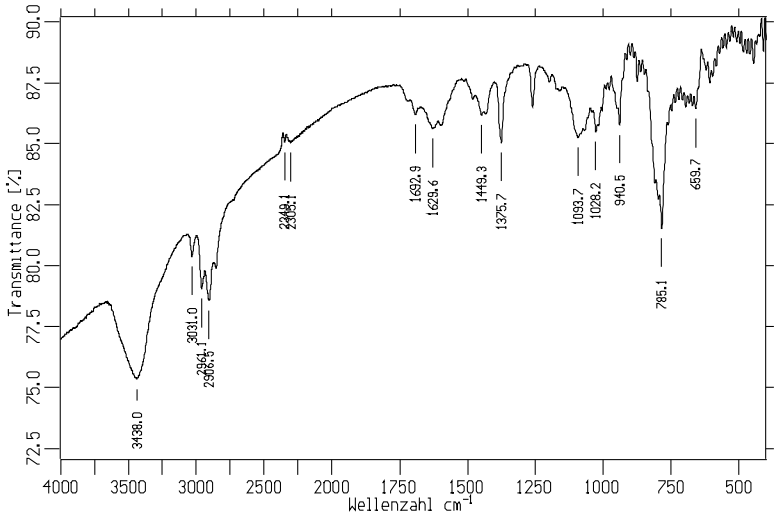

[1,8-(Diphenylsilanediyl)(η^7-cycloheptatrienyl)(η^5-cyclopentadienyl)vanadium], 24$^{\bullet}$

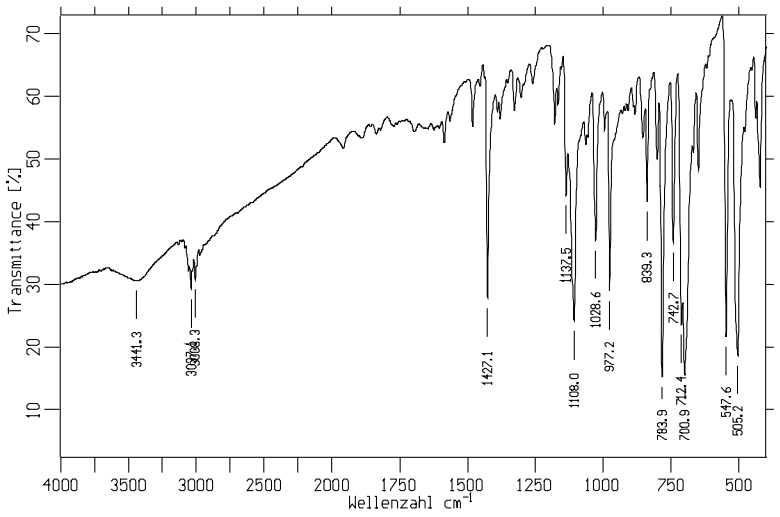

[1,8-(Tetramethyldisilane-1,2-diyl)(η^7-cycloheptatrienyl)(η^5-cyclopentadienyl)-vanadium], 25$^{\bullet}$

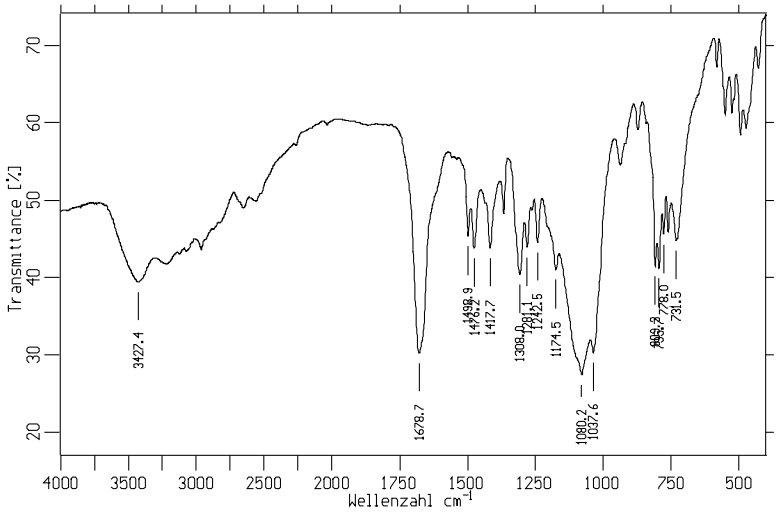

Bis(η^6-benzene)chromium, 3

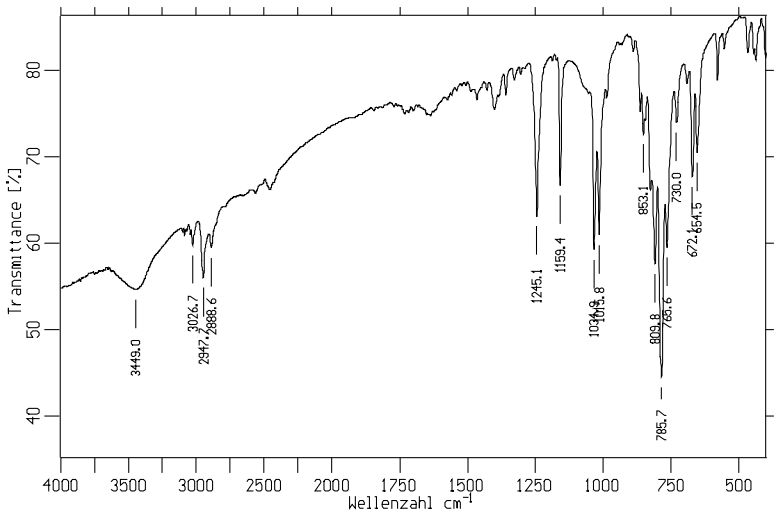

1,1'-Bis(carboxy-η^6-benzene)chromium, $4(H)_2$

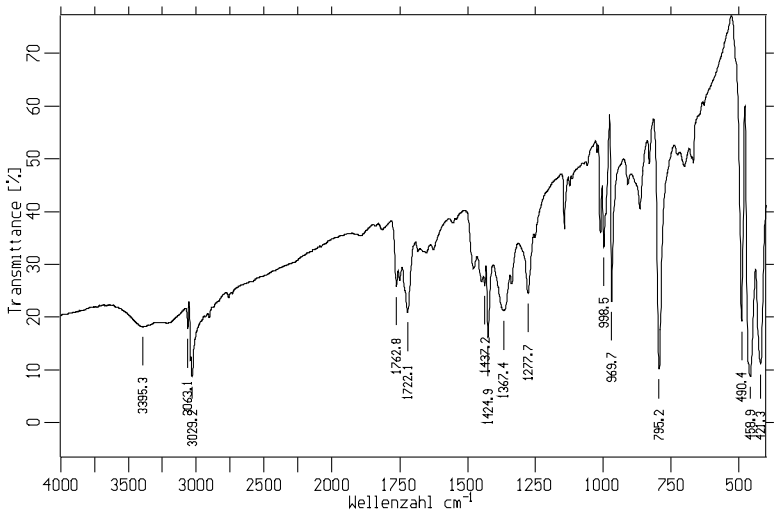

Appendix B: Experimental Data for the Crystal Structure Determinations

Trovacene, $1^{\bullet}$

Empirical formula	$C_{12}H_{12}V$
Formula weigh, g/mol	207.16
Crystal system	Orthorhombic
Space group	Pnma
Unit cell dimensions, Å	a=10.8759(8) b=10.6309(11) c=7.8757(6)
α, deg	90
β, deg	90
γ, deg	90
Volume, $Å^3$	910.59(13)
Z	4
F(000)	428
Calculated density, g/cm^3	1.511
Crystal size, mm	0.32x0.34x0.11
Temperature, K	100
Limiting indices	-14<=h<=15 -15<=k<=15 -10<=l<=11
Reflections collected	10935
Unique reflections	1515
min and max Transmittance (%)	0.8935-0.7337
Goodness of fit on F^2	1.066
R_1 (on F, $I > 2\sigma(I)$)	0.0308
wR_2 (on F^2, all data)	0.0845

(η^7-cycloheptatrienyl)(η^5-pentamethylcyclopentadienyl)vanadium, $2^{\bullet}$

Empirical formula	$C_{17}H_{22}V$
Formula weigh, g/mol	277.30
Crystal system	Orthorhombic
Space group	Pnma
Unit cell dimensions, pm	a=1021.1(1) b=1261.5(1) c=1103.1(1)
α, deg	90
β, deg	90
γ, deg	90
Volume, pm^3	$1429.3(2)\cdot10^6$
Z	4
F(000)	588
Calculated density, g/cm^3	1.289
Crystal size, mm	0.41x0.31x0.06
Temperature, K	193
Limiting indices	-12<=h<=12 -15<=k<=15 -13<=l<=13
Reflections collected	19739
Unique reflections	1515
Observed. Reflections with $F_o>4\sigma(F_o)$	1286
min and max Transmittance (%)	77/100
Goodness of fit on F^2	1.076
R_1 (on F, $I > 2\sigma(I)$)	0.037
wR_2 (on F^2, all data)	0.102

(Carboxy-η^7-cycloheptatrienyl)(carboxy-η^5-cyclopentadienyl)vanadium, 13$^{\bullet}$

Empirical formula	$C_{14}H_{12}O_4V$
Formula weight, g/mol	295.18
Crystal system	Monoclinic
Space group	$P2_1/c$
Unit cell dimensions, Å	a=6.9723(14) b=7.8419(16) c=21.642(4)
α, deg	90
β, deg	98.51(3)
γ, deg	90
Volume, Å^3	1170.3(4)
Z	4
F(000)	604
Calculated density, g/cm^3	0.854
Crystal size, mm	0.19x0.17x0.16
Temperature, K	243
θ range for data collection, deg	3.32-26.97
Limiting indices	-8<=h<=8 0<=k<=10 0<=l<=27
Reflections collected	2570
Unique reflections	2503
Goodness of fit on F^2	1.186
Final R indices (on F, $I > 2\sigma(I)$)	R_1=0.1030 wR_2=0.2582
R indices (all data)	R_1=0.2898 wR_2=0.3288

(Formyl-η^7-cycloheptatrienyl)(η^5-pentamethylcyclopentadienyl)vanadium, 16$^{\bullet}$

Empirical formula	$C_{18}H_{22}OV$
Formula weigh, g/molt	305.31
Crystal system	Orthorhombic
Space group	Pnma
Unit cell dimensions, pm	a=1061.7(1) b=1248.5(1) c=1115.5(1)
α, deg	90
β, deg	90
γ, deg	90
Volume, pm^3	$1478.6(2)\cdot10^6$
Z	4
F(000)	644
Calculated density, g/cm^3	1.371
Crystal size, mm	0.12x0.11x0.09
Temperature, K	193
Limiting indices	-13<=h<=13 -15<=k<=15 -13<=l<=13
Reflections collected	20251
Unique reflections	1568
Goodness of fit on F^2	0.097
R indices (all data)	R_1=0.0356 wR_2=0.0887

[1,8-(Diphenylsilanediyl)(η^7-cycloheptatrienyl)(η^5-cyclopentadienyl)vanadium], 24$^\bullet$

Empirical formula	$C_{24}H_{20}SiV$
Formula weight, g/mol	387.45
Crystal system	monoclinic
Space group	$P2_1/n$
Unit cell dimensions, pm	a=1114.3(2) b=1527.0(2) c=1190.7(2)
α, deg	90
β, deg	111.91(1)
γ, deg	90
Volume, pm^3	$1879.7(5)\cdot10^6$
Z	4
F(000)	804
Calculated density, g/cm^3	1.369
Crystal size, mm	0.23x0.2x0.08
Temperature, K	193
Limiting indices	13<=h<=13 -18<=k<=18 14<=l<=14
Reflections collected	26752
Unique reflections	3770
Observed. Reflections with $F_o>4\sigma(F_o)$	2544
Parameters	344
min and max Transmittance (%)	82/100
Goodness of fit on F^2	0.817
R_1 (on F, $I > 2\sigma(I)$)	0.0284
wR_2 (on F^2, all data)	0.0604

[1,8-(Tetramethyldisilane-1,2-diyl)(η^7-cycloheptatrienyl)(η^5-cyclopentadienyl)vanadium], 25•

Empirical formula	$C_{16}H_{22}Si_2V$
Formula weight, g/mol	321.47
Crystal system	monoclinic
Space group	$P2_1$
Unit cell dimensions, pm	a=664.0(1) b=1310.9(1) c=944.8(1)
α, deg	90
β, deg	104.72(1)
γ, deg	90
Volume, pm^3	$795.4(2)\cdot10^6$
Z	2
F(000)	338
Calculated density, g/cm^3	1.342
Crystal size, mm	0.40x0.34x0.012
Temperature, K	193
Limiting indices	-8<=h<=8 -16<=k<=14 11<=l<=11
Reflections collected	11497
Unique reflections	3064
Observed. Reflections with $F_o>4\sigma(F_o)$	2917
Parameters	134
min and max Transmittance (%)	74/100
Goodness of fit on F^2	1.097
R_1 (on F, $I > 2\sigma(I)$)	0.0631
wR_2 (on F^2, all data)	0.1755

1,1'-Bis(carboxy-η^6-benzene)chromium, 4(H)$_2$

Empiric formula	$C_{14}H_{12}CrO_4$
Formula weigh, g/mol	296.24
Crystal system	monoclinic
Space group	Cc
Unit cell dimensions, Å	11.482(5) 10.035(4) 19.669(5)
α, deg	90
β, deg	91.13(3)
γ, deg	90
Volume, Å^3	2265.9(15)
Z	8
F(000)	1216
Calculated density, g/cm^3	1.737
μ, mm^{-1}	1.016
Crystal size, mm	0.30 x 0.15 x 0.30
Temperature, K	253(2)
θ limits, deg	3-30
min/max h, k, l	-16/16,0/14,0/27
Reflections collected	3551
Unique reflections	3379
Reflections with I > 2σ(I)	1970
Parameters	344
min and max Transmittance	0.86-1.00
GOF on F^2	0.983
R_1 (on F, I > 2σ(I))	0.0381
wR_2 (on F^2, all data)	0.1142

[1,1'-Bis(carboxy-η^6-benzene)chromium][hexafluorophosphate], $[4(H_2)]^{\bullet+}\bullet[PF_6]^-$ α form

Empiric formula	$C_{14}H_{12}CrF_6O_4P$
Formula weigh, g/mol	441.21
Crystal system	monoclinic
Space group	C2/c
Unit cell dimensions, Å	7.649(4); 20.458(6); 10.044(3)
α, deg	90
β, deg	96.55(3)
γ, deg	90
Volume, $Å^3$	1562(1)
Z	4
F(000)	884
Calculated density, g/cm^3	1.877
μ, mm^{-1}	0.992
Crystal size, mm	0.22 x 0.20 x 0.18
Temperature, K	223(2)
θ limits, deg	3-30
min/max h, k, l	-10/10,0/28,0/14
Reflections collected	2401
Unique reflections	2285
Reflections with $I > 2\sigma(I)$	1655
Parameters	134
min and max Transmittance	0.94-1.00
GOF on F^2	1.020
R_1 (on F, $I > 2\sigma(I)$)	0.0424
wR_2 (on F^2, all data)	0.1300

[1,1'-Bis(carboxy-η^6-benzene)chromium][hexafluorophosphate], $[4(H_2)]^{\bullet+}\bullet[PF_6]^-$ β form

Empiric formula	$C_{14}H_{12}CrF_6O_4P$
Formula weigh, g/mol	441.21
Crystal system	triclinic
Space group	P1
Unit cell dimensions, Å	7.580(10); 7.902(9); 7.882(4)
α, deg	82.34(7)
β, deg	66.02(9)
γ, deg	65.90(10)
Volume, $Å^3$	393.5(7)
Z	1
F(000)	221
Calculated density, g/cm^3	1.862
μ, mm^{-1}	0.914
Crystal size, mm	0.20 x 0.18 x 0.12
Temperature, K	223(2)
θ limits, deg	3-25
min/max h, k, l	-8/8,-9/9,0/9
Reflections collected	1465
Unique reflections	1356
Reflections with $I > 2\sigma(I)$	920
Parameters	137
min and max Transmittance	0.85-1.00
GOF on F^2	0.987
R_1 (on F, $I > 2\sigma(I)$)	0.0918
wR_2 (on F^2, all data)	0.2971

[1,1'-Bis(carboxyl-η^6-benzene)chromium][ammoniumhexafluorophosphate], [4(H)$^{\bullet}$]•[NH_4PF_6]

Empiric formula	$C_{14}H_{15}CrF_6NO_4P$
Formula weigh, g/mol	458.24
Crystal system	monoclinic
Space group	$P2_1/c$
Unit cell dimensions, Å	7.518(2); 16.289(6); 13.791(5)
α, deg	90
β, deg	99.79(3)
γ, deg	90
Volume, Å^3	1664(1)
Z	4
F(000)	1784
Calculated density, g/cm^3	1.869
μ, mm^{-1}	1.378
Crystal size, mm	0.20 x 0.12 x 0.08
Temperature, K	223(2)
θ limits, deg	3-26
min/max h, k, l	-9/9,0/20,0/16
Reflections collected	3537
Unique reflections	3055
Reflections with I > 2σ(I)	955
Parameters	137
min and max Transmittance	0.87-1.00
GOF on F^2	0.784
R_1 (on F, I > 2σ(I))	0.0876
wR_2 (on F^2, all data)	0.3654

Appendix C: X-ray Powder Diffraction of $2[PF_6]\alpha$